Experiential Effects on the Neural Substrates of Visual Word and Number Processing

by

Joonkoo Park

A dissertation submitted in partial fulfillment
of the requirements for the degree of
Doctor of Philosophy
(Psychology)
in the University of Michigan
2011

Doctoral Committee:

Associate Professor Thad A. Polk, Chair
Professor Patricia A. Reuter-Lorenz
Professor Henry M. Wellman
Associate Professor Kerby A. Shedden

To Mom and Dad

Acknowledgements

When I was a child, I remember saying that I would like to become a scientist when I grow up. I did not know what it is that they did exactly, but they looked so cool to me that I wanted to become just like them, discovering and inventing new things. After many years and numerous transitions, my aspirations have finally come true.

The biggest transition, of course, has been the last five years of my life, with so many accomplishments that I could not have achieved without the help of others. The biggest credit goes to my advisor Professor Thad Polk. Thad knew exactly how to train an eager but naïve student into a scientist. He knew how to push me, how to pull me, and most importantly how to *wait* for me. I cannot imagine how I could have done any of these without his academic, social, and emotional support. Certainly, what I will miss the most from my life during Ph.D. training will be my interactions with Thad.

I would like to extend my appreciation to my dissertation committee members, Professors Kerby Shedden, Patti Reuter-Lorenz, and Henry Wellman. Kerby was the greatest gift I got in the later phase of my Ph.D. training. He played an enormous role in showing me the art of statistics and helping me earn a Master's degree in Statistics. I learned a great deal from his sharp intuitions and personable

being. Having Patti on the committee was a great advantage. She was full of insights, and always raised questions that helped me see the forest for the trees. Henry exemplified what I consider excellence in teaching. He has been my role model as a scholar and teacher. He ignited my interest in cognitive development so much that I decided to step into the field.

I would also like to thank Professor Denise Park and her group at the University of Texas at Dallas for always being supportive of me. Despite the fact that I worked with her remotely, she has helped me build my career in a variety of ways. Thanks to Professor Jun Zhang for introducing me to his mathematical intuitions that provided me a whole new way of viewing both cognitive psychology and cognitive neuroscience.

My friends in Ann Arbor and colleagues involved in my research projects have been a great source of support and help. Josh Carp has been a great friend, collaborator, and intellectual stimulant. Marc Berman and I have had great times discussing science and life. Lee Newman gave me tremendous support as a senior in school and in life. Taeyong Ahn has been a great friend as well as a great gym partner. Special thanks to the Polk Lab members: Agnes Jasinska, Rebecca Rhodes, and Cheng Wang. You girls will now take over the what-used-to-be-a-completely-male lab. I also thank Andy Hebrank and Bennet Fauber for providing me the best technical support that I could ever imagine, and Mary Mohrbach and Susan Douglas for their timely administrative support all the time. I also thank Kamin Kim, Natela Shanidze, Kevin Lim, and Dr. Kyoung-Uk Lee for making our life so much more

enjoyable. Additionally, I would like to thank all the grocery stores and restaurants for providing us with good ingredients and feeding us good food.

I cannot express more gratitude to my parents and family whose love I could feel from thousands of miles away. All my accomplishments in my entire life had been based on my parents' love and care as well as my sisters' support. In particular, my mom and dad have always had trust in me. In my entire life, they were completely supportive of whatever I decided to do and never tried to plan my life for me. I now realize that such unconditional love and trust was *exactly* their way of helping me plan my life. My parents-in-law have also been a source of great support and motivation during my Ph.D. training. I am grateful for their caring.

Finally, I would like to enjoy this moment of achievement with my lovely wife Youngbin. Meeting her and marrying her was the best thing that I have *ever* done in my life. I thank her for making my life so wonderful and beautiful. With her, this past five years of Ph.D. training has been so much fun and joyful.

Table of Contents

List of Figures

List of Tables

Abstract

Visual processing of words and numbers is a uniquely human cognitive ability. Evidence suggests that a region in left occipitotemporal cortex, the so-called visual word form area (VWFA), is crucially involved in this ability, particularly in the visual recognition of words. In this dissertation, I present a methodological study and two empirical studies to investigate the role of experience in shaping the VWFA, to explore ways to estimate the amount of this experiential influence, and to examine how the neural substrates of visual number recognition are different from those of visual letter recognition.

In the first study, I develop a novel statistical method to efficiently estimate correlation between paired spatial processes, and hence heritability in patterns of activation in neuroimaging datasets. The results demonstrate that the proposed method provides a better estimate of correlation and heritability than conventional voxelwise or region of interest methods.

The second study applies this method in a monozygotic twin sample to explore the role of unique environmental effects in shaping VWFA activation. The results demonstrate that there are greater unique environmental effects for neural activity associated with familiar word recognition than with unfamiliar word recognition.

The last study investigates whether the VWFA is also the crucial site for visual number recognition or whether number recognition is neurally dissociable from word recognition. I demonstrate letter-selective activation in left occipitotemporal cortex and number-selective activation in right lateral occipital cortex, thus establishing double dissociation. Furthermore, I show that individual differences in the laterality of visual number activation can be explained by individual differences in the laterality of numerical processing activation in parietal cortex.

In sum, this dissertation investigates experiential effects on the neural substrates of visual word and number processing. In a methodological study, I present a more powerful statistical method to estimate correlation and heritability in neuroimaging datasets. The findings from the two empirical studies suggest a critical role of environment in shaping the VWFA, demonstrate a novel double dissociation between the neural substrates of letter and number recognition, and provide evidence that top-down influences give rise to the functional neural organization for visual number recognition.

Chapter 1

Introduction

1.1 The Visual Word Form Area

Research in cognitive neuroscience has identified a part of left ventral visual cortex, the so-called visual word form area (VWFA) (Cohen, et al., 2000; McCandliss, Cohen, & Dehaene, 2003), as the primary neural substrate for processing written words and letters (for review see McCandliss, et al., 2003; Price & Devlin, 2003; Schlaggar & McCandliss, 2007). Neuroimaging and electrophysiological experiments demonstrate that the middle portion of the left occipitotemporal sulcus bordering the fusiform gyrus and the inferior temporal gyrus exhibits greater neural activity when processing written words compared to control stimuli (Allison, McCarthy, Nobre, Puce, & Belger, 1994; Baker, et al., 2007; Cohen & Dehaene, 2004; Cohen, et al., 2002; Dehaene, Le Clec'H, Poline, Le Bihan, & Cohen, 2002; Hashimoto & Sakai, 2004; Nobre, Allison, & McCarthy, 1994; Pernet, Celsis, & Demonet, 2005; Polk & Farah, 2002; Polk, et al., 2002). Neuropsychological studies with focal lesion patients demonstrating selective difficulty in reading letters and words support the causal role of this area in visual word processing (Anderson, Damasio, & Damasio,

1990; Ingles & Eskes, 2008; Philipose, et al., 2007; Reuter-lorenz & Brunn, 1990; Starrfelt, 2007).

The location of the VWFA is highly consistent across individuals and across people using different languages. A meta-analysis reports that the peak of the VWFA is located at approximately [-44, -58, -15] in MNI space in the right-handed population in general and that this peak is relatively consistent across cultures with different languages (Jobard, Crivello, & Tzourio-Mazoyer, 2003).

Although some evidence shows that subregions within VWFA show activation in response to auditory and tactile stimuli, VWFA primarily responds to visual word forms, suggesting that VWFA activity is largely modality specific (Cohen, et al., 2000; Dehaene, et al., 2002). Furthermore, the activity is invariant across visual space and across visual features (Cohen, et al., 2000; Polk & Farah, 2002). These findings suggest that the VWFA is involved in processing the abstract identity of letters and letter strings in the visual modality regardless of lower-level visual features.

One prominent model for the visual processing of letters and letter-strings is the Local Combination Detector (LCD) model (Dehaene, Cohen, Sigman, & Vinckier, 2005). This model, developed based on the "open bigrams" scheme (Whitney, 2001), proposes that neural encoding of letters and letter-strings is governed by the same principles known to exist in lower-level visual cortex. According to this model, the neurobiological basis of visual word recognition is organized in a hierarchical fashion from a pool of neurons with relatively small feature-specific receptive fields to a pool of neurons with relatively large feature-invariant receptive fields. For

example, the model proposes that local combination detectors encode local orientation bars in the bilateral V1, local contours in the bilateral V2, letter shapes in the bilateral V4, bank of abstract letter forms in V8, and finally local bigrams and recurring substrings in the left occipitotemporal region (i.e. putative VWFA). In the end, this model argues that words are processed by a sparsely distributed population of neurons that encode partially redundant combinations of local features. This model thus proposes that word-selectivity in VWFA arises from fine-tuning of these local combination detector neurons to better encode more frequently encountered features (e.g. letters and letter combinations) over the course of typical development.

Many recent functional magnetic resonance imaging (fMRI) studies provide empirical support for this model. The activation in VWFA is case invariant (Polk & Farah, 2002), for example, showing little activation difference between TABLE and table. VWFA also shows a posterior to anterior gradient in letter invariance (Dehaene, et al., 2004). That is, a more posterior region of the occipitotemporal cortex is sensitive to letter identity and its retinal location, while a more anterior region is sensitive to the retinal location but not to letter identity. In other studies, VWFA exhibits hierarchical organization from posterior to anterior along orthographic regularities (Binder, Medler, Westbury, Liebenthal, & Buchanan, 2006; Vinckier, et al., 2007). That is, VWFA activity is overall smaller in response to letter strings with infrequent letter combinations and larger in response to letter strings with frequent letter combinations.

1.2 What is the Role of Experience in Shaping the VWFA?

In this dissertation, I investigate the role of experience in shaping the VWFA. Word form recognition relies on the general visual mechanism as it makes unique demands of processing fine-grain local features quickly and in parallel. Some evidence suggests that this part-based recognition system is critical in reading (Farah & Wallace, 1991). Furthermore, some recent neuroimaging studies argue that the left occipitotemporal region serves its function as a shape processing system in general as opposed to having its specific role for word form processing (Ben-Shachar, Dougherty, Deutsch, & Wandell, 2007; Price & Devlin, 2003). So perhaps the VWFA is simply a more general part-based shape processing system that may be hardwired to some extent.

Nevertheless, reading is a relatively novel ability in evolutionary history. Written words (and numbers) are relatively recent cultural inventions on an evolutionary time scale that appeared only about 5,500 years ago. It was only until very recently that the majority of humans were educated to read and write. Reading is not shared by other species and does not develop without systematic training. It is therefore unlikely that humans have evolved to read words via natural selection. Thus, it seems likely that experience plays a crucial role in shaping the neural substrates of word and number processing (Dehaene & Cohen, 2007).

Consistent with this hypothesis, developmental studies show that children who have not yet learned to read show no evidence for VWFA in the ventral visual cortex (Cantlon, Pinel, Dehaene, & Pelphrey, 2011; Maurer, Brem, Bucher, & Brandeis, 2005). Furthermore, illiterate adults show negligible VWFA activation

(Dehaene, et al., 2010), which suggests that neural specialization for words is not simply the result of maturation, but requires the experience of learning to read. Training studies also show that VWFA activation is modulated as a result of extensive experience with word forms. In particular, training on the visual word form and associated phonology of an artificial language modulate the VWFA activation in response to the artificial script (Hashimoto & Sakai, 2004; Xue, Chen, Jin, & Dong, 2006).

While these findings are informative and important in understanding the role of experience in shaping the VWFA, it is difficult to assess the relative contribution of this experiential influence. Twin studies provide a direct approach to assessing the role of genetics and environment in neural processes and representations. Using a classical twin study design, it is possible to decompose the phenotypic variance into parts that can be explained by genetic (e.g. general visual mechanisms) and environmental factors (e.g. learning to visually process letters and words). However, heritability (i.e. proportion of phenotypic variance explained by genetic effects) has traditionally been measured for univariate, scalar traits, and it is challenging to assess the heritability of a spatial process, such as a pattern of neural activity. In Chapter 2, I present a novel statistical method to estimating intraclass correlation and heritability of spatial datasets. The method involves spatial decomposition of the neuroimaging data, and spatial variation and covariation in paired images is captured by a dimensionally-reduced model. I report that this novel statistical method provides a better estimator for intraclass correlation and heritability of spatial datasets than other conventional methods.

In Chapter 3, I assess the direct contribution of unique environment in explaining the variance of VWFA activity evoked by familiar words (e.g., in one's own language) and unfamiliar words (e.g., in a foreign language or in false fonts). Previous studies have compared the response magnitudes for familiar words and unfamiliar words in an attempt to see whether experience (associated with familiar words) modulates VWFA activity. However, the results have been mixed. Some studies showed greater VWFA activation for familiar words compared to unfamiliar words (Baker, et al., 2007; Vinckier, et al., 2007), while other studies showed the opposite (Hashimoto & Sakai, 2004; Xue, et al., 2006) or no difference (Xue & Poldrack, 2007). Thus, it is difficult to assess the role of experience in VWFA when only considering the magnitude of neural activation. By studying monozygotic twins, I quantified the unique environmental effects in VWFA activity patterns evoked by familiar (words) and unfamiliar words (false fonts). I show greater environmental contributions to VWFA activity associated with word recognition than false font recognition. These results overcome limitations of previous studies that interpret data based exclusively on response magnitude, and provide more direct evidence for environmental contributions to the neural architecture of VWFA. In addition, I show that the unique environmental effects are modulated by different subcomponents of reading, including orthographic, phonological, and semantic processing. In particular, the results suggest that experience with phonological processing in particular may exert the greatest influence in shaping the VWFA. In sum, findings reported in Chapter 3 illustrate how the environment we experience

can make qualitative changes in the brain and may even induce neural specialization for a cultural convention.

1.3 How is Neural Representation of Numbers Different from Words?

While the neural representation of words has been extensively investigated in the literature, the neural representation of numbers (Arabic numerals) has received little attention despite the fact that numbers are also predominant in our daily lives. Numbers are especially interesting stimuli because, like letters, they are cultural inventions that must be learned. But they are also fundamentally different from letters in that they primarily convey meanings of quantity and order. Supporting these ideas, behavioral studies show the visual processing of numbers is qualitatively different from that of letters (Hamilton, Mirkin, & Polk, 2006; Jonides & Gleitman, 1972; Polk & Farah, 1995). Thus, it is reasonable to suspect that visual processing of letters and numbers may depend on different neural systems. So how does the neural representation of numbers differ from the neural representation of words?

To date, relatively little is known about the neural basis for visual number recognition. According to the triple-code model (Dehaene, 1992; Dehaene & Cohen, 1995), numbers are represented in three different codes: an analogue magnitude code, a verbal word frame, and a visual Arabic number form. This model proposes that the visual Arabic number form is primarily encoded in bilateral ventral visual cortex (Dehaene & Cohen, 1995). However, there has been little empirical support for this hypothesis. Neuroimaging studies show greater neural activation in

response to letters compared to numbers, showing a single dissociation for letters over numbers, in VWFA (Baker, et al., 2007; Polk, et al., 2002), but the opposite dissociation has not been shown.

In the first part of Chapter 4, I investigate the neural segregation between visual processing of letters and numbers. In this experiment, participants viewed letters and numbers while their brain activity was measured in the fMRI scanner. I show that letter recognition is dissociable from number recognition in the left occipitotemporal region replicating previous studies, and more importantly that number recognition is dissociable from letter recognition in the right lateral occipital cortex, thus establishing a double dissociation.

In the second part of Chapter 4, I investigate the role of top-down influences on this neural dissociation. In particular, what causes the neural specialization for visual number recognition? I tested whether individual differences in the neural representation for visual number recognition could be explained by individual differences in parietal activity associated with numerical processing. Here, I show that the lateralization of the ventral visual activity in response to numbers can be predicted by the lateralization of numerical processing in parietal cortex. This finding suggests that top-down influences play an important role in determining the neural organization for number recognition.

1.4 Remarks

This is a staple dissertation that consists of three independent manuscripts. The chapters therefore are written to stand on their own. However, all three

chapters share the general theme of exploring and investigating experiential effects on the neural substrates of visual word and number processing. As of now, one of the chapters (Chapter 4) is accepted for publication in the *Journal of Cognitive Neuroscience*, one chapter (Chapter 2) is under review, and the other (Chapter 3) is ready to be submitted.

1.5 References

Allison, T., McCarthy, G., Nobre, A., Puce, A., & Belger, A. (1994). Human extrastriate visual cortex and the perception of faces, words, numbers, and colors. *Cereb Cortex, 4*(5), 544-554.

Anderson, S. W., Damasio, A. R., & Damasio, H. (1990). Troubled letters but not numbers - Domain specific cognitive impairments following focal damage in frontal-cortex. *Brain, 113*, 749-766.

Baker, C. I., Liu, J., Wald, L. L., Kwong, K. K., Benner, T., & Kanwisher, N. (2007). Visual word processing and experiential origins of functional selectivity in human extrastriate cortex. *Proceedings of the National Academy of Sciences of the United States of America, 104*(21), 9087-9092.

Ben-Shachar, M., Dougherty, R. F., Deutsch, G. K., & Wandell, B. A. (2007). Differential sensitivity to words and shapes in ventral occipito-temporal cortex. *Cereb Cortex, 17*(7), 1604-1611.

Binder, J. R., Medler, D. A., Westbury, C. F., Liebenthal, E., & Buchanan, L. (2006). Tuning of the human left fusiform gyrus to sublexical orthographic structure. *Neuroimage, 33*(2), 739-748.

Cantlon, J. F., Pinel, P., Dehaene, S., & Pelphrey, K. A. (2011). Cortical representations of symbols, objects, and faces are pruned back during early childhood. *Cereb Cortex, 21*(1), 191-199.

Cohen, L., & Dehaene, S. (2004). Specialization within the ventral stream: the case for the visual word form area. [doi: DOI: 10.1016/j.neuroimage.2003.12.049]. *NeuroImage, 22*(1), 466-476.

Cohen, L., Dehaene, S., Naccache, L., Lehericy, S., Dehaene-Lambertz, G., Henaff, M. A., et al. (2000). The visual word form area - Spatial and temporal characterization of an initial stage of reading in normal subjects and posterior split-brain patients. *Brain, 123*, 291-307.

Cohen, L., Lehericy, S., Chochon, F., Lemer, C., Rivaud, S., & Dehaene, S. (2002). Language-specific tuning of visual cortex functional properties of the Visual Word Form Area. *Brain, 125*, 1054-1069.

Dehaene, S. (1992). Varieties of numerical abilities. *Cognition, 44*(1-2), 1-42.

Dehaene, S., & Cohen, L. (1995). Towards an anatomical and functional model of number processing. *Mathematical Cognition, 1*, 83-120.

Dehaene, S., & Cohen, L. (2007). Cultural recycling of cortical maps. *Neuron, 56*(2), 384-398.

Dehaene, S., Cohen, L., Sigman, M., & Vinckier, F. (2005). The neural code for written words: a proposal. *Trends in Cognitive Sciences, 9*(7), 335-341.

Dehaene, S., Jobert, A., Naccache, L., Ciuciu, P., Poline, J. B., Le Bihan, D., et al. (2004). Letter binding and invariant recognition of masked words - Behavioral and neuroimaging evidence. *Psychological Science, 15*(5), 307-313.

Dehaene, S., Le Clec'H, G., Poline, J. B., Le Bihan, D., & Cohen, L. (2002). The visual word form area: a prelexical representation of visual words in the fusiform gyrus. *Neuroreport, 13*(3), 321-325.

Dehaene, S., Pegado, F., Braga, L. W., Ventura, P., Nunes Filho, G., Jobert, A., et al. (2010). How learning to read changes the cortical networks for vision and language. *Science, 330*(6009), 1359-1364.

Farah, M. J., & Wallace, M. A. (1991). Pure alexia as a visual impairment – a reconsideration. *Cognitive Neuropsychology, 8*(3-4), 313-334.

Hamilton, J. P., Mirkin, M., & Polk, T. A. (2006). Category-level contributions to the alphanumeric category effect in visual search. *Psychonomic Bulletin & Review, 13*(6), 1074-1077.

Hashimoto, R., & Sakai, K. L. (2004). Learning Letters in Adulthood: Direct Visualization of Cortical Plasticity for Forming a New Link between Orthography and Phonology. [doi: DOI: 10.1016/S0896-6273(04)00196-5]. *Neuron, 42*(2), 311-322.

Ingles, J. L., & Eskes, G. A. (2008). A comparison of letter and digit processing in letter-by-letter reading. *Journal of the International Neuropsychological Society, 14*(1), 164-173.

Jobard, G., Crivello, F., & Tzourio-Mazoyer, N. (2003). Evaluation of the dual route theory of reading: a metanalysis of 35 neuroimaging studies. [doi: DOI: 10.1016/S1053-8119(03)00343-4]. *NeuroImage, 20*(2), 693-712.

Jonides, J., & Gleitman, H. (1972). Conceptual category effect in visual search - O as letter or as digit. *Perception & Psychophysics, 12*(6), 457-460.

Maurer, U., Brem, S., Bucher, K., & Brandeis, D. (2005). Emerging neurophysiological specialization for letter strings. *J Cogn Neurosci, 17*(10), 1532-1552.

McCandliss, B. D., Cohen, L., & Dehaene, S. (2003). The visual word form area: expertise for reading in the fusiform gyrus. *Trends in Cognitive Sciences, 7*(7), 293-299.

Nobre, A. C., Allison, T., & McCarthy, G. (1994). Word recognition in the human inferior temporal-lobe. *Nature, 372*(6503), 260-263.

Pernet, C., Celsis, P., & Demonet, J. F. (2005). Selective response to letter categorization within the left fusiform gyrus. *Neuroimage, 28*(3), 738-744.

Philipose, L. E., Gottesman, R. F., Newhart, M., Kleinman, J. T., Herskovits, E. H., Pawlak, M. A., et al. (2007). Neural regions essential for reading and spelling of words and pseudowords. *Annals of Neurology, 62*(5), 481-492.

Polk, T. A., & Farah, M. J. (1995). Brain localization for arbitrary stimulus categories: A simple account based on Hebbian learning. *Proceedings of the National Academy of Sciences of the United States of America, 92*(26), 12370-12373.

Polk, T. A., & Farah, M. L. (2002). Functional MRI evidence for an abstract, not perceptual, word-form area. *Journal of Experimental Psychology-General, 131*(1), 65-72.

Polk, T. A., Stallcup, M., Aguirre, G. K., Alsop, D. C., D'Esposito, M., Detre, J. A., et al. (2002). Neural specialization for letter recognition. *Journal of Cognitive Neuroscience, 14*(2), 145-159.

Price, C. J., & Devlin, J. T. (2003). The myth of the visual word form area. *Neuroimage, 19*(3), 473-481.

Reuter-lorenz, P. A., & Brunn, J. L. (1990). A prelexical basis for letter-by-letter reading: A case study. *Cognitive Neuropsychology, 7*(1), 1 - 20.

Schlaggar, B. L., & McCandliss, B. D. (2007). Development of neural systems for reading. *Annual Review of Neuroscience, 30*, 475-503.
Starrfelt, R. (2007). Selective alexia and agraphia sparing numbers-a case study. *Brain Lang, 102*(1), 52-63.
Vinckier, F., Dehaene, S., Jobert, A., Dubus, J. P., Sigman, M., & Cohen, L. (2007). Hierarchical coding of letter strings in the ventral stream: Dissecting the inner organization of the visual word-form system. *Neuron, 55*(1), 143-156.
Whitney, C. (2001). How the brain encodes the order of letters in a printed word: The SERIOL model and selective literature review. [Review]. *Psychonomic Bulletin & Review, 8*(2), 221-243.
Xue, G., Chen, C., Jin, Z., & Dong, Q. (2006). Language experience shapes fusiform activation when processing a logographic artificial language: an fMRI training study. *Neuroimage, 31*(3), 1315-1326.
Xue, G., & Poldrack, R. A. (2007). The neural substrates of visual perceptual learning of words: implications for the visual word form area hypothesis. *J Cogn Neurosci, 19*(10), 1643-1655.

Chapter 2

Correlation and heritability in neuroimaging datasets: A spatial decomposition approach with application to an fMRI study of twins

2.1 Introduction

In a classical twin study, the heritability of a trait is assessed by estimating genetic and phenotypic variation based on the similarity (i.e. intraclass correlation) of monozygotic (MZ) and dizygotic (DZ) twins. Conventionally, heritability is measured for univariate, scalar traits (e.g. IQ, body mass index, etc.); however, there are cases where the trait may be defined by a spatial process (e.g. a pattern of neural activation estimated from neuroimaging studies). For example, a number of neuroimaging studies have studied twins in order to investigate the heritability of brain structure and function (see Blokland, et al., 2008; Brun, et al., 2009; Cote, et al., 2007; Jahanshad, et al., 2010; Koten, et al., 2009; Lee, et al., 2010; Matthews, et al., 2007; Polk, Park, Smith, & Park, 2007; Schmitt, et al., 2009; Thompson, et al., 2001). These studies make structural measurements and/or estimate neural activation at tens of thousands of data points. Even if the researcher restricts the focus of investigation to a smaller region of interest (ROI), these regions still often include hundreds or thousands of voxels. So how we can assess the heritability of a measure that is multivariate and spatial in nature?

One straightforward way is to estimate heritability at each voxel (or vertex) separately. In this approach, images from all twins are first normalized into a standard space. Then, genetic modeling is performed using the classical twin design at each voxel, which provides a measure of heritability at every voxel across the entire brain. This "voxelwise" approach has been used in many studies investigating heritability in structural neuroimaging data (e.g. Thompson, et al., 2001). Since the voxelwise approach ignores the spatial relationships among voxels, it does not make the most efficient use of the information in the data. With relatively high signal-to-noise ratio and reliability in high-resolution anatomical images, the voxelwise approach may maintain adequate power for some structural neuroimaging studies. But the voxelwise approach becomes more troublesome in functional neuroimaging studies in which the data typically have much lower signal-to-noise ratio at the voxel level (Huettel, Song, & Gregory, 2004), which may result in highly variable estimates, particularly with smaller sample size.

One way to account for the noisy nature of functional neuroimaging data is to restrict heritability estimation to a smaller region of interest (ROI). Except for one study using an extended twin design that maximizes power to detect heritability (Koten, et al., 2009), most functional neuroimaging twin studies have adopted the "mean-ROI" approach, in which heritability estimation is based on mean intensity values across voxels within an ROI (Blokland, et al., 2008; Cote, et al., 2007; Matthews, et al., 2007). The mean-ROI approach estimates the heritability of a function of the data (i.e. spatial average) and allows traditional heritability estimation schemes for scalar-valued traits to be applied in an imaging study. If the

ROI is functionally homogeneous, averaging intensity values within the ROI increases the signal-to-noise ratio. However, if there are inherent spatial correlations and inhomogeneity within the ROI (which is likely), this approach may result in a significant loss of power (Friston, Rotshtein, Geng, Sterzer, & Henson, 2006). For example, if only a subregion of the ROI shows heritable activation, this mean-ROI approach would show an intermediate level of heritability at a constant level throughout the ROI. Furthermore, recent fMRI studies have demonstrated that multivariate spatial patterns can contain unique information over and above univariate intensity values (Haynes & Rees, 2006; Norman, Polyn, Detre, & Haxby, 2006).

Finally, it is possible to assess genetic influences on a spatially measured trait using statistical association measures that are not directly related to heritability. For example, Polk and colleagues (2007) considered the correlation across voxels within each twin pair, and compared the averages of these correlations for MZ and DZ twin pairs. This provides a quantitative assessment of familiality using a familiar and stable statistical approach, but does not provide estimates of genetic heritability.

In the present work, we develop a statistical method for heritability estimation in functional neuroimaging studies of twins that addresses the main limitation of the mean-ROI method as well as the voxelwise method. The proposed method estimates correlation for MZ and for DZ twin pairs at each position in an ROI (or the whole brain), which in turn are used to estimate heritability. The method for estimating the correlation values is based on a statistical model in which the

variation in the measured trait at each spatial position is viewed as arising from a linear combination of spatial basis volumes. In a simulation study, we report the feasibility of this "spatial decomposition" method and explore its relative advantages compared to the conventional mean-ROI method and the voxelwise method. The relative advantage of the proposed method is also examined in a real fMRI study of a simple visuomotor task. We first assess the role of genetics in the functional neural architecture by comparing the intraclass correlation (ICC) of activation maps from MZ and DZ pairs. We then utilize the proposed spatial decomposition method to estimate the heritability of neural patterns in the visual and motor cortices by incorporating the structural equation model (SEM) approach to estimating heritability (Neale, 1998, 2003).

2.2 Statistical Method

2.2.1 Overall description

The spatial data Y for each individual is modeled as a linear combination of basis volumes X_p, scaled by unobserved random coefficients β_p. The X_p's represent underlying spatial patterns for the given phenotypic trait. The β_p's have unknown mean and variance, and unknown covariance between individuals in a twin pair, but are independent between twin pairs. The goal is to use the model to estimate these variance and covariance parameters, which in turn determine the correlation (or ICC[1]) at each spatial point. As demonstrated below, these parameters can be

[1] See Section 2.6 Appendix for the working definition of intraclass correlation.

estimated using fixed effects regression (i.e. ordinary least-squares regression), followed by some additional processing of the fitted regression parameters to account for uncertainty in the fixed effects estimates.

2.2.2 Model

Let Y_{ij} represent spatial data from a given ROI (possibly the whole brain) from the jth twin in the ith pair (i=1… n, j=1,2). For instance, Y_{ij} can be a vectorized representation of three-dimensional volumetric fMRI data (e.g. contrast maps, percent signal change maps, or t-maps) as a vector of v elements where v is the size of the ROI. Conditioning on the β_p's, the data Y_{i1} and Y_{i2} for a single twin pair is then modeled as a linear combination of a number of basis volumes X_p as follows:

$$\begin{pmatrix} Y_{i1} \\ Y_{i2} \end{pmatrix} = \begin{pmatrix} X_0, X_1 \ldots X_P & 0 \\ 0 & X_0, X_1 \ldots X_P \end{pmatrix} \cdot \begin{pmatrix} \beta_{0i1} \\ \vdots \\ \beta_{Pi1} \\ \beta_{0i2} \\ \vdots \\ \beta_{Pi2} \end{pmatrix} + \varepsilon . \qquad (1)$$

In this paper, particularly in the subsequent real data study, the basis volumes X_p were constructed from the neural activation patterns of an independent group of subjects performing the same task. The eigenvectors obtained from a singular value decomposition of these data were used as the basis volumes[2]. This serves to focus the heritability analyses on the more variable spatial components in the data. The coefficients, β_{pij}, are viewed as random variables with unknown mean

[2] X_0 is an intercept volume that is created to be orthogonal to the rest of the basis volumes.

and variance. The residual, ε, is viewed as centered errors uncorrelated across the voxels with constant variance across voxels.

2.2.3 Correlation Estimation

Using the model, we now estimate the voxel-level variance of Y_{ij}, $var(Y_{\bullet j})$, and the voxel-level covariance between Y_{i1} and Y_{i2}, $cov(Y_{\bullet 1}, Y_{\bullet 2})$. That is, $var(Y_{\bullet j})$ and $cov(Y_{\bullet 1}, Y_{\bullet 2})$ are both vectors, with as many elements as there are voxels in the ROI. We note that in the conventional voxelwise approach, these variance and covariance values are estimated directly using the usual sample variance and covariance estimators at each voxel separately. We also note that in the conventional mean-ROI approach, the mean Y_{ij} across the entire ROI is first computed, after which variance and covariance of the mean values are estimated. Our aim here is to use the regression model to improve the precision of these estimates, by borrowing information within spatial regions.

The first step is to use ordinary least squares, applied separately to each twin pair, to predict the β_{pij} values. The model-implied variance, $var(Y_{\bullet j})$, and covariance, $cov(Y_{\bullet 1}, Y_{\bullet 2})$, can then be estimated as follows:

$$\hat{\mathrm{var}}\left(Y_{\bullet j}\right) = \sum_p X_p^2 \,\hat{\mathrm{var}}\left(\beta_{p\bullet j}\right) + \sigma^2 \qquad (2)$$

$$\hat{\mathrm{cov}}\left(Y_{\bullet 1}, Y_{\bullet 2}\right) = \sum_p X_p^2 \,\hat{\mathrm{cov}}\left(\beta_{p\bullet 1}, \beta_{p\bullet 2}\right), \qquad (3)$$

where X_p^2 represents element-wise squares. Here, $\hat{\mathrm{var}}\left(\beta_{p\bullet j}\right)$ and $\hat{\mathrm{cov}}\left(\beta_{p\bullet 1}, \beta_{p\bullet 2}\right)$ are bias corrected versions of the standard empirical variance and the empirical covariance, respectively (see Section 2.6 Appendix). The residual variance (σ^2) can

be estimated from the mean of the error variance across all voxels. The covariance of residuals between pairs is assumed to be zero, and is therefore omitted in Equation 3.

As correlation is defined by the ratio of covariance and variance, the correlation of two spatial patterns can then be estimated by performing element-wise divisions as follows:

$$corr\left(Y_{\bullet 1}, Y_{\bullet 2}\right) = \frac{\hat{\mathrm{cov}}\left(Y_{\bullet 1}, Y_{\bullet 2}\right)}{\sqrt{\hat{\mathrm{var}}\left(Y_{\bullet 1}\right) \times \hat{\mathrm{var}}\left(Y_{\bullet 2}\right)}}. \quad (4)$$

2.2.4 Genetic Effects and Heritability Estimation

A classical twin study asserts that the variance of a phenotype can be decomposed into additive genetics, common environment, and unique environment with twins that are reared together (Falconer & Mackay, 1996). The comparison between the ICC of MZ pairs and of DZ pairs provides a quick and easy way to assess genetic effects on the phenotypic trait. Since MZ pairs share all of their alleles while DZ twins share 50% on average, phenotypic covariance for MZ twins should be more similar than that of DZ twins if genes account for variation between individuals.

While the comparison between the ICC of MZ twins and DZ twins can be a useful tool to examine the genetic influence in the phenotypic trait, modern covariance modeling methods provide a quantitative estimate of heritability (Christian, Norton, Sorbel, & Williams, 1995; Neale, 2003). As described above, the variance $var(Y_{\bullet j})$ and the sibling covariance $cov(Y_{\bullet 1}, Y_{\bullet 2})$ can be estimated using the spatial decomposition approach. These values can then be fed into a maximum-

likelihood model-fitting algorithm using structural equation modeling (SEM) implemented in Mx (Neale, Boker, Xie, & Maes, 2003) in order to estimate genetic and environmental components of phenotypic variance.

2.3 Simulation Study

2.3.1 Methods

A simulation study was conducted in order to evaluate the model-based point estimates of the correlation parameters in terms of bias, variance, and mean squared error. Patterns of neural activation (Y_{ij}) were simulated in a 3-D space of 512 (8×8×8) voxels from pairs (n = 10, 20, 40) of data as in Equation 1. The set of basis volumes ($X_0 \ldots X_P$) was derived from the eigenvectors of the covariance matrix of the entire voxel space. A rational quadratic covariance function with both parameters equal to 1 was used to determine the spatial structure of the simulated trait data. In this simulation study, we wanted to examine in particular the effect of underspecification (i.e. a model with fewer basis volumes than what was used to construct the full data) and overspecification (i.e. a model with more basis volumes than what was used to construct the full data). Therefore, we arbitrarily decided to use the first 32 eigenvectors of the covariance matrix as the spatial structure of the trait values.

The coefficients for each these 32 basis volumes, β_{pij}, are drawn randomly from a bivariate normal distribution. The mean of this bivariate normal distribution was 0, and the variance was set in a monotonically decreasing order to mimic real

data[3]. The covariance of this bivariate random distribution was manipulated so that the correlation was fixed at r. Various levels of correlation between 0 and 1 were considered in order to examine the effect of similarity between pairs on the point estimates. The errors (ε) were drawn from a normal distribution with mean of zero and standard deviation of σ, which was set at various values between 0 and 1.

For each case in the parameter space, simulated data were generated 500 times and the correlation was estimated for each sample using three different methods. Firstly, the correlation was estimated using the proposed spatial decomposition method. Here, five different types of models were used to estimate the correlation. Note that the simulated data were generated based on 32 basis volumes. In five different models, the first 4, the first 8, the first 16, the first 32, and the first 64 (i.e. including all the basis volumes used in the simulated data but also 32 more basis volumes from the initial set of eigenvectors) were used, respectively, to estimate the correlation. In the first three cases, the model is underspecified in terms of the basis volumes, and in the last case, the model is overspecified. Secondly, the correlation was estimated using the conventional voxelwise method. Thirdly, the correlation was estimated using the mean-ROI approach, in which mean values of the entire voxel space for pairs were correlated.

In all three of these methods, the mean root squared error (RMSE), root integrated squared bias (RISB), and integrated variance (IVAR) were computed by comparing the simulated results and the voxel-level true correlation. Given the

[3] That is, the variance of the coefficients associated with pth basis volume was exponentially decreasing defined as $\exp(33-p) / \exp(32) \times 3{,}000$, where $p = 1, 2, \ldots 32$.

parameters r and σ and the basis volumes that went into simulating the data, the true voxel-level correlation at each voxel can be computed from Equation 4. Then, RMSE between the estimated correlation and the true correlation was computed at every repetition, and the mean RMSE over 500 repetitions was computed. The variance of the correlation estimates over 500 repetitions at each voxel was also computed, and the integrated variance (IVAR) was measured by computing the mean of these variance measures across all voxels. Likewise, the mean of the correlation estimates over 500 repetitions was compared with the true correlation, which resulted in root integrated squared bias (RISB).

2.3.2 Results

Figure 2-1 illustrates RMSE, IVAR, and RISB of the correlation estimates from three different methods simulating data from 20 pairs[4]. Similar RMSE values were observed among the results from the five different model-fitting approaches in the spatial decomposition method. However, a closer look at RISB revealed some systematic patterns in underspecified (P=4, 8, or 16) models. That is, RISB increased (particularly when r was high) as the model was more underspecified, although this reduced RISB was not visually observable after P=8. There were no visually observable effects of overspecification at least in this parameter space. In general, RISB remained low in the entire parameter space, which indicates that the bias introduced when estimating the ratio between two unbiased estimates (the

[4] See Figure 2-7 for results with 10 and 40 pairs.

numerator and denominator of Equation 4) is small in the setting of this simulation study (see Stuart & Ord, 2009).

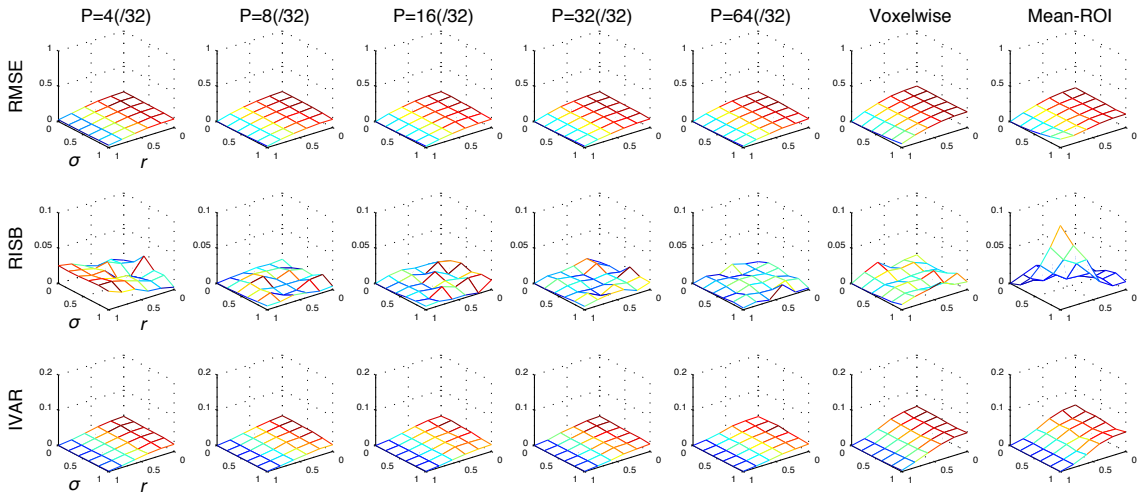

Figure 2-1 Results of the simulation study using the proposed spatial decomposition method (columns 1-5), the voxelwise method (column 6), and the mean-ROI method (column 7) with 20 pairs. Patterns of neural activation for twin pairs were simulated with 32 basis volumes while varying the degree of correlation between pairs (r) and the error variability (σ). The estimated correlation was compared with the true correlation, and root mean squared error (RMSE), root integrated squared bias (RISB), and integrated variance (IVAR) were computed over the parameter space. In the case of the spatial decomposition method, the correlation was estimated using a subset of basis volumes (4, 8, or 16, as represented in the first three columns), all 32 basis volumes (represented in the fourth column), and 64 basis volumes (represented in the fifth column).

The results from the voxelwise method and the mean-ROI method demonstrate that RMSE from these two methods is larger than RMSE from the spatial decomposition method. This increase was driven by larger RISB and IVAR in both methods compared to the spatial decomposition method (except in the cases when the model was extremely underspecified). There was a slight advantage of reduced IVAR in the mean-ROI method (average IVAR across the parameter space was 0.0294) compared to the voxelwise method (average IVAR was 0.0300). The

mean-ROI approach resulted in much greater RISB than the voxelwise method (particularly when σ and r were high).[5]

2.4 Real Data Study

2.4.1 Method

Participants

Thirteen pairs of right-handed MZ twins (nine female pairs, four male pairs, ages 18-29 with a mean age of 21.3) and eleven pairs of DZ twins (seven female pairs, four male pairs, ages 18-23, mean age 19.9) reared together participated in the study. Zygosity was determined by comparing seven to eight highly variable DNA markers (D5S818, D13S317, D7S820, D16S539, vWA, TH01, TPOX, CSF1PO) from the buccal cells of twins collected by swabbing the cheek of each participant. DNA was amplified using the polymerase chain reaction technique. Twins in whom all the markers matched were classified as monozygotic and twins in whom some markers mismatched were classified as dizygotic. Additionally, data from an independent group of nineteen subjects (12 females, ages 18-23, mean age of 19.9) were collected.

Experimental Procedure and Data Acquisition

During a functional MRI session, participants performed a simple visuomotor task. Participants were instructed to fixate on the "+" at the center of the screen.

[5] See Figure 2-8 for a discussion about the bias in the mean-ROI method.

Every 16 seconds, a circular checkerboard flickered at the rate of 8 Hz at the center of the screen for 2 seconds, and the participants were asked to press a button once with the right index finger as soon as they saw the flickering checkerboard. This session lasted for five minutes.

High-resolution T1-weighted anatomical images were collected in a GE 3T scanner using spoiled-gradient-recalled acquisition (SPGR) in axial slices parallel to the AC/PC line with a resolution of 0.9375×0.9375×5.0 mm. Neural activity was estimated based on the blood-oxygen level dependent (BOLD) signal using a spiral acquisition sequence with the following parameters: TR = 2000 ms, TE = 30 ms, flip angle = 90°, slice thickness = 5 mm, in-plane resolution = 3.75×3.75 mm, number of slices = 30, and field of view = 24cm.

Preprocessing and Data Modeling

The functional images for each participant underwent reconstruction, slice timing correction, and realignment as part of preprocessing. The high-resolution anatomical image for each participant was coregistered to the mean of all functional images. Then, the anatomical image was segmented using SPM8 (Wellcome Department of Cognitive Neurology, London) to separate gray and white matter voxels using the International Consortium of Brain Mapping (ICBM) tissue probability maps, and affine normalization parameters were calculated from those maps in standard MNI space. The functional images for each individual were then normalized to the template space with a resolution of 3×3×3 mm and spatially smoothed with a Gaussian kernel of 8×8×8mm.

We followed a conventional voxel-by-voxel approach for reducing the temporal data to a single activation map. For each participant, a general linear model (GLM) corrected for temporal autocorrelation (using an AR(1) model) with regressors corresponding to the experimental condition (i.e. presentation of the flickering checkerboard) using SPM8. The resulting parameter estimates of the GLM, henceforth referred to as the activation maps, were used in further analyses.

Regions of Interest

The regions of interest (ROIs) were defined in the left visual cortex, right visual cortex, and the left motor cortex. The left and right visual cortices were constructed as the union of the calcarine sulcus, lingual gyrus, and cuneus separately in the left and the right hemisphere using the PickAtlas AAL software toolbox (Maldjian, Laurienti, Kraft, & Burdette, 2003; Tzourio-Mazoyer, et al., 2002). The left motor cortex was constructed as the pre-central gyrus from the same toolbox. These three masks were resliced to match the voxel space of the functional data. This procedure resulted in a mask with 783 voxels in the left visual cortex, 913 voxels in the right visual cortex, and 428 voxels in the left motor cortex.

Intraclass Correlation Differences

The brain activation maps within the left and the right visual cortex from an independent group of nineteen subjects were mean-centered and underwent singular value decomposition which resulted in nineteen eigenvectors. These eigenvectors served as the basis volumes of the given neural pattern elicited by the

visuomotor task within the two masks. Then, the brain activation maps from twin participants were entered into the proposed model (Eq. 1) separately for MZ twin pairs and DZ twin pairs. After fixed effects regression and a bias correction procedure (see Statistical Model), the variances and covariances of the β values were estimated (see Equation 2 and 3) from which the ICC for each twin group was estimated[6]. The estimated error standard deviation, σ, was 0.686 (left visual), 0.823 (right visual), and 0.435 (left motor) in MZ pairs and 0.547 (left visual), 0.606 (right visual), and 0.393 (left motor) in DZ pairs.

There were no significant effects of age (β = 0.0591, p=0.429 in the left visual cortex; β = 0.0246, p = 0.783 in the right visual cortex; β = 0.0883, p = 0.073 in the left motor cortex) or sex (β = 0.4200, p = 0.278 in the left visual cortex; β = 0.2668, p = 0.566 in the right visual cortex; β = 0.2144, p = 0.410 in the left motor cortex) on the mean activation values across all subjects, and therefore the activation maps were not adjusted for age or sex when estimating ICC.

ICC maps of MZ and DZ pairs[7] were then compared by taking the difference between the two, $ICC_{MZ} - ICC_{DZ}$. If there is genetic influence on the neural activation pattern, then the difference map should be positive. Regions with positive differences were identified, and the statistical significance of the cluster size was computed based on a clusterwise correction for multiple comparisons (Holmes, Blair, Watson, & Ford, 1996; Nichols & Holmes, 2002). To be specific, a simulation was used to derive the distribution of the maximum cluster size under the null

[6] ICC is truncated at zero if negative.
[7] See Supplementary Figure 2-9 and Figure 2-10 for ICC maps of MZ and DZ pairs computed using the spatial decomposition method.

hypothesis. The null distribution, under the assumption that there is no difference between the ICC_{MZ} and ICC_{DZ}, was constructed by permuting the zygosity label of each twin pair (Chiang, et al., 2008). First, a heritability map was derived from many repetitions (10,000) while permuting the zygosity. At each repetition, clusters of heritable regions were defined by contiguous voxels exceeding a certain magnitude threshold (i.e. the top 95 percentile value). The volume of the largest cluster defined at this magnitude threshold level was recorded after each repetition, and these measures served as the null distribution of the size of the cluster at a given threshold.

Heritability

Heritability of the neural activation pattern was estimated using a maximum-likelihood model fitting approach via SEM (using the Mx software). Variance maps (Eq. 2) and covariance maps (Eq. 3) were constructed[8] from twins separately for MZ and DZ pairs using the proposed spatial decomposition method. The variance and covariance measures at each voxel were fit to a univariate AE model to estimate additive genetic (A) and unique environmental (E) contributions to the variation in the neural activation pattern (see Voxelwise Method below for the motivation for an AE model). Heritability (h^2) was defined as the proportion of variance from all components (additive genetics and unique environmental, A+E) that was explained by additive genetics (A) alone. As in the case of identifying regions showing greater

[8] Conventional variance and covariance were used with appropriate bias correction instead of the covariance and variance formula used in Fisher's ICC.

ICC_{MZ} than ICC_{DZ} within the bilateral visual cortex, clusterwise correction for multiple comparisons incorporating permutation (1,000) was used to assess significantly heritable regions within the visual cortex.

Voxelwise Method

ICC difference and heritability was also estimated using the conventional voxelwise method. More specifically, ICC was computed at each voxel separately for MZ twin pairs and DZ twin pairs[9], and the difference between the resulting ICC maps was computed. For the voxelwise estimation of heritability, variance and covariance measures were computed at each voxel, then heritability was estimated at each voxel initially using the ACE model in Mx. The ACE model, however, returned negligible estimation of common environmental effect in many of the voxels (73.6% of the voxels in the left visual ROI, 71.3% of the voxels in the right visual ROI, and 64.0% of the voxels in the left motor ROI). In addition, the observation of the ICC_{MZ} and ICC_{DZ} maps revealed that ICC_{DZ} was less than half of ICC_{MZ} in the majority of voxels. Thus, an AE model was fit for parsimony. As in the case of the spatial decomposition method, statistical inference on the ICC difference and heritability was made using a clusterwise correction for multiple comparisons.

Mean-ROI Method

[9] See Supplementary Figure 2-11 and Figure 2-12 for ICC maps of MZ and DZ pairs computed using the voxelwise method.

Lastly, ICC difference and heritability were estimated using the conventional mean-ROI method. Neural activity values were averaged across all the voxels within each ROI, and these summary measures were used in the subsequent ICC and heritability estimation. As in the other methods, an AE model was used for heritability estimation, and the statistical significance of the estimates was assessed using the permutation method.

Residual Diagnostics

The model (Eq. 1) assumes that the errors are spatially unstructured, or at least contain no covarying information between pairs. In practice, however, it is possible that some spatially defined covarying information is not fully captured by the given basis volumes. This is particularly likely when the model is underspecified as shown in the simulation study. In the data from the real study, we empirically tested how much covarying information was left in the errors. Residual maps for individual twins were constructed. Then the intraclass correlation of the residual values between twins across pairs was computed at each voxel. If there is no covarying information left in the errors, we should expect negligible correlation across all voxels on average.

The mean residual correlation (± standard deviation) across all thirteen MZ pairs was 0.2377 (± 0.3013) in the left visual cortex, 0.1151 (± 0.3033) in the right visual cortex, and 0.1510 (± 0.2628) in the left motor cortex. The mean residual correlation across all eleven DZ pairs was -0.0421 (± 0.2960) in the left visual cortex, -0.0734 (± 0.2780) in the right visual cortex, and 0.0523 (± 0.3028) in the left

motor cortex. Slightly positive residual correlation on average in MZ pairs indicates that some covarying information may not have been captured by the given basis volumes. This is empirically plausible since the basis set from nineteen singleton participants might not contain enough spatial structure to capture all possible similarity between siblings. Ideally, the basis volumes should be created from a larger sample. Not being able to capture a small amount of covariance structure in MZ pairs results in underestimation of the covariance for MZ pairs. Any significant effects of genetics are therefore still significant; but the analysis becomes somewhat conservative in assessing heritability.

2.4.2 Results

We first examined the activation and variability measures within the bilateral visual cortex separately in the twins and in the independent group of subjects. The group-level activation map constructed from a univariate one-sample t-test across twins was moderately correlated with the group-level activation map constructed from an independent group of nineteen subjects in all ROI's (r = 0.519 in the left visual cortex, r = 0.561 in the right visual cortex, and r = 0.507 in the left motor cortex) (Fig. 2). The variability map constructed from a univariate standard deviation measures across twins was also highly correlated with the variability map constructed from an independent group of nineteen subjects in all ROI's (r = 0.793 in the left visual cortex, r = 0.784 in the right visual cortex, and r = 0.763 in the left motor cortex) (Figure 2-2). High similarity between the activation and variability maps from these two groups of subjects suggests that the activation maps from the

singleton subjects can be used as a representative sample of the population of interest.

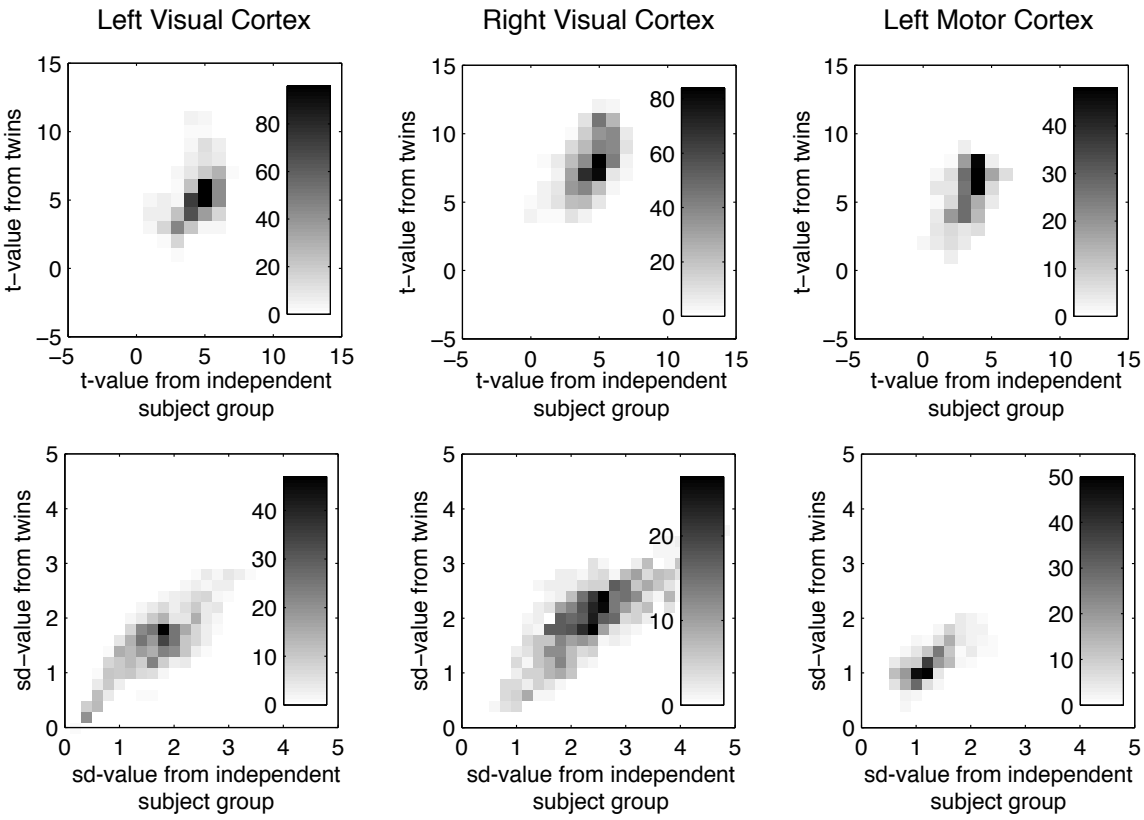

Figure 2-2 Density plots for the activation map and variability map computed from two groups of subjects. Group-level one-sample t-maps and standard deviation (sd) maps were constructed from twins in the left and right visual cortex and the left motor cortex. These maps were then compared against the t-maps and sd-maps from the independent group of subjects. The plots indicate the number of voxels that exhibited a specific statistical value in both groups of subjects.

Intraclass Correlation Differences

We then examined genetic influences on neural activity in the left and right visual cortex as well as the left motor cortex using the proposed spatial decomposition method, the voxelwise method, and the mean-ROI method. In the spatial decomposition method, ICC's for MZ and DZ pairs were estimated first by

estimating volume coefficients in the model (Eq. 1) and then by transforming the variance and covariance of these coefficients in the basis space onto the voxel space (Eq. 2 to 4). Table 1 summarizes results from these three methods. Figure 2-3 shows the ICC difference map computed using the spatial decomposition method and the voxelwise method displaying suprathreshold clusters that exceed clusterwise correction for multiple comparisons. The spatial decomposition approach identified two suprathreshold clusters in the left visual cortex one suprathreshold cluster in the right visual cortex, and one suprathreshold cluster in the left motor cortex (red clusters in Figure 2-3). All three clusters were statistically significant in terms of cluster size (see Table 2-1).

Table 2-1 Cluster analysis of the ICC difference map estimated from the spatial decomposition method and the voxelwise method, and mean ICC difference value from the mean-ROI method.

ROI	Method	Magnitude threshold (95 percentile)	Cluster threshold ($p < 0.05$)	Cluster sizes (p-values)	Mean ICC Difference (p-value)
Left Visual Cortex	Spatial Decomposition	0.6206	0 voxels	36 voxels (p=0.0020) 4 voxels (p=0.0055)	-
	Voxelwise	0.7998	3 voxels	23 voxels (p=0.0023) 4 voxels (p=0.0329) 6 voxels (p=0.0223) 7 voxels (p=0.0190)	-
	Mean-ROI	-	-	-	0.7264 (p=0.0016),
Right Visual	Spatial Decomposition	0.5763	0 voxels	46 (p=0.0183)	-

Cortex					
	Voxelwise	0.7235	28 voxels	1 voxel (p=0.3155) 18 voxels (p=0.0792) 1 voxel (p=0.3155) 26 voxels (p=0.0536)	-
	Mean-ROI	-	-	-	0.5808 (p=0.0513),
Left Motor Cortex	Spatial Decomposition	0.7457	0 voxels	22 (p=0.0022)	-
	Voxelwise	0.8467	2 voxels	22 (p=0.0021)	-
	Mean-ROI	-	-	-	0.8446 (p=0.0149)

The conventional voxelwise method identified four suprathreshold clusters in the left visual cortex and one suprathreshold cluster in the left motor, all of which were statistically significant in terms of cluster size (blue clusters in Figure 2-3). However, it failed to find any clusters in the right visual cortex that reached statistical significance in cluster size at the alpha level of 0.05 (Table 2-1).[10] The range of the voxelwise ICC difference measures was also more variable than the results from the spatial decomposition method in both hemispheres (Figure 2-4). The correlation across voxels between the results from the spatial decomposition method and the voxelwise method was 0.7068 in the left visual cortex, 0.5714 in the right visual cortex, and 0.6613 in the left motor cortex (Figure 2-4).

[10] Examination of cluster size significance was also performed using varying magnitude threshold. In general, clusters identified from the spatial decomposition method showed greater statistical significance than clusters identified from the voxelwise method. See Supplementary Figure 2-13 for further details.

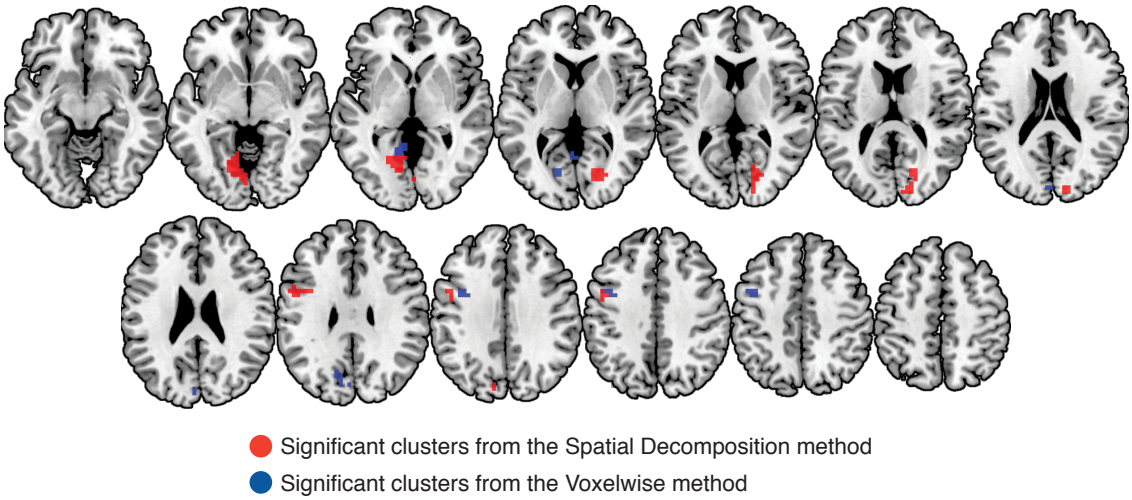

Figure 2-3 Map of ICC difference estimated from the spatial decomposition (red) and the voxelwise (blue) methods. Only statistically significant clusters ($p < 0.05$ using clusterwise correction for multiple comparisons incorporating permutation with a magnitude threshold of 95 percentile) are overlaid on a canonical brain in MNI space with axial slices from $z = -10$ to $z = 50$ in increments of 5 mm. The left hemisphere appears on the left for all brain images.

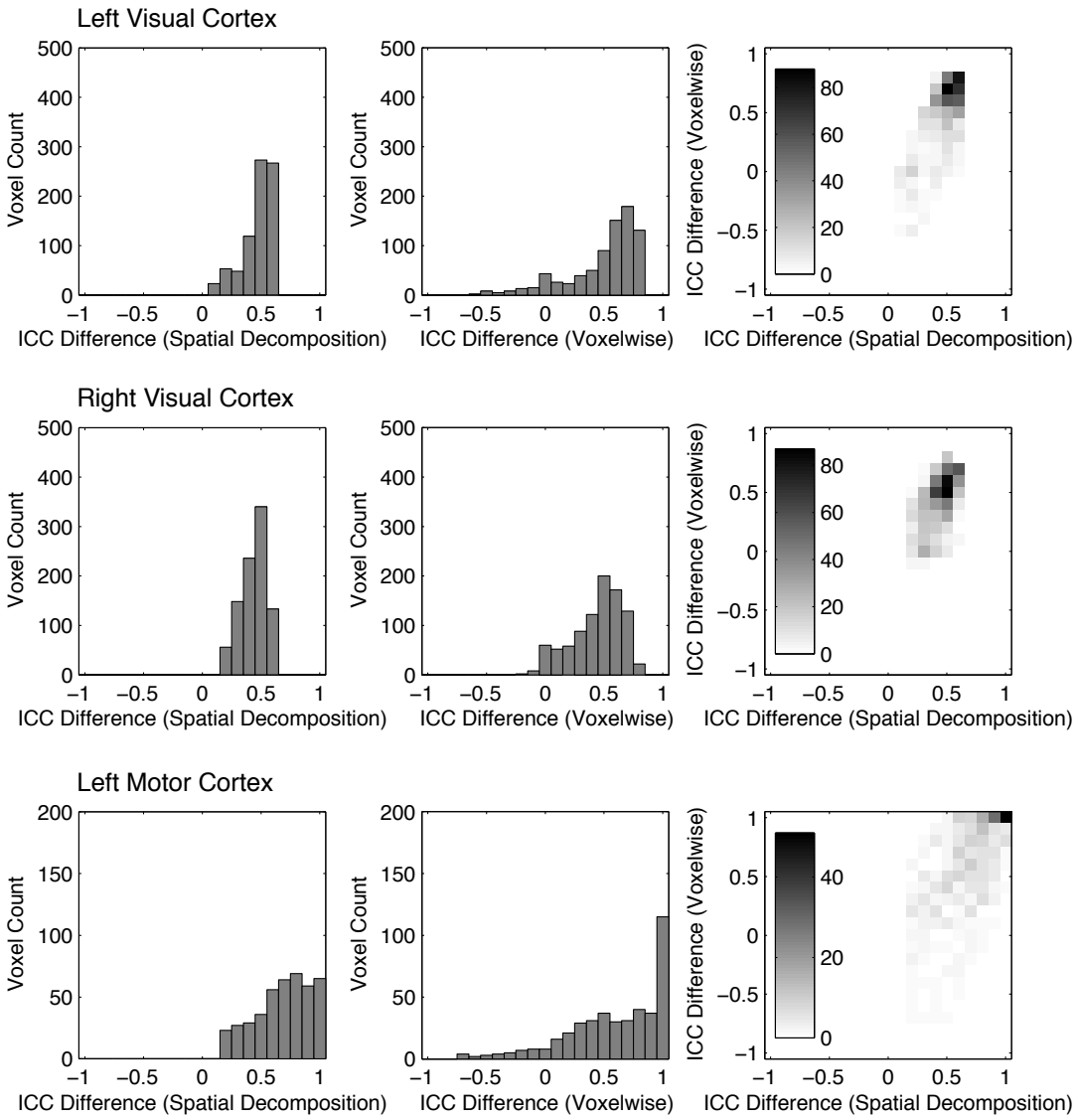

Figure 2-4 Histograms of ICC difference in the left and right visual cortex estimated from the spatial decomposition method and the voxelwise method, as well as the joint histogram of ICC difference estimates between the two methods across the whole brain.

The mean-ROI method found a significant difference between MZ ICC and DZ ICC in the left visual cortex ($p = 0.0016$) and the left motor cortex ($p = 0.0149$) overall (Table 2-1). In the right visual cortex, the difference just failed to reach significance ($p = 0.0513$).

Heritability

Using the maximum-likelihood model fitting method implemented in Mx, heritability of the neural activity was estimated using three different methods. Table 2 summarizes results from the spatial decomposition method, the voxelwise method, and the mean-ROI method. Figure 2-5 shows the heritability map computed using the spatial decomposition method displaying suprathreshold clusters that exceed clusterwise correction for multiple comparisons. As in the case of the ICC difference measure, two suprathreshold clusters were identified in the left visual cortex, one of which was statistically significant in terms of cluster size. Additionally, one suprathreshold cluster in the left motor cortex was statistically significant in terms of cluster size.

Table 2-2 Cluster analysis of the heritability map estimated from the spatial decomposition method and the voxelwise method, and mean ICC difference value from the mean-ROI method.

ROI	Method	Magnitude threshold (95 percentile)	Cluster threshold ($p < 0.05$)	Cluster sizes (p-values)	Heritability (p-value)
Left Visual Cortex	Spatial Decomposition	0.6055	11 voxels	36 voxels (p=0.028) 4 voxels (p=0.058)	-
	Voxelwise	0.7780	46 voxels	33 voxels (p=0.096) 7 voxels (p=0.458)	-
	Mean-ROI	-	-	-	0.7218 (p=0.048)
Right Visual Cortex	Spatial Decomposition	0.5262	70 voxels	46 voxels (p=0.070)	-
	Voxelwise	0.6570	145 voxels	1 voxel (p=0.949)	-

				8 voxels (p=0.831) 4 voxel (p=0.903) 33 voxels (p=0.556)	
	Mean-ROI	-	-	-	0.5551 (p=0.096)
Left Motor Cortex	Spatial Decomposition	0.6509	16 voxels	22 voxels (p = 0.044)	-
	Voxelwise	0.7784	31 voxels	20 voxels (p = 0.122) 2 voxel (p = 0.571)	-
	Mean-ROI	-	-	-	0.7451 (p=0.123)

Heritability was also estimated using the voxelwise method. None of the suprathreshold clusters in any of the three ROIs reached statistical significance (see Table 2-2; no blue clusters in Figure 2-5).[11] The correlation across voxels between the results from the spatial decomposition method and the voxelwise method was 0.7437 in the left visual cortex, 0.5691 in the right visual cortex, and 0.6222 in the left motor cortex (Figure 2-6).

[11] As in the ICC difference measures, examination of the cluster size significance was also performed using varying magnitude threshold. Clusters identified from the spatial decomposition method showed greater statistical significance than clusters identified from the voxelwise method. See Figure 2-14 for further details.

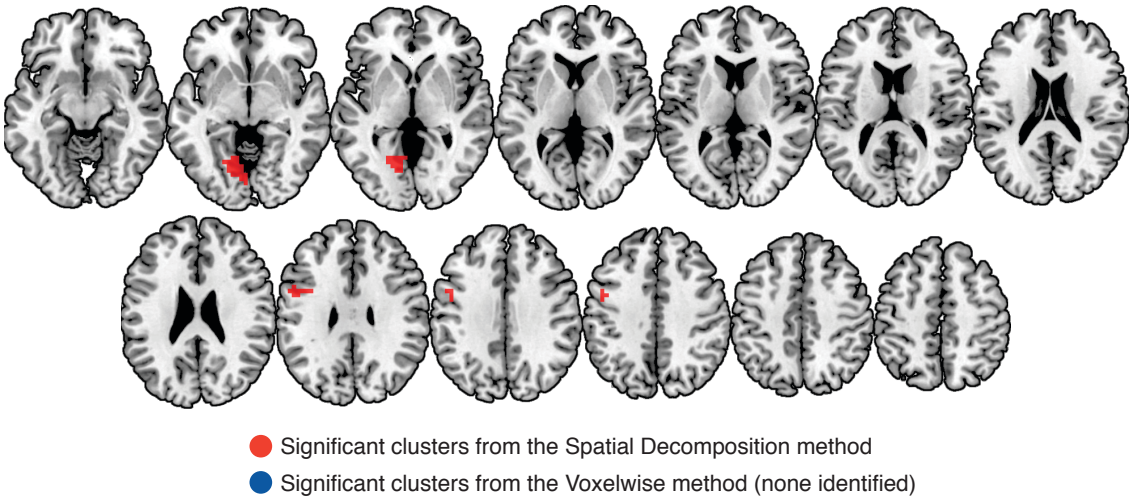

Figure 2-5 Map of heritability (h^2) estimated from the spatial decomposition method. Only statistically significant clusters ($p < 0.05$ using clusterwise correction for multiple comparisons incorporating permutation with a magnitude threshold of 95 percentile) are overlaid on a canonical brain in MNI space with axial slices from $z = -10$ to $z = 50$ in increments of 5 mm. None of the clusters identified from the voxelwise method was statistically significant.

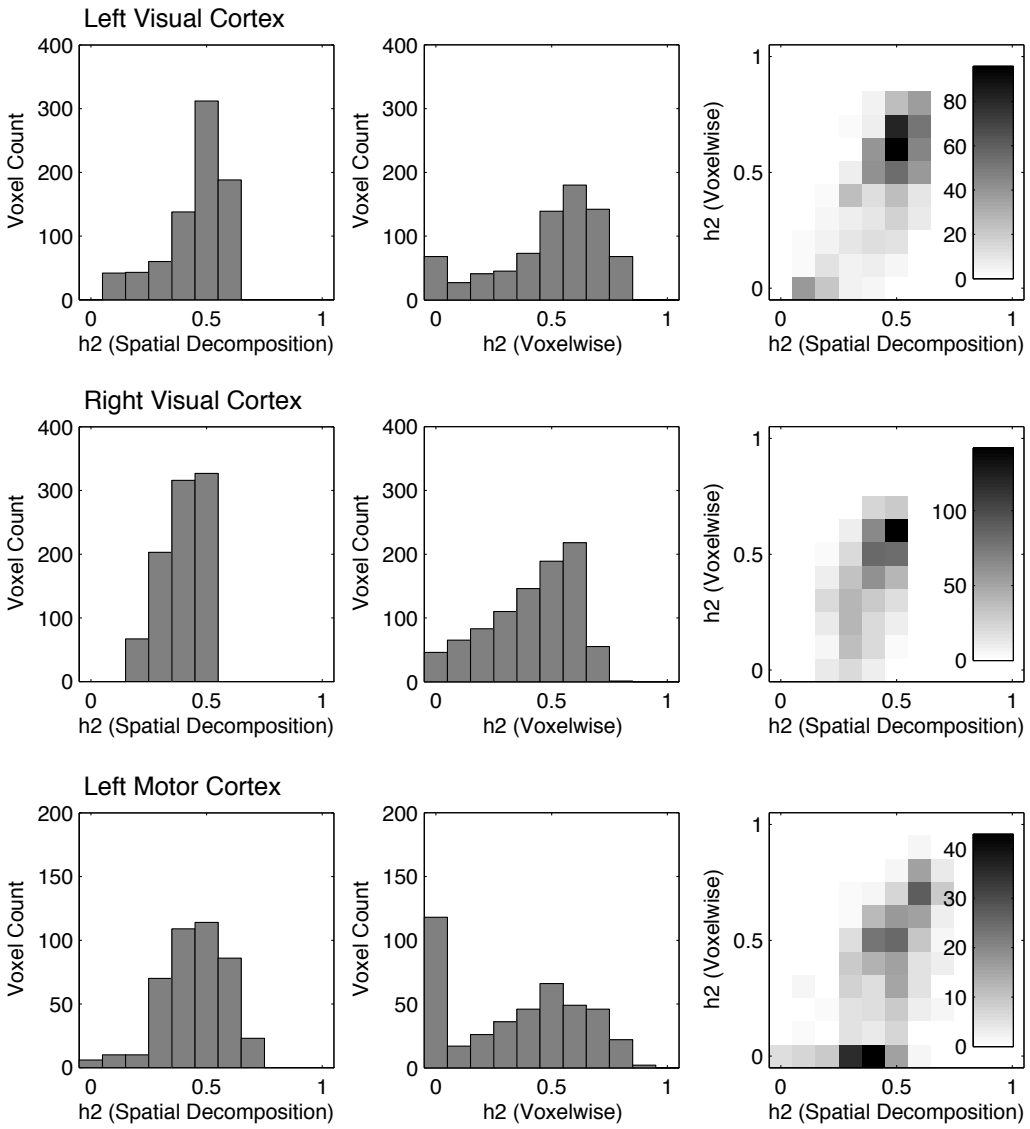

Figure 2-6 Histograms of heritability (h^2) in the left and right visual cortex estimated from the spatial decomposition method and the voxelwise method, as well as the joint histogram of *h2* estimates between the two methods across the whole brain.

The mean-ROI method showed that the average neural activity in the left visual cortex was significantly heritable ($h^2 = 0.7218$, $p = 0.048$), but no other ROI's were shown to be heritable at the alpha level 0.05.

2.5 Discussion

In this work, we developed a statistical method to estimate correlation between related subjects at each location of a spatial process. The feasibility and the relative advantage of this spatial decomposition method over conventional methods were demonstrated using a simulation study. Correlation estimates from the spatial decomposition method had lower variance and bias compared to estimates from the voxelwise or the mean-ROI approach. This discrepancy between the RMSE from the spatial decomposition method and that from the two other conventional methods tended to be greater as the overall noise increased. These results collectively suggest that the spatial decomposition method has better control over noise than the conventional methods.

Using a real fMRI dataset from a twin study, we then applied the spatial decomposition method to assess the genetic influence and heritability of brain activation in the primary visual and motor cortex during a simple visuomotor task. The results from the spatial decomposition method showed greater statistical significance, compared to the results from the voxelwise and the mean-ROI methods, both in the measure of ICC difference and in the measure of heritability. The left visual cortex showed greater genetic influence both in terms of magnitude and statistical significance than the right visual cortex.

In general, ICC difference and heritability estimates from the spatial decomposition method were less variable than the voxelwise method, as expected. Along with the results from the simulation study, the proposed method showed greater power in realistic settings compared to the voxelwise and mean-ROI

approaches. The spatial decomposition method controls the noise by using spatial basis volumes. In a way, the voxelwise method can be considered to be a special case of the spatial decomposition method. If the number of basis volumes is equal to the number of voxels in the ROI (e.g. imagine a basis set of an identity matrix), the spatial decomposition method becomes identical to the voxelwise approach. On the other hand, if a single constant map is used as a basis volume then the spatial decomposition method is conceptually similar, although not identical, to the mean-ROI method.

In the proposed spatial decomposition method, we used an independent set of data to construct the basis volumes for the given neural activation pattern. Since the basis volumes were limited to nineteen (the number of independent group of subjects), our model could have been underspecified especially when we tried to capture over 700 voxels in each mask. Underspecification of the model results in bias as shown in the simulation study, although this bias is more likely to result in bias toward zero, that results in a conservative assessment of genetic influence (see Methods). In addition, note that our results show better detectability of heritability in the spatial decomposition method than any other conventional methods in the three ROIs[12]. Nonetheless, an adequate construction of the basis volumes can

[12] The exact same analyses were also performed in the whole brain. After heritability estimation using an AE model and setting the magnitude threshold as the 99 percentile of the entire h^2 range, 81 suprathreshold clusters were identified from the voxelwise method and 8 suprathreshold clusters were identified from the spatial decomposition method. After 200 repetitions using the permutation scheme, the cluster size significance of the largest cluster identified from the voxelwise method was p=0.485 and the cluster size significance of the largest cluster identified from the voxelwise method was p=0.100. These results demonstrate that the spatial decomposition method, even though it may be extremely underspecified to capture the spatial dependencies of the whole brain, is more powerful than the voxelwise method.

improve the model even further. One potential method is to use either functional localizer data or images from orthogonal contrasts (Berman, et al., 2010; Friston, et al., 2006; Saxe, Brett, & Kanwisher, 2006) as independent datasets to construct the basis volumes. This way, there is no need to collect data from independent subjects and it will result in a much larger basis set given that modern fMRI twin studies have a few tens, if not hundreds, of subjects.

There has been some recent advance in the heritability estimation in diffusion tensor imaging data (Brun, et al., 2009; Jahanshad, et al., 2010; Lee, et al., 2010) and genetic covariance estimation in structural imaging data (Schmitt, et al., 2007). While these studies incorporate multivariate statistical analyses in heritability estimation, our study is quite different in a number of ways. The goal of our work is to borrow information from neighboring voxels to improve the precision of voxelwise heritability estimates. This is particularly a critical issue in functional neuroimaging studies, as the noise level is substantially higher than in the structural studies. In addition recent research in functional neuroimaging has started to emphasize the spatial and network-like nature of brain activity. Many studies have demonstrated that information is encoded over a large number of brain regions in a distributed and overlapping fashion (Haynes & Rees, 2006; Norman, et al., 2006). In addition, many studies have shown that multiple brain regions are intrinsically organized into networks (Achard, Salvador, Whitcher, Suckling, & Bullmore, 2006; Greicius, Krasnow, Reiss, & Menon, 2003) so that analyzing the functional role of a particular brain region may be impossible without considering other regions. It is therefore important to understand and consider the spatial

dependencies in patterns of brain activation when estimating the heritability of such patterns.

In summary, we developed a statistical method to estimate correlation and heritability at each position in a spatial dataset. We then applied this method to assess the influence of genetics on the pattern of neural activities evoked by a visuomotor task. The proposed spatial decomposition method was shown to be more efficient than the conventional voxelwise and mean-ROI methods in our experiments. The results also showed that neural activity evoked by a simple visuomotor task is under significant genetic influence particularly in the left visual cortex and the left motor cortex.

2.6 Appendix

2.6.1 Fisher's ICC

Given *N* paired data values (x_{n1}, x_{n2}) where n=1…N, the following defines Fisher's ICC (Fisher, 1954):

$$\bar{x} = \frac{1}{2N}\sum_{n=1}^{N}(x_{n1} + x_{n2}),$$

$$\mathrm{cov}(x_{\bullet 1}, x_{\bullet 2}) = \frac{1}{N-1}\sum_{n=1}^{N}(x_{n1} - \bar{x})(x_{n2} - \bar{x}),$$

$$\mathrm{var}(x_{\bullet\bullet}) = \frac{1}{2N-1}\left(\sum_{n=1}^{N}(x_{n1} - \bar{x})^2 + \sum_{n=1}^{N}(x_{n2} - \bar{x})^2\right),$$

$$ICC\left(x_{\bullet 1}, x_{\bullet 2}\right) = \frac{\mathrm{cov}(x_{\bullet 1}, x_{\bullet 2})}{\mathrm{var}(x_{\bullet\bullet})}.$$

2.6.2 Bias correction for the plug-in estimates

The estimators we use follow standard approaches from fixed effects modeling (Allison, 2005; Robinson, 1991; Searle, Casella, & McCulloch, 2008). The bias correction procedure was adopted because the sample variance of the estimated fixed effects is biased due to uncertainty in the fixed effects estimates. The adjustment we use removes this bias. The variance and covariance ($\hat{\text{var}}\left(\beta_{p\bullet\bullet}\right)$ and $\hat{\text{cov}}\left(\beta_{p\bullet 1},\beta_{p\bullet 2}\right)$) of the random effects can be estimated starting from the empirical variance and covariance of the fitted fixed effects ($\text{var}\left(\hat{\beta}_{p\bullet\bullet}\right)$ and $\text{cov}\left(\hat{\beta}_{p\bullet 1},\hat{\beta}_{p\bullet 2}\right)$). The empirical estimates are subject to a bias correction:

$$\text{var}\left(\hat{\beta}\right)=\frac{1}{2n-1}\sum_{i}^{2n}\left(\hat{\beta}_i-\bar{\hat{\beta}}\right)^2=\frac{1}{2n-1}\left(Q\hat{\beta}\right)'\left(Q\hat{\beta}\right)=\frac{1}{2n-1}\hat{\beta}'Q\hat{\beta}$$

where Q is an idempotent centering matrix. Matrix Q can be constructed so that the above equation can yield $\text{var}\left(\hat{\beta}_{p\bullet 1}\right)$, $\text{var}\left(\hat{\beta}_{p\bullet 2}\right)$, or pooled variance $\text{var}\left(\hat{\beta}_{p\bullet\bullet}\right)$ to be used for intraclass correlation.

Taking the expected value,

$$E\left(\frac{1}{2n-1}\hat{\beta}'Q\hat{\beta}\right)=\frac{1}{2n-1}tr\left(Q\cdot\ E\left(\hat{\beta}\hat{\beta}'\right)\right)=\frac{1}{2n-1}tr\left(Q\cdot\left[\left(X'X\right)^{-1}\sigma^2+\beta\beta'\right]\right)$$

$$=\frac{1}{2n-1}tr\left(Q\left(X'X\right)^{-1}\sigma^2\right)+\frac{1}{2n-1}tr\left(Q\beta\beta'\right)=\frac{1}{2n-1}tr\left(Q\left(X'X\right)^{-1}\sigma^2\right)+\frac{1}{2n-1}\beta Q\beta'$$

Thus, the term $\frac{1}{2n-1}tr\left(Q\left(X'X\right)^{-1}\sigma^2\right)$ can be subtracted from the plug-in estimates to correct for bias.

Likewise,

$$\operatorname{cov}\left(\hat{\beta}_1,\hat{\beta}_2\right)=\frac{1}{n-1}\left(Q_1\hat{\beta}\right)'\left(Q_2\hat{\beta}\right)=\frac{1}{n-1}\hat{\beta}'Q_1'Q_2\hat{\beta}=\frac{1}{n-1}tr\left(Q_1'Q_2\hat{\beta}\hat{\beta}'\right)$$

where n-by-$2n$ matrices Q_1 and Q_2 represent a centering matrix. Matrices Q_1 and Q_2 can be constructed so that the above equation can either yield interclass covariance or intraclass covariance.

Taking the expected value,

$$E\left(\frac{1}{n-1}tr\left(Q_1'Q_2\hat{\beta}\hat{\beta}'\right)\right)=\frac{1}{n-1}tr\left(Q_1'Q_2\left(X'X\right)^{-1}\sigma^2\right)+\frac{1}{n-1}tr\left(Q_1'Q_2\beta\beta'\right)$$

$$=\frac{1}{n-1}tr\left(Q_1'Q_2\left(X'X\right)^{-1}\sigma^2\right)+\frac{1}{n-1}\left(Q_1\beta\right)'\left(Q_2\beta\right)$$

Thus, the bias $\frac{1}{n-1}tr\left(Q_1'Q_2\left(X'X\right)^{-1}\sigma^2\right)$ can be subtracted from the plug-in estimates to correct for bias.

2.7 Supplementary Figures

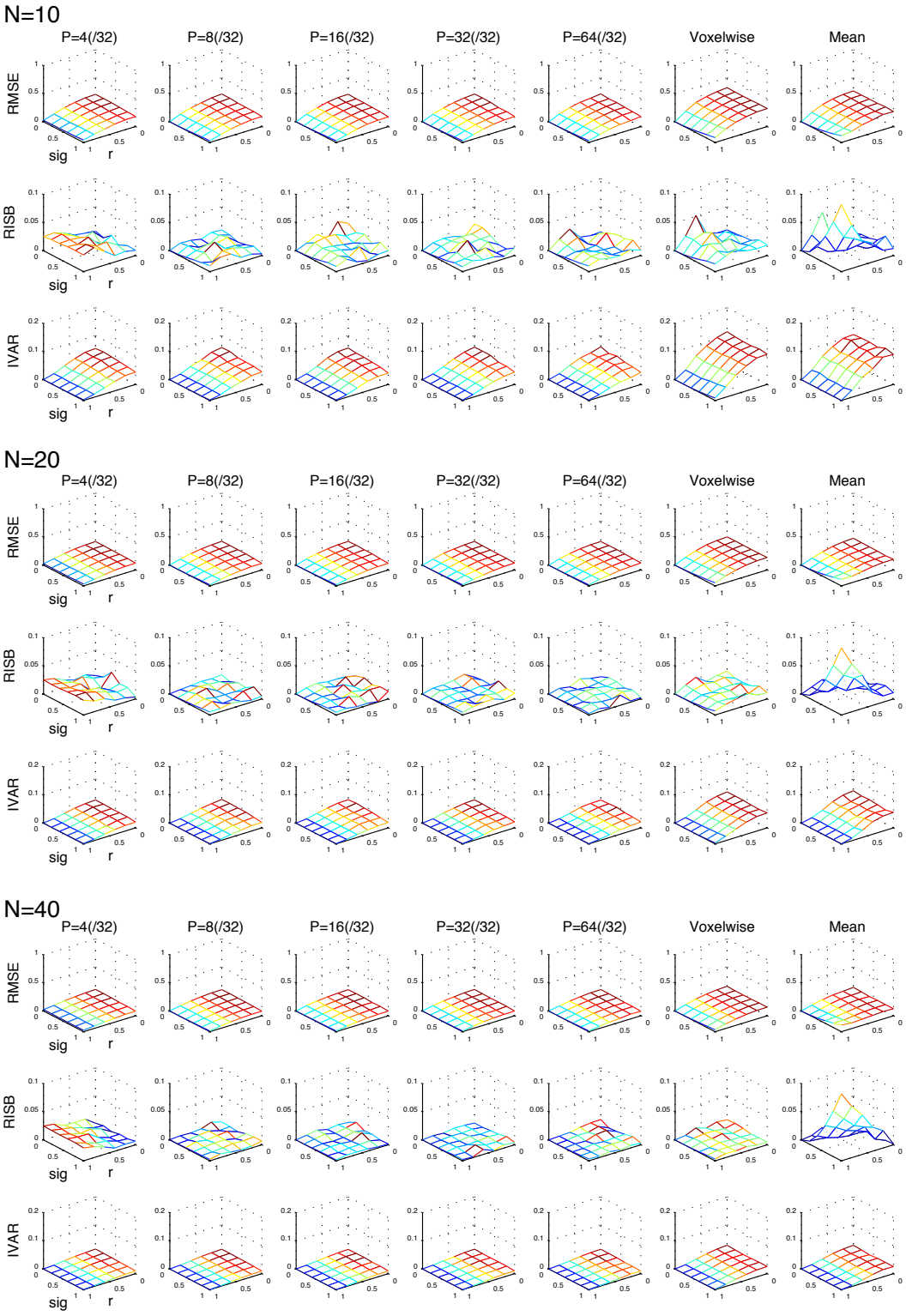

Figure 2-7 Results of the simulation study using the proposed spatial decomposition method (columns 1-5), the voxelwise method (column 6), and the mean-ROI method (column 7) with 10, 20,

and 40 pairs. Patterns of neural activation for twin pairs were simulated with 32 basis volumes while varying the degree of correlation between pairs (*r*) and the error variability (*sig*). The estimated correlation was compared with the true ICC, and root mean squared error (RMSE), integrated variance (IVAR), and root integrated squared bias (RISB) were computed over the parameter space. In the case of the spatial decomposition method, correlation was estimated using a subset of 32 basis volumes (4, 8, or 16, as represented in the first three columns), all 32 basis volumes (represented in the fourth column), and 64 basis volumes (represented in the fifth column). IVAR decreased as a function of number of pairs suggesting statistical consistency of the estimators.

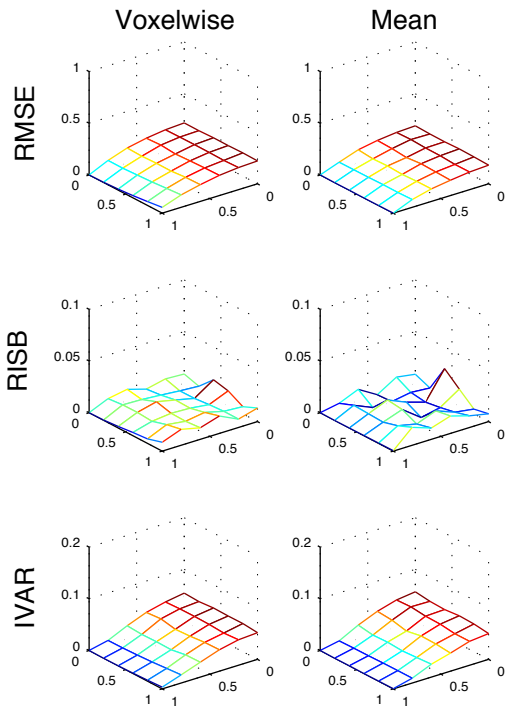

Figure 2-8 Simulation of the mean-ROI method while the simulated estimates are compared against the ROI-level true correlation. In our simulation study, the simulated correlations were compared against the the voxel-level true correlation computed from Equations 2 to 4 with given parameters *r* and *σ*. This was based on the idea that the conventional voxelwise method estimates correlation at the voxel level. The proposed spatial decomposition method also estimates correlation at the voxel level. Thus, the estimands are the same between the two methods while the estimators are different. The mean-ROI method estimates a different quantity, however. It estimates the correlation of a function of the data (i.e. spatial average). Thus, it is in some sense more reasonable to assess the bias of the mean-ROI estimator against the ROI-level true correlation (i.e. *r* in our simulation study). This figure shows the results of the simulation study (N=20) using the voxelwise method (comparing the simulated estimates to the voxel-level true correlation) and the mean-ROI method (comparing the simulated estimates to the ROI-level true correlation). The bias that existed in the mean-ROI method (as shown in Figure 2-1 and Figure 2-7) is reduced in this case, and there are little differences between the two methods. The critical difference is more at the conceptual level that the voxelwise method (and the spatial decomposition method) does not assume spatial homogeneity while the mean-ROI method assumes spatial homogeneity.

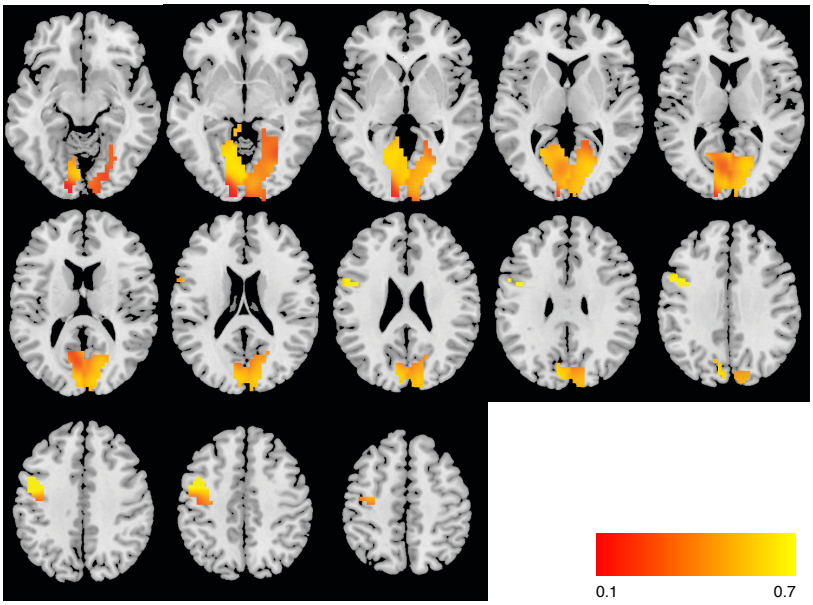

Figure 2-9 ICC estimates of MZ pairs computed using the spatial decomposition method, arbitrarily thresholded at 0.10. The ICC were estimated separately in the three ROI's (the left and right visual cortex and the left motor cortex) and then were overlaid on a canonical brain in MNI space with axial slices from *z* = -10 to 50 mm with increments of 5 mm. The same axial slices and the same color scale are used in Figures S4 through S6. Left hemisphere appears on the left for all brain images.

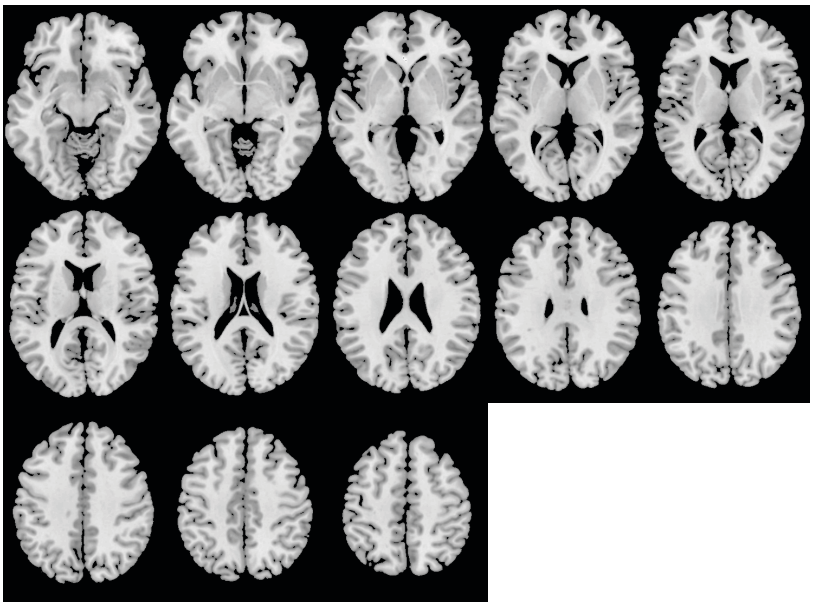

Figure 2-10 ICC estimates of DZ pairs computed using the spatial decomposition method. There was no suprathreshold cluster at this arbitrary threshold of 0.1.

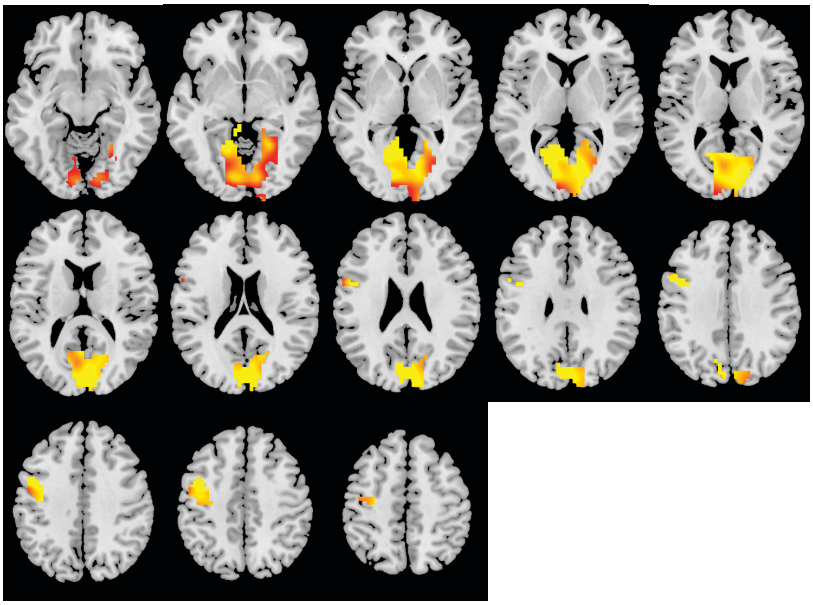

Figure 2-11 ICC estimates of MZ pairs computed using the voxelwise method.

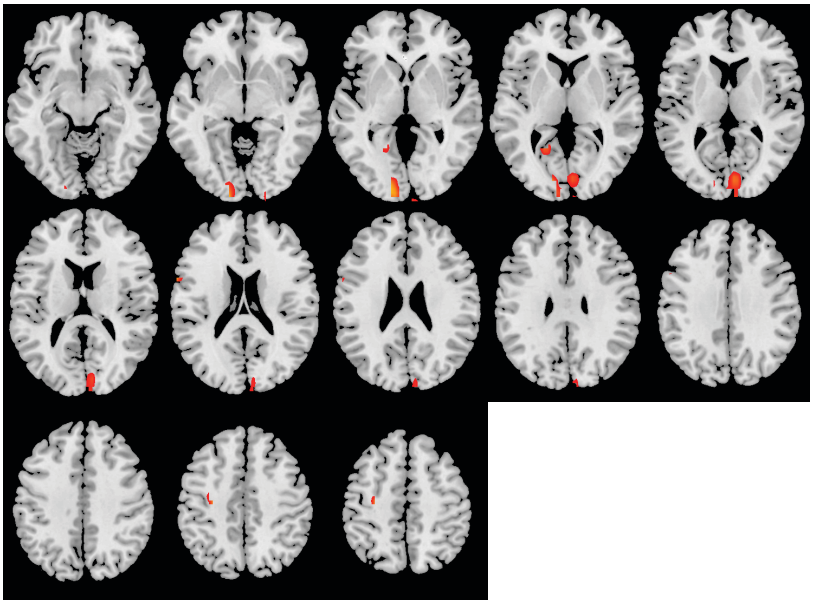

Figure 2-12 ICC estimates of DZ pairs computed using the voxelwise method.

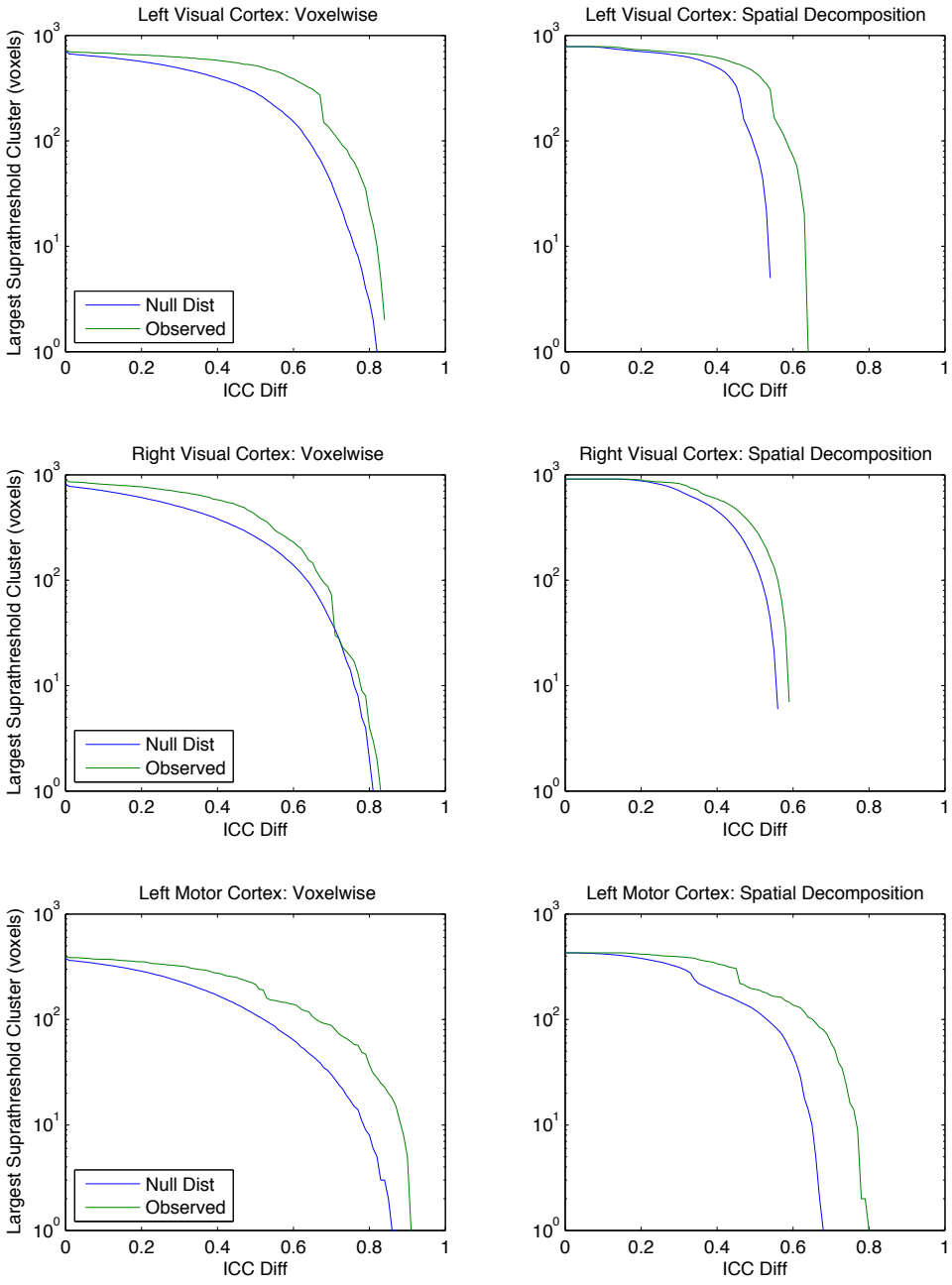

Figure 2-13 Statistical significance of the cluster size as a function of magnitude threshold in the estimation of ICC difference in the left visual cortex (top), the right visual cortex (middle), and the left motor cortex (bottom). While varying the magnitude threshold from 0 to 1 in increments of 0.01, the size of the largest suprathreshold cluster (green) was recorded and compared with the null distribution of the maximum cluster size. The null distribution was constructed from 10,000 permutations of zygosity. These graphs demonstrate that overall the spatial decomposition method yielded greater statistical significance (i.e. how much the green line is above the blue line) of the largest cluster size than the voxelwise method regardless of the magnitude threshold.

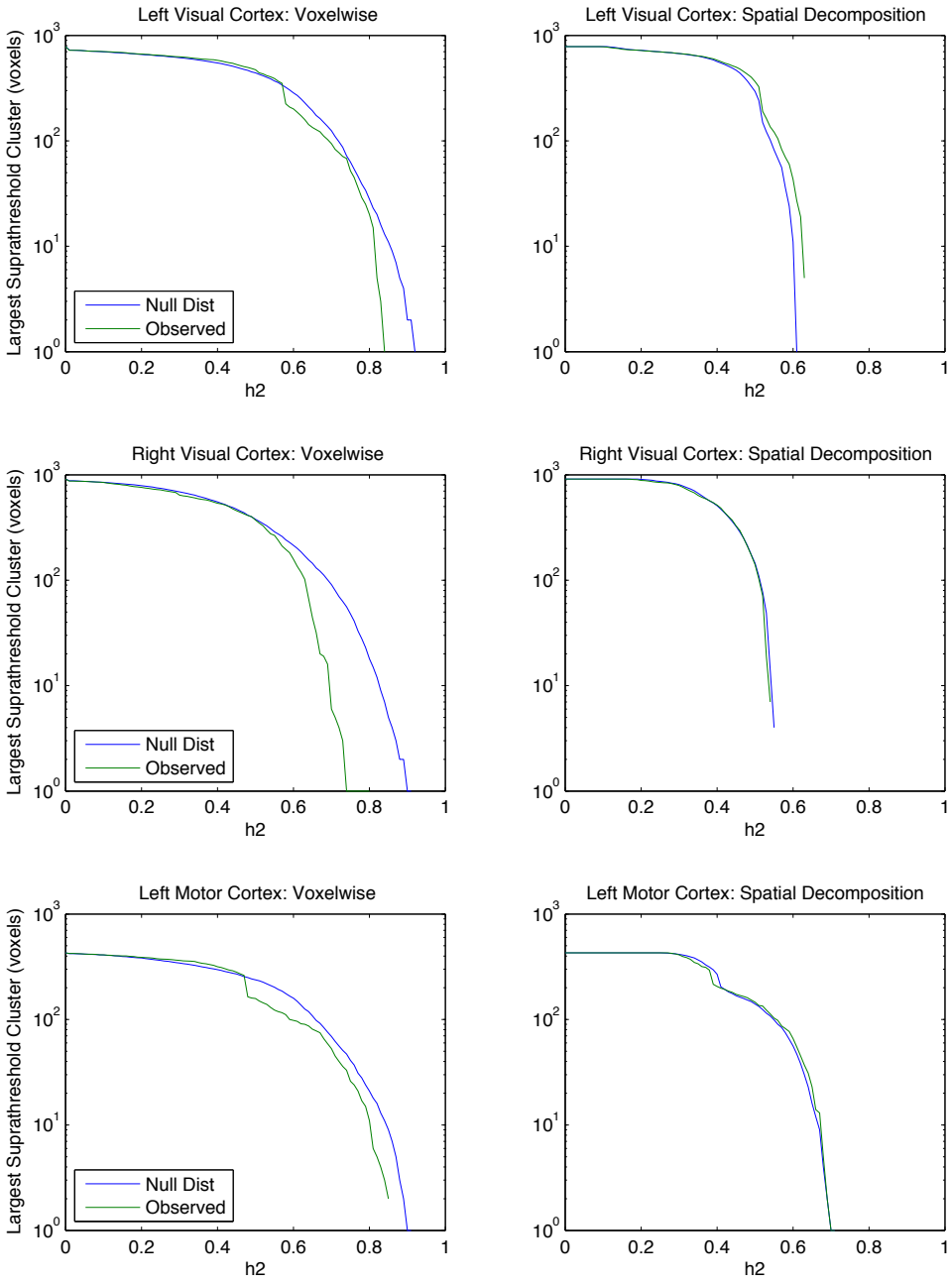

Figure 2-14 Statistical significance of the cluster size as a function of magnitude threshold in the estimation of heritability (h^2) in the left visual cortex (top), the right visual cortex (middle), and the left motor cortex (bottom). While varying the magnitude threshold from 0 to 1 in increments of 0.01, the size of the largest suprathreshold cluster (green) was recorded and compared with the null distribution of the maximum cluster size. The null distribution was constructed from 1,000 permutations of zygosity. These graphs demonstrate that overall the spatial decomposition method yielded greater statistical significance (i.e. how much the green line is above the blue line) of the largest cluster size than the voxelwise method regardless of the magnitude threshold.

2.8 References

Achard, S., Salvador, R., Whitcher, B., Suckling, J., & Bullmore, E. (2006). A resilient, low-frequency, small-world human brain functional network with highly connected association cortical hubs. *Journal of Neuroscience, 26*(1), 63-72.

Allison, P. (2005). *Fixed Effects Regression Methods for Longitudinal Data Using SAS*: SAS Publisher.

Berman, M. G., Park, J., Gonzalez, R., Polk, T. A., Gehrke, A., Knaffla, S., et al. (2010). Evaluating functional localizers: the case of the FFA. *Neuroimage, 50*(1), 56-71.

Blokland, G. A. M., McMahon, K. L., Hoffman, J., Zhu, G., Meredith, M., Martin, N. G., et al. (2008). Quantifying the heritability of task-related brain activation and performance during the N-back working memory task: A twin fMRI study. *Biological Psychology, 79*(1), 70-79.

Brun, C. C., Lepore, N., Pennec, X., Lee, A. D., Barysheva, M., Madsen, S. K., et al. (2009). Mapping the regional influence of genetics on brain structure variability - A Tensor-Based Morphometry study. *Neuroimage, 48*(1), 37-49.

Chiang, M. C., Barysheva, M., Lee, A. D., Madsen, S., Klunder, A. D., Toga, A. W., et al. (2008). Mapping genetic influences on brain fiber architecture with high angular resolution diffusion imaging (HARDI). *2008 Ieee International Symposium on Biomedical Imaging: From Nano to Macro, Vols 1-4*, 871-874.

Christian, J. C., Norton, J. A., Sorbel, J., & Williams, C. J. (1995). Comparison of analysis of variance and maximum-likelihood based path-analysis of twin data - Partitioning genetic and environmental sources of covariance. *Genetic Epidemiology, 12*(1), 27-35.

Cote, C., Beauregard, M., Girard, A., Mensour, B., Mancini-Marie, A., & Perusse, D. (2007). Individual variation in neural correlates of sadness in children: A twin fMRI study. *Human Brain Mapping, 28*(6), 482-487.

Falconer, D. S., & Mackay, T. F. C. (1996). *Introduction to Quantitative Genetics* (4 ed., pp. 160-183). Harlow, Essex, UK: Longmans Green.

Fisher, R. A. (1954). *Statistical Methods for Research Workers* (12th ed.): Oliver and Boyd.

Friston, K. J., Rotshtein, P., Geng, J. J., Sterzer, P., & Henson, R. N. (2006). A critique of functional localisers. *Neuroimage, 30*(4), 1077-1087.

Greicius, M. D., Krasnow, B., Reiss, A. L., & Menon, V. (2003). Functional connectivity in the resting brain: A network analysis of the default mode hypothesis. *Proceedings of the National Academy of Sciences of the United States of America, 100*(1), 253-258.

Haynes, J. D., & Rees, G. (2006). Decoding mental states from brain activity in humans. *Nature Reviews Neuroscience, 7*(7), 523-534.

Holmes, A. P., Blair, R. C., Watson, J. D. G., & Ford, I. (1996). Nonparametric analysis of statistic images from functional mapping experiments. *Journal of Cerebral Blood Flow and Metabolism, 16*(1), 7-22.

Huettel, S. A., Song, A. W., & Gregory, M. (2004). *Functional Magnetic Resonance Imaging* (pp. 217-251). Sunderland, MA: Sinauer Associates, Inc.
Jahanshad, N., Lee, A. D., Barysheva, M., McMahon, K. L., de Zubicaray, G. I., Martin, N. G., et al. (2010). Genetic influences on brain asymmetry: A DTI study of 374 twins and siblings. *Neuroimage, 52*(2), 455-469.
Koten, J. W., Wood, G., Hagoort, P., Goebel, R., Propping, P., Willmes, K., et al. (2009). Genetic Contribution to Variation in Cognitive Function: An fMRI Study in Twins. *Science, 323*(5922), 1737-1740.
Lee, A. D., Lepore, N., de Leeuw, J., Brun, C. C., Barysheva, M., McMahon, K. L., et al. (2010). Multivariate variance-components analysis in DTI. *2010 7th Ieee International Symposium on Biomedical Imaging: From Nano to Macro*, 1157-1160.
Maldjian, J. A., Laurienti, P. J., Kraft, R. A., & Burdette, J. H. (2003). An automated method for neuroanatomic and cytoarchitectonic atlas-based interrogation of fMRI data sets. *Neuroimage, 19*(3), 1233-1239.
Matthews, S. C., Simmons, A. N., Strigo, I., Jang, K., Stein, M. B., & Paulus, M. P. (2007). Heritability of anterior cingulate response to conflict: An fMRI study in female twins. *Neuroimage, 38*(1), 223-227.
Neale, M. C. (1998). Twin analysis. In P. Armitage & T. Colton (Eds.), *Encyclopedia of Biostatistics*. New York: John Wiley.
Neale, M. C. (2003). Twin studies: Software and algorithms. In D. N. Cooper (Ed.), *Encyclopedia of the Human Genome*: Macmillan Publishers Ltd.
Neale, M. C., Boker, S. M., Xie, G., & Maes, H. (2003). *Mx Statistical Modeling*: Medical College of Virginia.
Nichols, T. E., & Holmes, A. P. (2002). Nonparametric permutation tests for functional neuroimaging: A primer with examples. *Human Brain Mapping, 15*(1), 1-25.
Norman, K. A., Polyn, S. M., Detre, G. J., & Haxby, J. V. (2006). Beyond mind-reading: multi-voxel pattern analysis of fMRI data. *Trends in Cognitive Sciences, 10*(9), 424-430.
Polk, T. A., Park, J., Smith, M. R., & Park, D. C. (2007). Nature versus nurture in ventral visual cortex: A functional magnetic resonance Imaging study of twins. *Journal of Neuroscience, 27*(51), 13921-13925.
Robinson, G. K. (1991). That BLUP is a Good Thing: The Estimation of Random Effects. *Statistical Science*, 6(1), 15-32.
Saxe, R., Brett, M., & Kanwisher, N. (2006). Divide and conquer: A defense of functional localizers. *Neuroimage, 30*(4), 1088-1096.
Schmitt, J. E., Lenroot, R. K., Ordaz, S. E., Wallace, G. L., Lerch, J. P., Evans, A. C., et al. (2009). Variance decomposition of MRI-based covariance maps using genetically informative samples and structural equation modeling. *Neuroimage, 47*(1), 56-64.
Schmitt, J. E., Wallace, G. L., Rosenthal, M. A., Molloy, E. A., Ordaz, S., Lenroot, R., et al. (2007). A multivariate analysis of neuroanatomic relationships in a genetically informative pediatric sample. *Neuroimage, 35*(1), 70-82.
Searle, S. R., Casella, G., & McCulloch, C. E. (2008). *Variance Components*: John Wiley & Sons, Inc.

Stuart, A., & Ord, K. (2009). *Kendall's Advanced Theory of Statistics* (Vol. 1, pp. 351): Wiley.

Thompson, P. M., Cannon, T. D., Narr, K. L., van Erp, T., Poutanen, V. P., Huttunen, M., et al. (2001). Genetic influences on brain structure. *Nature Neuroscience, 4*(12), 1253-1258.

Tzourio-Mazoyer, N., Landeau, B., Papathanassiou, D., Crivello, F., Etard, O., Delcroix, N., et al. (2002). Automated anatomical labeling of activations in SPM using a macroscopic anatomical parcellation of the MNI MRI single-subject brain. *Neuroimage, 15*(1), 273-289.

Chapter 3

Investigating environmental contributions to the neural representation of written words

3.1 Introduction

The left lateral occipitotemporal cortex has been identified as a critical site for the visual processing of written words. Brain imaging experiments collectively demonstrate that the middle portion of the left occipitotemporal sulcus bordering the fusiform gyrus and the inferior temporal gyrus exhibits greater neural activation in response to written words compared to other control stimuli in a variety of tasks (for review see McCandliss, Cohen, & Dehaene, 2003; Schlaggar & McCandliss, 2007). While debate over the specialization of this region for abstract word forms exists, this region has often termed as the visual word form area (VWFA) (Cohen, et al., 2002).

The location of VWFA is quite consistent across individuals and cultures (Bolger, Perfetti, & Schneider, 2005; Cohen, et al., 2002; Jobard, Crivello, & Tzourio-Mazoyer, 2003), which suggests that some innate mechanisms play a role in the development of this neural architecture. On the other hand, reading is a recent development on an evolutionary time scale, it is not shared with other species, and it does not develop without extensive experience. It is therefore unlikely that our

brain has been genetically programmed, via natural selection, to specifically process written words (Dehaene & Cohen, 2007; McCandliss, et al., 2003; Polk & Farah, 1998). Therefore, experience must be playing a critical role in shaping the neural architecture for written words in the left occipitotemporal area in literate adults.

Whether and how experience shapes VWFA has been tested in a variety of different ways in previous studies. In some studies, VWFA activation in response to known script versus unknown script was compared (Baker, et al., 2007; Dehaene, et al., 2010; Hashimoto & Sakai, 2004; Vinckier, et al., 2007; Xue, Chen, Jin, & Dong, 2006). If our experience with visual word forms influences the neural signature of VWFA, then it would be natural to hypothesize differential neural activation levels between known and unknown scripts. The results, however, have been mixed across studies. For example, one study shows greater VWFA activation in response to known script than unknown script (Baker, et al., 2007) while another study shows the opposite results (Xue, et al., 2006).

Some other studies examined patterns of VWFA activation as a function of word regularity or frequency (Binder, Medler, Westbury, Liebenthal, & Buchanan, 2006; Kronbichler, et al., 2004; Vinckier, et al., 2007). The idea behind these studies is that VWFA activation will be modulated by the frequency with which we encounter word forms. However, there is no clear consensus on the findings either. Some studies show that VWFA activity increases as a function of orthographic regularity (Binder, et al., 2006; Vinckier, et al., 2007) while another study shows that VWFA activity decreases as a function of word frequency (Kronbichler, et al., 2004).

The reasons for such inconsistent findings are largely unknown. One thing we do know, however, is that factors such as attentional engagement, task difficulty, and time on task play critical roles in the magnitude of neural activation in the context of visual word form recognition (Ben-Shachar, Dougherty, Deutsch, & Wandell, 2007; Mechelli, Humphreys, Mayall, Olson, & Price, 2000; Nobre, Allison, & McCarthy, 1994; Starrfelt, 2007). Therefore, subtle differences in tasks and other experimental parameters can easily influence the response magnitude and may therefore obscure the results making it difficult to examine experience-dependent properties in VWFA. So, how else can we empirically test the role of experience in shaping the neural architecture for written words?

Twin studies make it possible to directly assess the amount of genetic and environmental contributions in explaining individual differences in a trait. In particular, monozygotic (MZ) twins make it possible to quantify the effect of unique environmental variance. Because MZ twins reared together share all their genetic alleles and potential common environmental effects, the correlation of the phenotypic trait in MZ twins provides an estimate of variability explained by these common factors (genetics and common environment) (Falconer & Mackay, 1996). The complement of this correlation therefore provides an estimate of the variability explained by unique environmental effects. In other words, a trait that is more susceptible to environmental influence, making MZ twins less similar to each other, will exhibit a smaller correlation between MZ twins than a trait that is less susceptible to environmental influence. The unique environmental effects are

broadly defined to include any possible prenatal experiences and epigenetic effects, and are simply the factors that make the MZ siblings different from each other.

In the present study, we examine how the unique environment that we experience over time influences neural activation in VWFA. We measured VWFA activity evoked by words, pseudowords, consonant strings, and false fonts in MZ twins. By taking MZ correlations, it is possible to quantify the proportion of the variability in VWFA activation that can be attributed to unique environmental effects. Assuming that the neural representation of written words is influence by experience, we expected to find a greater environmental effect in the familiar word condition than in the unfamiliar false fonts condition. We also tested how environmental effects modulate subcomponents of reading. Reading involves multiple subcomponents including visual, orthographic, phonological, and semantic processing, but the stimulus types that we studied involve different subsets on these processes. Processing false fonts involves visual processing, but not orthographic, phonological, or semantic processing. Processing consonant strings involves both visual and orthographic processing, but not phonological or semantic processing. Processing pseudowords involves visual, orthographic, and phonological processing, but not semantic processing. Finally, processing words involves all these subcomponents (Pugh et al., 1996). By investigating unique environmental effects on all four stimulus types, we expected to delineate how different subcomponents of reading may be influenced by the environment that we experience over time.

3.2 Methods

3.2.1 Participants

Sixteen MZ pairs (7 male pairs, ages 18-29 with median age of 22.5) participated in the study. All participants were screened to ensure they were right-handed, native English speakers, psychologically and physically healthy, not taking medications with psychotropic or vascular effects, and free of any other MRI safety contraindications. Zygosity was determined by comparing up to fifteen genetic markers (D3S1358, TH01, D21S11, D18S51, Penta E, D5S818, D13S317, D7S820, D16S539, CSF1PO, Penta D, vWA, D8S1179, TPOX, FGA) from the buccal cells of twins collected by swabbing the cheek of each participant. Twins in whom all the markers matched were classified as monozygotic. All study procedures were reviewed and approved by the Institutional Review Boards at the University of Texas at Dallas, the University of Texas Southwestern, and the University of Michigan. All participants provided detailed written consent prior to their involvement in the study.

3.2.2 Stimulus Materials

The primary goal of this study was to compare unique environmental effects in the neural activation evoked by words and false fonts. To this end, words (WD) were randomly chosen from the MCWord database (Medler & Binder, 2005, MCWord: An On-Line Orthographic Database of the English Language, http://www.neuro.mcw.edu/mcword) with word frequency ranging from 205.4 to 497.3 per million. False fonts (FF) were adapted from Vinckier et al. (2007). These

false fonts were designed to be visually similar to upper case letters. All strings were composed of four characters (mono-spaced type-face with 2° visual angle in height), and only capital letters were used (see Figure 3-1).

In addition to real words and false fonts, pseudowords (PW) and consonant strings (CS) were also included to study how subcomponents of reading are modulated by unique environment. If orthographic, phonological, and semantic processing trained and acquired over time make different contributions in shaping the VWFA, then the amount of unique environmental effects should vary across different subcomponents of reading. Pseudowords, or pronounceable nonwords, were created from constrained trigram-based strings from the MCWord database. Consonant strings were random combinations of consonants. Additionally, random combinations of Arabic numbers (NB) were included, which served as a contrast when functionally identifying the VWFA.

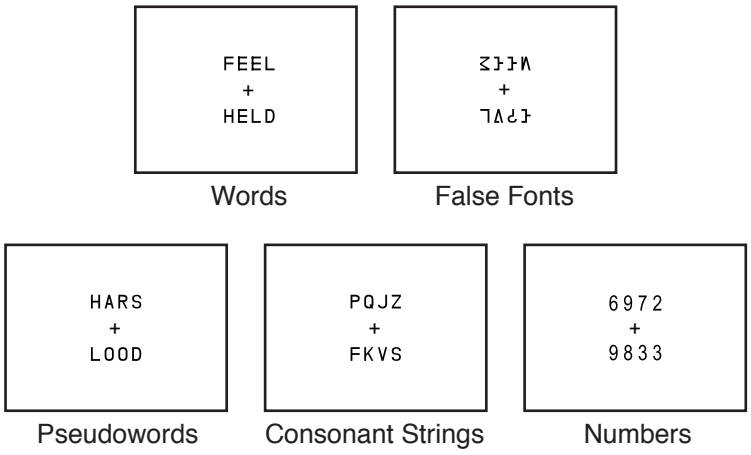

Figure 3-1 Examples of stimuli used in this study. Monozygotic twin participants performed a visual matching task on pairs of real words (WD), false fonts (FF), pseudowords (PW), consonant strings (CS), and numbers (NB), and judged whether the two items were the same or different.

3.2.3 Procedure

The fMRI experiment consisted of five 5-minute runs with eighteen 16-sec blocks, pseudorandomly ordered. Eighteen blocks were composed of three of each of the five stimulus categories in addition to three blocks of fixation viewing. Each block consisted of 8 trials (1.5 sec of presentation and 0.5 sec of inter-trial interval). On each trial, two strings from the same stimulus category were presented 4.2° above and below the central cross as shown in Figure 3-1. Participants judged whether the two strings were the same or different. The correct answer was "same" in half of all the trials. All visual stimuli were presented via E-prime (Psychology Software Tools, Pittsburgh, PA) and displayed by a back-projection system. Participants made responses using buttons under the right index and middle fingers (Lumina response pad; Cedrus, San Pedro, CA).

3.2.4 Data Acquisition

Brain images were acquired with a Philips Achieva 3T whole-body scanner at UT Southwestern using the Philips SENSE parallel acquisition technique. Functional scans were acquired as axial slices, with a voxel size of 3.4 mm × 3.4 mm × 3.5 mm. At each of 148 BOLD acquisitions per run, 43 axial slices were acquired (covering the whole brain; TR = 2.0 s, TE = 25 ms). A high-resolution axial T1 MPRAGE was acquired (voxel size 1 mm isotropic; TR = 8.27 ms, TE = 3.82 ms).

3.2.5 Activation Analysis and Inter-individual Registration

Functional data were processed using SPM5 (Wellcome Department of Cognitive Neurology, London, UK, http://www.fil.ion.ucl.ac.uk). The functional

images underwent slice-timing correction and realignment to the mean volume. Then, activations in response to each stimulus (i.e. WD, FF, PW, CS, and NB) relative to fixation were estimated using the standard general linear model (GLM) with a high-pass filter at 128 Hz and correcting for temporal autocorrelation with an AR(1) model. The model included separate regressors for each of the experimental conditions in each run convolved with a canonical hemodynamic response function, as well as six nuisance covariates modeling head translation and rotation. In order to use independent data to define the region of interest (and construct basis volumes) and to test the effect of interest, the neural activations were estimated separately for odd and even runs. This procedure resulted in volumetric brain maps of parameter estimates (beta values from the GLM) from odd and even runs for each of the five categories in each participant.

In order to minimize the contribution of brain morphology in estimating the similarity in brain function in twin pairs, a cortex-based inter-individual registration technique was used by incorporating the FreeSurfer 4.5 (Martinos Center for Biomedical Imaging, http://surfer.nmr.mgh.harvard.edu) automated reconstruction stream. First, each participant's T1 anatomical image was coregistered with the mean functional image. Then, this image underwent a series of reconstruction streams in FreeSurfer, which resulted in the identification of gray/white matter boundaries and gyral/sulcal folding patterns. Inter-individual registration was performed using this surface-based atlas by mapping individual cortical folding patterns to the FreeSurfer average curvature map. This procedure allows direct

alignment of the anatomy instead of image intensities. The resulting surface map consisted of 163,842 vertices on each hemisphere.

This procedure also enabled inter-individual registration of the functional brain maps. First, individual volumetric parameter estimate maps computed from the functional data analysis were mapped onto individual surface maps. Then, these individual surface maps were mapped onto the FreeSurfer average surface map. The resulting maps were surface-smoothed using a Gaussian kernel with 6mm full-width-half-maximum.

3.2.6 Region of Interest

The VWFA was functionally constructed from the second-level random-effects group analysis on the surface maps of WD+PW+CS > NB from even runs ($p < 10^{-5}$, uncorrected; extent > 50 mm^2) (Table 3-1). This contrast resulted in one contiguous region in the left fusiform and inferior temporal area subtending 831 vertices (approximately 470 mm^2) (see Figure 3-2A). No region in the bilateral ventral visual cortex showed greater activation in the WD condition relative to the FF condition ($p < 10^{-5}$, uncorrected; extent > 50 mm^2), which prevented us from using FF as a control stimuli to identify VWFA.

Table 3-1 Cluster results of the second-level random-effects group analysis of WD+PW+CS > NB ($p < 10^{-5}$, uncorrected) for defining the VWFA. No suprathreshold activation was observed in the right hemisphere.

Coordinates (Talairach)	Maximum t-value	Size (mm^2)
-39.6 -42.9 -14.3	6.402	470.88
-42.0 3.0 20.7	5.648	27.59
-44.1 -32.9 -16.8	5.391	31.39
-39.7 -20.6 -17.6	5.344	10.58

-51.6 -40.4 7.2	5.241	7.49

In addition, another region was identified as a control region to assess whether any differences in the unique environmental effects are unique to VWFA. To this end, the left motor cortex was functionally defined from the group-level task-related activity (all tasks > fixation from even runs, $p < 10^{-5}$, uncorrected; extent > 50 mm^2) within the left sensorimotor cortex (see Figure 3-4A).

3.2.7 Monozygotic Twin Approach

The goal of the MZ twin analysis was to quantify the role of unique environmental effect in explaining the total phenotypic variance of VWFA activity. MZ twins reared together share all of their genetic alleles (A) and common environment (C), so any difference arising between MZ twins can be attributed to the unique environment effect (E). That is, P = A + C + E, and the intraclass correlation (ICC) between MZ twins becomes the proportion of phenotypic variation accounted for by genetics and shared environment (Var(G+C) / Var(P)). Therefore, the complement of this MZ correlation (1 – Var(E) / Var(P)) represents the proportion of phenotypic variance explained by the unique environmental effects. Note that the unique environmental effect also includes variance accounted for by measurement error, and that it is assumed in this study that this error variance is comparable across the four conditions.

3.2.8 Parameter Estimates and MZ Correlations

As in other previous studies, activation magnitude in the VWFA in response to various visual categories were observed. In order to do so, parameter estimates

for the WD, FF, PW and CS conditions from odd runs within the ROI were computed for each participant. Then, the mean parameter estimate in each condition was computed across all participants (see Figure 3-2B).

Then, in order to quantify the effect of unique environment, the ICC between MZ twins was computed (see Figure 3-3A). First, linear effect of age and sex was removed from parameter estimates to remove any variance explained by these covariates. Then, the ICC of the mean parameter estimate between MZ twins was computed in each condition (Fisher, 1954). To enable comparison between different correlation estimates, the computed ICC underwent Fisher's *r*-to-*z* transformation. MZ correlation (or ICC) reported in this paper refers to *z*-transformed ICC, and more specifically, ICC_{WD}, ICC_{PW}, ICC_{CS}, and ICC_{FF} refer to ICC estimates in each of the four conditions in subscripts.

See Section 3.5 Appendix for the same analysis using the spatial decomposition method (Chapter 2).

3.2.9 Statistical Significance

The statistical significance of the effect of interest (e.g. whether ICC_{FF} is greater than ICC_{WD} or whether there is a linear increase across the four conditions) was tested using a permutation method. To be specific, the observed difference value (i.e. $ICC_{FF} - ICC_{WD}$ for the difference between ICC_{FF} and ICC_{WD}, and $(3/4)\times ICC_{FF} + (1/4)\times ICC_{CS} - (1/4)\times ICC_{PW} - (3/4)\times ICC_{WD}$ for the linear contrast across the four conditions) was first computed and recorded. Then, in a total of 10,000 repetitions, the condition labels in each paired parameter estimates were permuted within each pair, and the difference value was computed from each of the permuted sample. This

permutation scheme is based on the null hypothesis that there is no difference between the ICC's for the WD versus the FF conditions. This procedure results in a null distribution of 10,000 estimates of the difference value. The *p*-value of the *observed* difference value was computed based on the proportion of the *null* distribution exceeding the observed value.

3.3 Results

3.3.1 Behavioral Results

Reaction times and accuracy in response to each experimental condition were analyzed (Table 3-2). There was a significant difference between the reaction times across conditions tested by a within-subject ANOVA design ($F_{2.72,\ 84.42}$ = 96.320, $p < 0.001$, Greenhouse-Geisser corrected). A post-hoc contrast analysis showed that this difference was mainly driven by slower RT for NB than CS ($F_{1,31}$ = 9.164, $p = 0.005$) and slower RT for FF than NB ($F_{1,31}$ = 204.456, $p < 0.001$). The same test for accuracy showed a significant difference between the conditions ($F_{3.00,\ 93.05}$ = 14.074, $p < 0.0001$, Greenhouse-Geisser corrected), and this difference was mainly driven by lower accuracy in the false fonts condition than the other conditions (A post-hoc contrast of FF < NB showed $F_{1,31}$ = 27.983, $p < 0.001$).

Table 3-2 Behavioral results of the visual matching task for each experimental condition performed in the scanner. Mean accuracy and median reaction time for the correct trials were measured for each MZ twin (*N*=32), and the average (standard deviations in parentheses) of these scores across subjects are reported.

	Word	Pseudoword	Consonant Strings	Number Strings	False Fonts
Accuracy	98.9	98.2	98.2	98.7	96.6

(%)	(1.25)	(2.02)	(2.16)	(1.98)	(2.64)
Reaction Time (ms)	659.05 (84.57)	663.66 (85.31)	670.78 (103.61)	678.28.60 (89.18)	781.23 (111.88)

3.3.2 Response Magnitude

Many previous studies have compared neural response magnitude evoked by familiar words to unfamiliar words (e.g., foreign words or false fonts) in VWFA (Fig. 2A). In order to directly compare our results to these previous studies, mean activation levels in the ROIs were computed as shown in Figure 3-2B. There was a significant difference in the response magnitude across the four experimental conditions in the VWFA ($F_{1.92, 59.63} = 23.455$, $p < 0.001$, Greenhouse-Geisser corrected within-subject ANOVA). This effect was driven by relatively smaller response magnitude in the CS condition ($F_{1,31} = 103.391$, $p < 0.001$). There was no difference across the WD, PW, and FF conditions ($F_{1.30, 40.34} = 1.116$, $p = 0.314$, Greenhouse-Geisser corrected within-subject ANOVA).

Smaller response magnitude in the CS condition compared to the WD and PW conditions is consistent with previous studies showing hierarchical organization of VWFA (Vinckier, et al., 2007) and sensitivity to bigram frequency (Binder, et al., 2006). However, comparable response magnitude in the FF condition compared to the WD and PW conditions is different from the previous study that used the same set of false font stimuli (Vinckier, et al., 2007). This nonsignificant difference between VWFA activity evoked by words and false fonts is somewhat consistent with a previous study showing negligible difference between a familiar script and unfamiliar script (Xue & Poldrack, 2007).

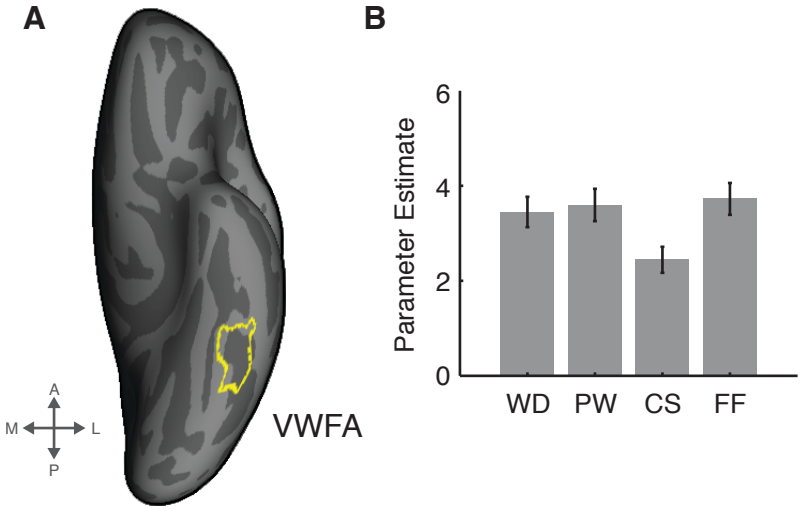

Figure 3-2 The region of interest and the mean response magnitude. A. The visual word form area (VWFA) is shown in a yellow boundary on an inflated surface of the ventral view of the left cerebral cortex. This region was defined from the second-level random-effects analysis ($p < 10^{-5}$, uncorrected; extent > 50 mm^2) of the contrast WD + PW + CS > NB from the even runs. (A: anterior; P: posterior; M: medial; L: lateral) B. Mean response magnitude in the VWFA from the odd runs. Error bars represent standard error across all participants.

3.3.3 Unique Environmental Effects in VWFA

ICC estimates between MZ twins' VWFA activation are shown in Figure 3-3A. There was a monotonic increase in ICC across the four conditions, with the smallest in ICC_{WD} and the greatest in ICC_{FF}. The difference between ICC_{FF} and ICC_{WD} was statistically significant ($p = 0.029$). This pattern is consistent with our primary hypothesis of greater unique environmental effects in the neural activity associated with familiar real word processing than unfamiliar false font processing in VWFA.

A linear contrast across the four conditions was also statistically significant ($p = 0.011$), consistent with the idea that unique environmental effects in VWFA are modulated by orthographic, phonological and semantic processing. In a post-hoc analysis, we also examined stepwise differences across the four conditions. The

difference between ICC_{WD} and ICC_{PW} was 0.023 (p = 0.426), between ICC_{PW} and ICC_{CS} was 0.188 (p = 0.080), and between ICC_{CS} and ICC_{FF} was 0.036 (p = 0.394). These results suggest that perhaps the unique environmental effect is most associated with the phonological information embedded in orthographic stimuli.

The scatter plots of the parameter estimates between MZ twins shown in Figure 3-3B show a much tighter correlation between MZ activation in the FF condition than in the WD condition as well as a monotonic trend toward tighter correlation across the conditions. Note also that these effects in ICC estimates cannot be explained by the effects of response magnitude (see Figure 3-2B).

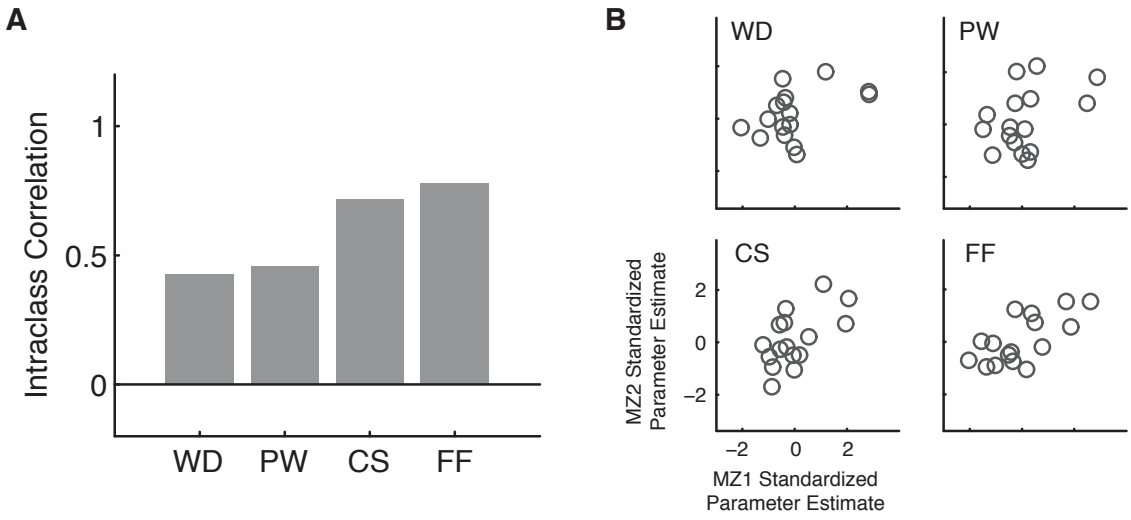

Figure 3-3 Z-transformed ICC estimates in the VWFA. A. The difference between ICC_{WD} and ICC_{FF} (p = 0.029) and the linear contrast across the four conditions (p = 0.011) was statistically significant. The difference between ICC_{PW} and ICC_{CS} was marginally significant (p = 0.080). B. The scatter plots of the standardized parameter estimates between MZ twins.

3.3.4 ICC in the Left Motor Cortex

In addition, we examined whether greater environmental effects in WD condition compared to the FF condition and the linear contrast effects are unique to the VWFA. We selected the left motor cortex as a control region to compare such effects (Figure 3-4A), because we expected little difference between the experimental conditions but robust activation in all conditions. There was a significant linear trend in the mean response magnitude in the left motor cortex as shown in Figure 4B ($F_{1,31}$ = 5.973, p = 0.020). However, there was no significant difference between ICC_{FF} and ICC_{WD} in the left motor cortex (p = 0.180) and no significant linear contrast in the ICC across the four conditions (p = 0.069) (Figure 3-4C).

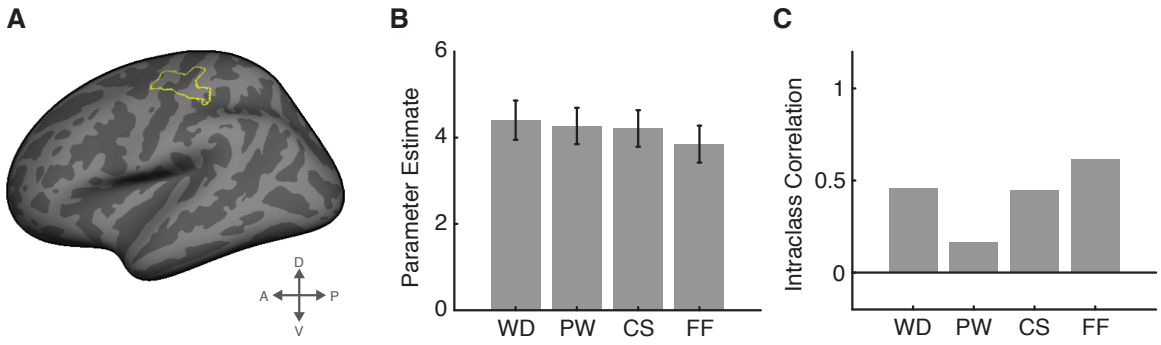

Figure 3-4 The left motor cortex serving as a control region. A. The left motor cortex was functionally defined from the group-level task-related activity (all tasks > fixation from even runs, p < 10-5, uncorrected; extent > 50 mm2) within the left sensorimotor cortex. B. Mean response magnitude in the left motor cortex from the odd runs. C. Z-transformed ICC estimates in the left motor cortex.

3.4 Discussion

In this study, we investigated how the environment that we experience influences the functional organization of the visual word form area (VWFA). Neural activations in response to words and false fonts were measured in monozygotic twins, and the proportion of phenotypic variability explained by unique environmental effects was estimated. The results showed greater unique environmental contributions to the variability of the neural activity evoked by words than false fonts, confirming the idea that the development of VWFA must be partially experientially driven. More importantly, there was a linear gradient of unique environmental effects across the four experimental conditions, i.e. greater effects of unique environment on words than pseudowords, on pseudowords than consonant strings, and on consonant strings than false fonts. Thus, the present findings support the idea that the VWFA is shaped by our experience with different subcomponents of reading over the course of development. The MZ twin correlation approach provides a unique way to investigate the role of experiential/environmental effects, which overcomes the limitations of previous studies based exclusively on mean activation magnitude.

There are two influential theoretical claims regarding the role of experience in shaping the neural architecture for written words. One theory proposes that the neurons in the left occipitotemporal region, with genetic predispositions for processing fine-grain visual features, become tuned to encode abstract representations of visual word forms (Dehaene & Cohen, 2007, 2011), thus termed the "visual word form area" (VWFA) (Cohen, et al., 2000). Another theory argues

that neurons in this occipitotemporal region become responsive to words (and possibly to other stimuli as well) due to unique top-down feedback connections from phonological and semantic processing areas (Price & Devlin, 2003, 2011). While the underlying mechanism for the development of the so-called VWFA is explained differently in the two theories, there are some common predictions that they make regarding the neural response in VWFA evoked by various types of orthographic stimuli.

One of the predictions regarding experience-dependent properties in VWFA is that the neural response will be greater when viewing known script than unknown script. This simple prediction has been tested in many previous studies using various stimuli and tasks. The results to date, however, have been somewhat mixed. One study demonstrated greater left occipitotemporal activation for native words compared to foreign words (Baker, et al., 2007), while another study demonstrated greater activation for foreign words compared to native words (Xue, et al., 2006). Another study found a non-significant difference between the two (Xue & Poldrack, 2007), and yet another reported that false fonts activated more than random letter sequences but less than real words in this region (Vinckier, et al., 2007). Lastly, one study showed greater activation for foreign words than native words in the more lateral region of the occipitotemporal cortex but the opposite pattern in the more medial region (Hashimoto & Sakai, 2004). Collectively, these studies report differences in the response magnitude for native words versus foreign words and false fonts, supporting the idea that experience leads to changes

in the neural architecture of the VWFA. However, the direction of this effect is inconsistent across studies.

Inconsistent results across studies are also apparent in studies that examine VWFA as a function of the frequency with which we encounter orthographic stimuli. Binder et al. (2006) found that the putative VWFA region is sensitive to bigram frequency showing greater activation in response to letter strings with more frequent bigrams. Vinckier et al. (2007) also found that this region is hierarchically organized showing greater activation in response to more orthographically regular letter strings. On the other hand, Kronbichler et al. (2004) found decreasing putative VWFA activation as a function of increasing word frequency even while the bigram frequency was controlled for.

In this study, we used an alternative approach to investigating the role of experience in a monozygotic twin study. Monozygotic twins (MZ) provide ways to quantify the role of unique environment in explaining differences between individuals. MZ twins are genetically identical, so it is unique environmental factors that make MZ twins different from one another. Greater MZ correlation in the false font condition than in the word condition suggests that environment plays a significantly stronger role in shaping the VWFA activation in response to words than false fonts. Furthermore, this effect was specific to the VWFA: a control region in the motor cortex showed no evidence for such an ICC difference between words and false fonts.

We also found a monotically increasing influence of unique environmental effects from false fonts to consonant strings, then to pseudowords and words in the

VWFA. This linear contrast across the four conditions suggests that there are greater unique environmental contributions as more subcomponents of reading are involved. This linear contrast, however, is mainly driven by the difference between ICC_{PW} and ICC_{CS}, which suggests that individual experience with phonological processing may be the most important experiential factor in shaping the VWFA. Nonsignificant differences between ICC_{CS} and ICC_{FF} and between ICC_{WD} and ICC_{PW} suggest that individual experiences in orthographic and semantic processing may not be as important in shaping the VWFA.

The unique role of subcomponents of reading has been tested in previous training studies (Hashimoto & Sakai, 2004; Xue, et al., 2006). Xue et al. (2006) studied how visual, phonological, and semantic training on an artificial language influence the putative VWFA activity. They found that VWFA activity decreased after visual training but increased after phonological training. Hashimoto & Sakai (2004) trained subjects to match an artificial symbol with a sound that could either be a speech sound or a nonspeech sound. They found that VWFA activity selectively increased in the speech condition, suggesting that associated phonological processing drives the development of VWFA. Our findings are consistent with these previous studies showing the relative importance of experience with phonological information in shaping the VWFA. Furthermore, our results show an effect of long-term experience overcoming the limited interpretations of the training studies. In addition, our results show a full range of experiential effects from false fonts to words.

Because reading is an acquired skill, we argue that there is no genetic advantage in processing one type of orthographic stimuli versus another. Imagine a person who has absolutely no knowledge about English letters (or any other similar Roman letters). It would be very difficult for him/her, if not impossible, to tell whether an item presented in our experiment is a word, pseudoword, consonant string, or a string of false fonts. Thus, any difference in MZ correlation observed in our study can be attributed to differences in environmental effects on the four conditions. Importantly, the observed differences among MZ correlations cannot be explained by overall response magnitude effects (Fig. 2B). This study, therefore, provides a unique way to investigate environmental effects on neural activity, overcoming limitations in previous studies where interpretations are based exclusively on response magnitude.

The present findings provide direct evidence for environmental contributions to the neural representations of written words. These results overcome limitations of previous studies that interpret data based exclusively on response magnitude. In addition, our results suggest that phonological processing may have the largest contribution in shaping the neural representation of words in the VWFA. In sum, they illustrate how the environment we experience can make qualitative changes in the brain and may even induce neural specialization for a cultural convention.

3.5 Appendix

3.5.1 Voxel-level MZ Correlation

While the MZ correlations can be estimated from the mean activation values within the region of interest as presented in the main section of this study, this mean-ROI method imposes a strong assumption of spatial homogeneity. If this assumption is not met, then the estimate may result in bias (see Chapter 2). In addition, the mean-ROI method prevents us from identifying a possible correlated subregion within the ROI. One way to overcome these limitations in the mean-ROI analysis is to use the novel statistical method that is introduced in Chapter 2. This spatial decomposition method allows us to efficiently estimate a correlation between patterns of neural activity, by incorporating information about spatial patterns inherent in the neural activity.

Intraclass correlation (ICC) maps of neural activity in response to WD, FF, PW, and CS between MZ twins were estimated by applying this spatial decomposition approach (Chapter 2). First, the basis volumes were derived from the task-related neural activation patterns (all conditions > fixation) estimated from the even runs. This procedure resulted in a matrix of 831 vertices by 33 (= 32 subjects + 1 intercept) images of neural activation patterns. Then, the eigenvectors of its covariance matrix served as the basis volumes.

Using these basis volumes, the spatial decomposition method was used to estimate the ICC of the activation patterns estimated from odd runs of WD, FF, PW, and CS conditions, with linear effects of age and sex removed. This procedure resulted in an ICC map of WD (ICC_{WD}), FF (ICC_{FF}), PW (ICC_{PW}), and CS (ICC_{CS}) in two

separate ROIs (the VWFA and the left motor cortex). Then, Fisher's r-to-z transformation was applied to these ICC maps for comparisons between different ICC estimates.

3.5.2 ICC Difference Between WD and FF

We first tested whether any region within a particular ROI showed significantly greater ICC_{FF} than ICC_{WD}. Statistical significance of this effect was computed using a permutation method incorporating a clusterwise correction for multiple comparisons (Holmes, Blair, Watson, & Ford, 1996; Nichols & Holmes, 2002). In this method, a magnitude threshold is first determined, and the size of the suprathreshold clusters undergoes the statistical significance test.

To be specific, the observed difference map (i.e. $ICC_{FF} - ICC_{WD}$) was first computed and recorded. Then, in order to set a magnitude threshold, we computed a *z*-score map of this difference map using a permutation scheme. In a total of 10,000 repetitions, the condition labels in each paired patterns were permuted within each pair, and the difference map was computed from each of the permuted sample. This permutation scheme is based on the null hypothesis that there is no difference between the ICC's for the WD versus the FF conditions. This procedure results in a null distribution of 10,000 estimates in each vertex. Then, the observed difference map was divided by the standard deviation of this null distribution, which resulted in a *z*-score map of the effect of interest (i.e. $ICC_{FF} - ICC_{WD}$). Among all the vertices that resulted in $p < 0.05$ ($z > 1.645$), the median difference value was set as the magnitude threshold. For instance, the resulting magnitude threshold was 0.188 in the VWFA. Note that if none of the vertices exceed $z > 1.645$ in the *z*-score map of

the effect of interest, then no magnitude threshold is set, which in turn simply means that the effect of interest is not statistically significant.

Using the magnitude threshold, a clusterwise correction for multiple comparisons was performed in order to test whether the size of any of the suprathreshold clusters was statistically significant. For example, there was one suprathreshold cluster (169 vertices) in the VWFA. The null distribution of the cluster size in these ROIs was constructed by recording the size of the largest suprathreshold cluster (under the identical magnitude threshold setting) from the difference maps of the *permuted* sample. The *p*-values of the size of the suprathreshold clusters from the *observed* difference map were computed based on the proportion of the null distribution exceeding the observed sizes.

3.5.3 Linear Contrast of ICC

While our primary hypothesis was that ICC_{FF} is greater than ICC_{WD}, we also tested how ICC_{PW} and ICC_{CS} are different from ICC_{FF} and ICC_{WD}. Previous studies have suggested that the acquisition of phonological and semantic knowledge about words may be critical in the development of VWFA (Hashimoto & Sakai, 2004; Xue, et al., 2006). The PW condition lacks semantics relative to the WD condition, and the CS condition further lacks phonology relative to the PW condition. Thus, if the acquisition of phonology and semantics over the course of schooling affects VWFA activation, then we should expect ICC_{PW} to be greater than ICC_{WD}, and ICC_{CS} to be greater than ICC_{PW} but smaller than ICC_{FF}.

We therefore tested for a significant linear contrast over the four conditions. First, a linear contrast map was constructed from a weighted average of the four ICC

maps (i.e. $(3/4)\times ICC_{FF} + (1/4)\times ICC_{CS} - (1/4)\times ICC_{PW} - (3/4)\times ICC_{WD}$). Then, using a clusterwise correction for multiple comparisons procedure and a permutation scheme, we tested whether any of the suprathreshold clusters (exceeding a magnitude threshold derived from the *z*-score map) were statistically significant in size.

3.5.4 ICC in the VWFA

ICC estimates between MZ twins' neural activation in the VWFA are shown in Figure 3-5A. Visually, ICC_{FF} was greater than ICC_{WD}, particularly in the middle portion of the VWFA, consistent with our primary hypothesis that there exists more environmental effects in the neural activity associated with real word processing than false fonts processing in VWFA. Numerically, the difference map ($ICC_{FF} - ICC_{WD}$, Figure 3-5B) resulted in a significant cluster in the center of the VWFA ($p = 0.0481$).

Additionally, we tested whether there was a significant linear relationship among ICC estimates of the four conditions. A linear contrast map (Figure 3-5C) indeed resulted in a significant cluster in the center of the VWFA ($p = 0.0378$).

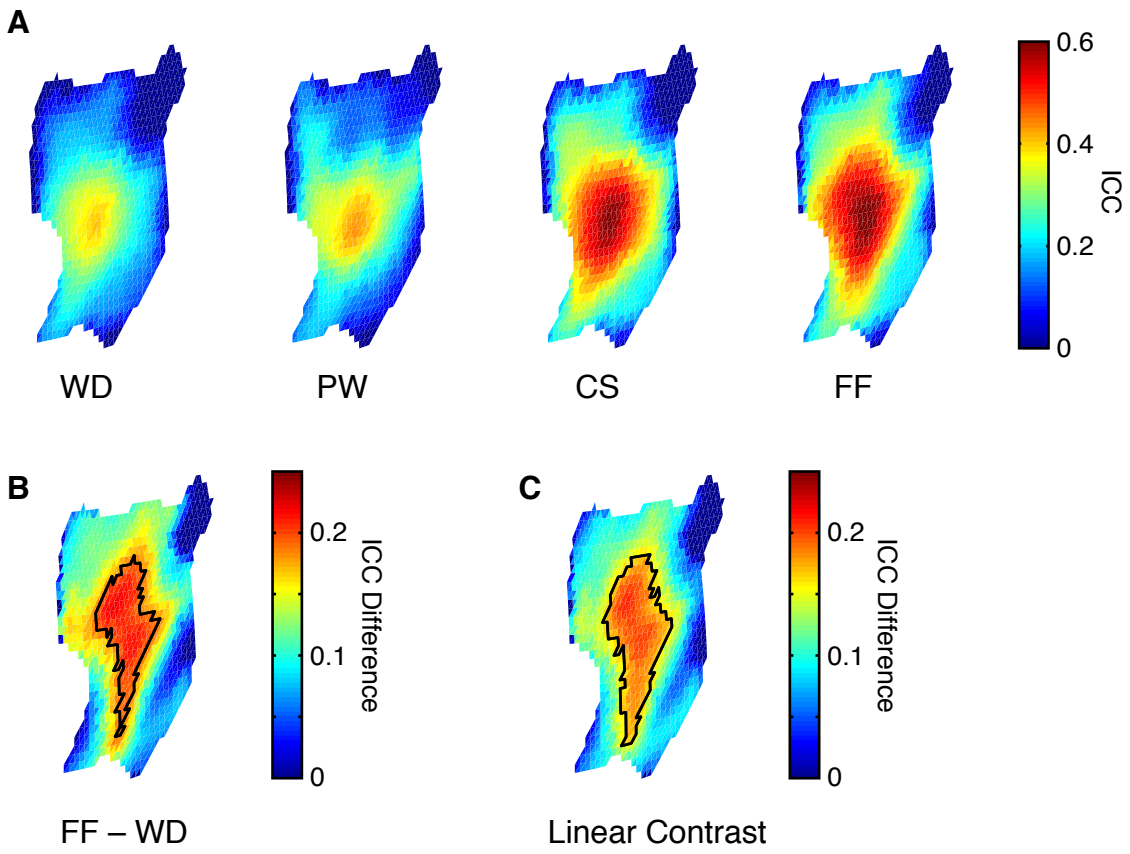

Figure 3-5 ICC maps in the VWFA. A. Topographic maps of ICC_{WD}, ICC_{PW}, ICC_{CS}, and ICC_{FF} within the VWFA. B. ICC difference map between the WD and FF conditions. The suprathreshold cluster (magnitude threshold = 0.188, cluster size = 169 vertices) was statistically significant in size (p = 0.0481). C. The linear contrast map among all conditions. The suprathreshold cluster (magnitude threshold = 0.163, cluster size = 218 vertices) was statistically significant in size (p = 0.0378) as well. The color bars in all topographic figures represent an r-to-z transformed ICC estimate. Suprathreshold cluster is identified in a thick black boundary.

3.5.5 ICC in the left motor cortex

In addition, we examined whether greater environmental effects in WD condition compared to the FF condition and the linear contrast effects are unique to the VWFA. In the left motor cortex (Figure 3-6), none of these effects were statistically significant (p > 0.2046 in the difference map and p > 0.1345 in the linear contrast map).

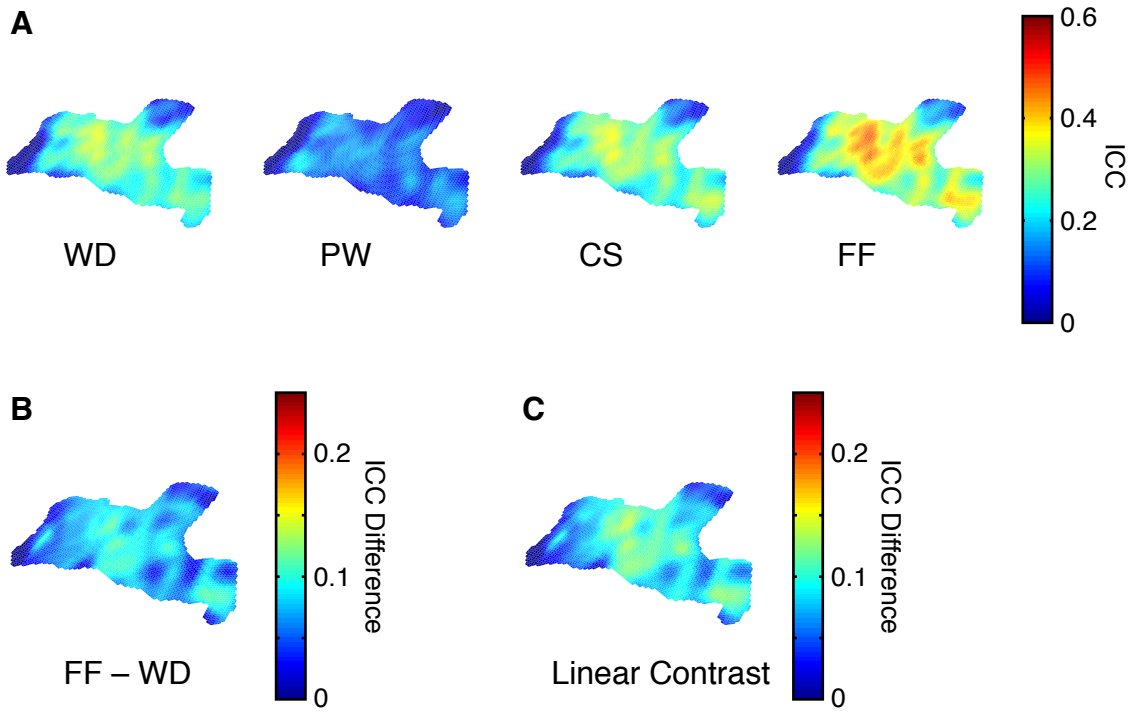

Figure 3-6 ICC maps in the left motor cortex derived from the spatial decomposition method. A. Topographic maps of ICC_{WD}, ICC_{PW}, ICC_{CS}, and ICC_{FF} within the left motor cortex. B. ICC difference map between the WD and FF conditions. This difference map had a magnitude threshold of 0.069, which resulted in four suprathreshold clusters (10, 65, 366, and 1978 vertices). None of them was statistically significant in size ($p > 0.2046$). C. The linear contrast map among all conditions. This map had a magnitude threshold of 0.079, which resulted in three suprathreshold clusters (35, 395, and 1934 vertices). None of them was statistically significant in size ($p > 0.1345$).

3.5.6 Mean-ROI vs. Spatial Decomposition Methods

In Chapter 2, I described several relative advantage of the spatial decomposition method compared to the mean-ROI method. First, the spatial decomposition method relaxes the assumption of spatial homogeneity, so it enables us to identify correlated subregion within the ROI. Second, if this assumption is highly violated, then the mean-ROI method is likely to result in biased estimates. In investigating the MZ correlations in the VWFA in this Chapter, however, the

performance of the spatial decomposition method and the mean-ROI method was comparable. That is, both methods were able to detect significant MZ correlations in VWFA. That is, incorporating the spatial decomposition method did not add much value to the more conventional mean-ROI method. This may have been due to the special characteristics of the ROI in the current study. It is possible that this relatively small ROI is somewhat spatially homogeneous. So, relaxation of this assumption at a cost of slight conservative bias in the spatial decomposition method perhaps did not result in overall advantage of this novel method.

3.6 References

Baker, C. I., Liu, J., Wald, L. L., Kwong, K. K., Benner, T., & Kanwisher, N. (2007). Visual word processing and experiential origins of functional selectivity in human extrastriate cortex. *Proceedings of the National Academy of Sciences of the United States of America, 104*(21), 9087-9092.

Ben-Shachar, M., Dougherty, R. F., Deutsch, G. K., & Wandell, B. A. (2007). Differential sensitivity to words and shapes in ventral occipito-temporal cortex. *Cereb Cortex, 17*(7), 1604-1611.

Binder, J. R., Medler, D. A., Westbury, C. F., Liebenthal, E., & Buchanan, L. (2006). Tuning of the human left fusiform gyrus to sublexical orthographic structure. *Neuroimage, 33*(2), 739-748.

Bolger, D. J., Perfetti, C. A., & Schneider, W. (2005). Cross-cultural effect on the brain revisited: universal structures plus writing system variation. *Hum Brain Mapp, 25*(1), 92-104.

Cohen, L., Dehaene, S., Naccache, L., Lehericy, S., Dehaene-Lambertz, G., Henaff, M. A., et al. (2000). The visual word form area - Spatial and temporal characterization of an initial stage of reading in normal subjects and posterior split-brain patients. *Brain, 123*, 291-307.

Cohen, L., Lehericy, S., Chochon, F., Lemer, C., Rivaud, S., & Dehaene, S. (2002). Language-specific tuning of visual cortex functional properties of the Visual Word Form Area. *Brain, 125*, 1054-1069.

Dehaene, S., & Cohen, L. (2007). Cultural recycling of cortical maps. *Neuron, 56*(2), 384-398.

Dehaene, S., & Cohen, L. (2011). The unique role of the visual word form area in reading. *Trends Cogn Sci, 15*(6), 254-262.

Dehaene, S., Pegado, F., Braga, L. W., Ventura, P., Nunes Filho, G., Jobert, A., et al. (2010). How learning to read changes the cortical networks for vision and language. *Science, 330*(6009), 1359-1364.

Falconer, D. S., & Mackay, T. F. C. (1996). Introduction to Quantitative Genetics (4 ed., pp. 160-183). Harlow, Essex, UK: Longmans Green.

Fisher, R. A. (1954). *Statistical Methods for Research Workers* (12th ed.): Oliver and Boyd.

Hashimoto, R., & Sakai, K. L. (2004). Learning Letters in Adulthood: Direct Visualization of Cortical Plasticity for Forming a New Link between Orthography and Phonology. [doi: DOI: 10.1016/S0896-6273(04)00196-5]. *Neuron, 42*(2), 311-322.

Holmes, A. P., Blair, R. C., Watson, J. D. G., & Ford, I. (1996). Nonparametric analysis of statistic images from functional mapping experiments. *Journal of Cerebral Blood Flow and Metabolism, 16*(1), 7-22.

Jobard, G., Crivello, F., & Tzourio-Mazoyer, N. (2003). Evaluation of the dual route theory of reading: a metanalysis of 35 neuroimaging studies. [doi: DOI: 10.1016/S1053-8119(03)00343-4]. *NeuroImage, 20*(2), 693-712.

Kronbichler, M., Hutzler, F., Wimmer, H., Mair, A., Staffen, W., & Ladurner, G. (2004). The visual word form area and the frequency with which words are encountered: evidence from a parametric fMRI study. *Neuroimage, 21*(3), 946-953.

McCandliss, B. D., Cohen, L., & Dehaene, S. (2003). The visual word form area: expertise for reading in the fusiform gyrus. *Trends in Cognitive Sciences, 7*(7), 293-299.

Mechelli, A., Humphreys, G. W., Mayall, K., Olson, A., & Price, C. J. (2000). Differential effects of word length and visual contrast in the fusiform and lingual gyri during reading. *Proc Biol Sci, 267*(1455), 1909-1913.

Nichols, T. E., & Holmes, A. P. (2002). Nonparametric permutation tests for functional neuroimaging: A primer with examples. *Human Brain Mapping, 15*(1), 1-25.

Nobre, A. C., Allison, T., & McCarthy, G. (1994). Word recognition in the human inferior temporal-lobe. *Nature, 372*(6503), 260-263.

Polk, T. A., & Farah, M. J. (1998). The neural development and organization of letter recognition: Evidence from functional neuroimaging, computational modeling, and behavioral studies. *Proceedings of the National Academy of Sciences of the United States of America, 95*(3), 847-852.

Price, C. J., & Devlin, J. T. (2003). The myth of the visual word form area. *Neuroimage, 19*(3), 473-481.

Price, C. J., & Devlin, J. T. (2011). The Interactive Account of ventral occipitotemporal contributions to reading. *Trends Cogn Sci,* 15(6), 246-253.

Pugh, K. R., Shaywitz, B. A., Shaywitz, S. E., Constable, R. T., Skudlarski, P., Fulbright, R. K., et al. (1996). Cerebral organization of component processes in reading. Brain, 119 (Pt 4), 1221-1238.

Schlaggar, B. L., & McCandliss, B. D. (2007). Development of neural systems for reading. *Annual Review of Neuroscience, 30*, 475-503.

Starrfelt, R. (2007). Selective alexia and agraphia sparing numbers-a case study. *Brain Lang, 102*(1), 52-63.

Vinckier, F., Dehaene, S., Jobert, A., Dubus, J. P., Sigman, M., & Cohen, L. (2007). Hierarchical coding of letter strings in the ventral stream: Dissecting the inner organization of the visual word-form system. *Neuron, 55*(1), 143-156.

Xue, G., Chen, C., Jin, Z., & Dong, Q. (2006). Language experience shapes fusiform activation when processing a logographic artificial language: an fMRI training study. *Neuroimage, 31*(3), 1315-1326.

Xue, G., & Poldrack, R. A. (2007). The neural substrates of visual perceptual learning of words: implications for the visual word form area hypothesis. *J Cogn Neurosci, 19*(10), 1643-1655.

Chapter 4

Neural dissociation of number from letter recognition and its relationship to parietal numerical processing

4.1 Introduction

Despite the fact that letters and numbers are cultural inventions and the distinction between them is physically arbitrary, the visual recognition of letters is dissociable from the visual recognition of numbers. This dissociation of letter recognition from number recognition has been found in behavioral studies (Hamilton, Mirkin, & Polk, 2006; Jonides & Gleitman, 1972; Polk & Farah, 1995), neuropsychological studies (Anderson, Damasio, & Damasio, 1990; Ingles & Eskes, 2008; Starrfelt, 2007), electrophysiological studies (Allison, McCarthy, Nobre, Puce, & Belger, 1994; Wong, Gauthier, Woroch, DeBuse, & Curran, 2005), and neuroimaging studies (Flowers et al., 2004; James, James, Jobard, Wong, & Gauthier, 2005; Joseph, Cerullo, Farley, Steinmetz, & Mier, 2006; Pernet, Celsis, & Demonet, 2005; Polk & Farah, 1998; Polk et al., 2002; Puce, Allison, Asgari, Gore, & McCarthy, 1996). These findings are significant because letters and numbers are arbitrary symbols and the distinction between them is simply a cultural convention. If they are processed differently at both behavioral and neural levels, it suggests that early

schooling experiences can lead to qualitative changes in neurocognitive architecture.

Nevertheless, inferring that two tasks depend on separate underlying processes based on single or one-way dissociations is problematic (Shallice, 1988). For example, if task A is harder than task B, then brain damage might selectively impair task A even if the two tasks depend on the same neural substrates. Similarly, if task A produces greater breadth or more areas of activation than task B in a neuroimaging experiment, it might merely reflect the fact that task A is more demanding, not that the tasks depend on dissociable neural systems.

Ideally then, one would like to demonstrate that number recognition is also dissociable from letter recognition, thereby establishing a double dissociation and undermining alternative hypotheses. Some electrophysiological studies have found number-specific responses from specific inferotemporal electrodes (Allison et al., 1994; Roux, Lubrano, Lauwers-Cances, Giussani, & Demonet, 2008) consistent with the hypothesis that number recognition is dissociable from letter recognition, but evidence from patient studies and neuroimaging is scarce. Although patients with numerical processing deficits (acalculia) are commonly reported, we know of no reports of patients with a specific deficit in the visual recognition of numbers relative to letters and words (but see the following reports for descriptions of patients with deficits in the verbal production of number names: Cipolotti, Warrington, & Butterworth, 1995; Marangolo, Nasti, & Zorzi, 2004). And very few neuroimaging studies have directly contrasted the visual recognition of numbers with the recognition of letters. Polk et al. (2002) attempted to do so, but only

reported significant activation for numbers in three subjects, and no significant activation was reported at the group level. In Experiment 1, we use new procedures and study a larger group of subjects to examine directly the neural dissociation of number recognition from letter recognition.

If letter and number recognition rely (at least in part) on different neural systems, a natural question is why. Dehaene and colleagues' neuronal recycling hypothesis proposes that acquired functions like letter and number recognition exploit and reorganize evolutionarily older neural circuits originally performing similar functions (Dehaene & Cohen, 2007). According to this view, one of the reasons that the so-called visual word form area (VWFA) tends to develop in left occipitotemporal cortex is because this area has relatively direct connections to and from anterior language processing sites in the left hemisphere (McCandliss, Cohen, & Dehaene, 2003).

A recent electroencephalogram (EEG) study has provided indirect support for this hypothesis (Cai, Lavidor, Brysbaert, Paulignan, & Nazir, 2008). While it has been known that VWFA lies in the left inferior temporal region in most right-handed subjects (Cohen et al., 2002), Cai et al. (2008) tested its lateralization in left-handed subjects in whom anterior language processing regions are commonly right-lateralized. Four of the nine left-handed subjects showed right-lateralized frontal activity in a verb generation task, and these four subjects also exhibited stronger right-sided negativity in inferior temporal sites. Based on these results, they argued that the localization of word recognition in ventral visual cortex depends on the localization of spoken language processes in frontal cortex.

Following this reasoning, we hypothesized that the location of cortical areas involved in visual number recognition might depend on the location of cortical areas involved in higher-order numerical processing in parietal cortex. Specifically, participants whose higher-order numerical processing is more right-lateralized in parietal cortex would also tend to exhibit more right-lateralized number recognition in ventral visual cortex, and vice versa. We tested these predictions in Experiment 2 by measuring neural activity in response to higher-order numerical processing tasks (addition, subtraction, counting) in the same participants. We then investigated whether the lateralization of this higher-order numerical processing activity correlated with the lateralization of lower-order number recognition activity in ventral visual cortex.

4.2 Experiment 1

4.2.1 Methods

Participants. 20 healthy young adults (ages 18-29 with mean of 23.4; 9 males) participated in the study. All participants were screened to ensure they were right-handed, native English speakers, psychologically and physically healthy, not taking medications with psychotropic or vascular effects, and free of any other MRI safety contraindications. All study procedures were reviewed and approved by the Institutional Review Boards at the University of Texas at Dallas, the University of Texas Southwestern, and the University of Michigan, All participants provided detailed written consent prior to their involvement in the study.

Stimulus Materials. Five types of stimuli were created for use in the study. All five types consisted of two strings, 4.2° above and below the central cross (examples are shown in Figure 4-1). Participants made a "same/different" judgment on each pair of strings. The primary stimuli of interest were letter consonant strings and number strings. All strings were composed of four letters/numbers (mono-spaced type-face with 2° visual angle in height), and only capital letters were used. Three other types of stimuli—words, pseudowords, and false fonts (adapted from Vinckier et al., 2007)—were included, although the focus of this study was on consonant and number strings. Pseudowords (pronounceable nonwords) were created with constrained trigram-based strings (Medler & Binder, 2005, MCWord: An On-Line Orthographic Database of the English Language. http://www.neuro.mcw.edu/mcword/), and real words with mean word frequency of 323.6 per million (ranging from 205.4 to 497.3) were included.

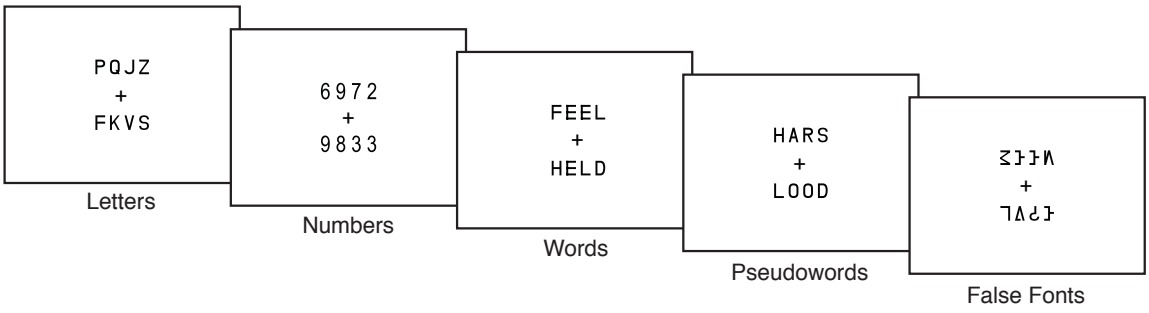

Figure 4-1 Examples of stimuli used in Experiment 1. Participants performed a visual matching task and judged whether the two items are same or different.

Procedure. The task consisted of five 5-minute runs with eighteen 16-sec blocks, pseudorandomly ordered (three for each of the five categories in addition to

three blocks of fixation). Each block consisted of 8 trials (1.5 sec of presentation and 0.5 sec of inter-trial interval) in which participants made a same/different judgment on each pair of strings. The correct answer was "same" in half of all the trials. All visual stimuli were presented via E-prime (Psychology Software Tools, Pittsburgh, PA) and displayed by a back-projection system. Participants made responses using buttons under the right index and middle fingers (Lumina response pad; Cedrus, San Pedro, CA).

Data Acquisition. Brain images were acquired with a Philips Achieva 3T whole-body scanner at UT Southwestern using the Philips SENSE parallel acquisition technique. Functional scans were acquired as axial slices, with a voxel size of 3.4 mm × 3.4 mm × 3.5 mm. At each of 148 BOLD acquisitions per run, 43 axial slices were acquired (covering the whole brain; TR = 2.0 s, TE = 25 ms). A high-resolution axial T1 MPRAGE was acquired primarily to facilitate group registration (voxel size 1 mm isotropic; TR = 8.27 ms, TE = 3.82 ms).

Activation Analysis. Data were preprocessed using SPM5 (Wellcome Department of Cognitive Neurology, London, UK, www.fil.ion.ucl.ac.uk). Functional images underwent slice-timing correction and realignment to the mean volume. Each participant's T1 anatomical image was coregistered with the functional images and then segmented into gray matter, white matter, and cerebral spinal fluid. The gray matter was normalized into the default gray matter probability template in standard MNI (Montreal Neurological Institute) space, and the acquired normalization parameters were used to normalize the functional images for each individual with a spatial resolution of 3 mm × 3 mm × 3 mm.

Activations in response to each stimulus type (numbers, letters, words, pseudowords, false fonts) in contrast to fixation were estimated using the standard general linear model (GLM) with a high-pass filter at 128 Hz and correcting for temporal autocorrelation with an AR(1) model. The model included separate regressors for each of the experimental conditions convolved with a canonical hemodynamic response function, as well as six nuisance covariates modeling head translation and rotation. In each subject, "letter-preferred activation" was defined by contrasting consonant strings to number strings, and "number-preferred activation" was defined by contrasting number strings to consonant strings. These contrast maps from each subject were then entered into a second-level random effects group analysis in order to identify letter- and number-preferred activity at the group level (see Figure 4-3).

Laterality Analysis. To assess laterality for letter-preferred activity, we first created a region of interest (ROI) based on the letter-preferred (letter vs. number) group activation map within a bilateral anatomical mask including the fusiform, inferior and middle temporal, and inferior occipital gyri (defined using Pick-Atlas toolbox, http://www.fmri.wfubmc.edu/cms/software). The activation map was thresholded at a relatively lenient threshold ($p < 0.05$, extent > 20 voxels) within the anatomical mask to accommodate individual differences in the location of letter-preferred activation in individual participants. This approach yielded 216 voxels all of which were in left ventral visual cortex. Finally, we added all the corresponding 216 voxels in the right hemisphere (flipping the sign of the x-coordinates) in order

to make this ROI symmetric. This bilateral ROI constructed from the group-level letter-preferred activation map is referred to as the visual letter ROI.

We applied the same procedure to create a visual number ROI. The number-preferred (number vs. letter) group activation yielded 343 voxels within the same anatomical mask, all in the right ventral visual cortex. We then added the 343 corresponding voxels from the left hemisphere to create the visual number ROI.

We then computed laterality indices for each individual participant's letter-preferred activity in the visual letter ROI and number-preferred activity in the visual number ROI using a threshold-independent laterality index that was computed following Suarez et al. (2009). This approach was validated to be more robust and unambiguous compared to threshold-dependent methods in a study determining language dominance validated against the intracarotid amytal test (Suarez et al., 2009). In this method, histograms of the number of voxels with positive *t*-values were generated separately in the left and the right hemisphere of each bilateral ROI. These histograms were multiplied by a weighting function defined as t^2 (as suggested by Suarez et al., 2009), and areas under the each of the weighted histograms were computed. Then, the laterality index (LI) was computed using the conventional ratio $LI = (Q_L - Q_R) / (Q_L + Q_R)$, where Q_L denotes the area under the weighted histograms from the left hemisphere and Q_R denotes the same area from the right hemisphere. An LI of 1 indicates complete left hemisphere dominance, and an LI of -1 indicates complete right hemisphere dominance.

4.2.2 Results

Behavioral Results. Accuracy on the visual matching task was above 95% for all conditions (Table 4-1). Reaction time for the letter (consonant strings) condition was slightly faster than for the number condition ($t_{19} = 2.007$, $p < 0.059$, paired t-test). The reaction times for the three orthographic conditions (real words, pseudowords, and consonant strings) did not show any significant difference ($p > 0.220$ for the three paired t-tests). Reaction time to the false fonts was the slowest of all the conditions ($t_{19} = 11.602$, $p < 0.001$ for the contrast of false fonts versus all other conditions).

Table 4-1 Behavioral results of the visual matching task for each experimental condition performed in the scanner (N=20). Mean accuracy and median reaction time for the correct trials were measured for each subject, and the average (standard deviations in parentheses) of these scores across subjects are reported.

	Word	Pseudoword	Consonant Strings	Number Strings	False Fonts
Accuracy (%)	98.9 (1.20)	97.9 (1.85)	98.1 (1.70)	99.0 (1.29)	96.2 (2.91)
Reaction Time (ms)	679.30 (91.21)	679.65 (95.16)	691.00 (111.49)	712.60 (98.68)	801.75 (111.02)

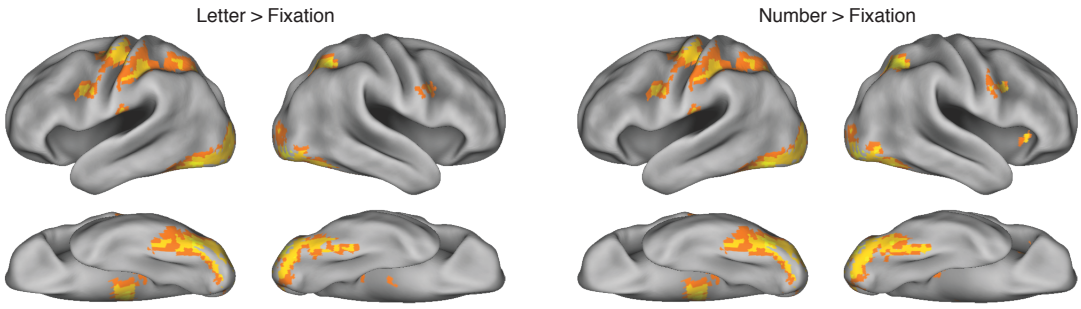

Figure 4-2 Group-level (N=20) activation maps of letters and numbers relative to fixation, thresholded at $p < 0.001$ (uncorrected) with extent greater than 20 voxels, overlaid on to a 3D inflated surface using Caret PALS atlas (http://brainvis.wustl.edu/wiki/index.php/Caret:About) for visualization.

Letter- and Number-Preferred Activation. Both the letter and number conditions showed greater BOLD response compared to the fixation condition in various regions including the bilateral ventral visual cortex and the left sensorimotor cortex (Figure 4-2). Moreover, when the letter condition and the number condition were contrasted directly, letters activated an area in left ventral visual cortex more than numbers while numbers activated an area in right ventral visual cortex more than letters at the group level (Figure 4-3). The left mid-fusiform and inferior temporal area and the left angular gyrus were the only two regions that passed the cluster-level threshold in the letter-preferred (letter vs. number) activation map, and the right lateral occipital area was the only region that passed the threshold in the number-preferred (number vs. letter) activation map (Table 4-2).

Table 4-2 Statistics on the clusters of letter-preferred activation (letter vs. number) and number-preferred activation (number vs. letter) surviving the threshold of $p < 0.005$ and extent greater than 20. The peak *z*-scores and coordinates (in MNI space) are reported with the voxelwise uncorrected *p*-value and cluster-level corrected *p*-value.

	Z-score (*t*-score)	Coordinates (x, y, z in mm)	*p* (cluster-level corrected)	*p* (voxelwise uncorrected)
Letter > Number	4.60 (6.36)	-57 -28 28	< 0.001	2.11×10^{-6}
	4.12 (5.33)	-36 -37 -23	0.005	1.91×10^{-5}
	3.81 (4.75)	24 -43 58	0.328	0.005
	3.47 (4.16)	51 -25 34	0.118	0.002
	3.32 (3.92)	3 20 34	0.721	0.016
Number > Letter	3.65 (4.47)	48 -73 -2	0.010	7.12×10^{-5}

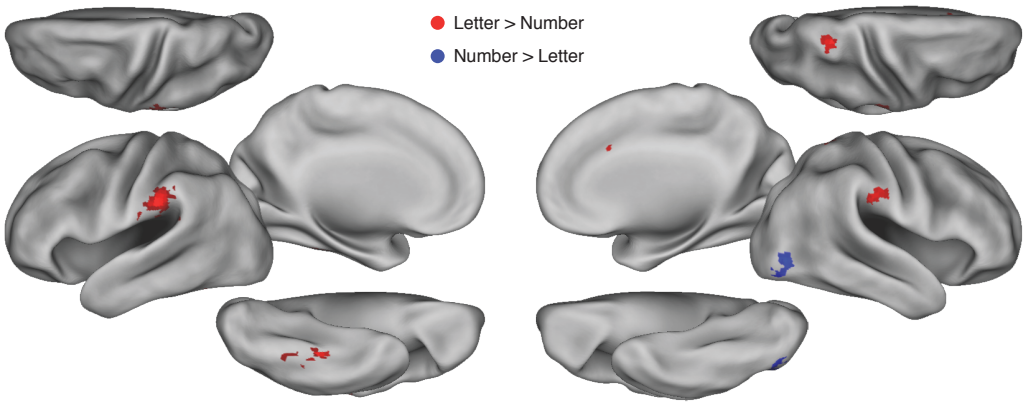

Figure 4-3 Letter- and number-preferred activation maps. Letters in contrast to numbers activated the left mid-fusiform/inferior temporal area (p = 0.005, cluster-level correction for multiple comparisons) while numbers in contrast to letters activated the right lateral occipital area (p = 0.010). Complete coordinates of clusters are reported in Table 4-2. For visualization, these group-level functional maps (p < 0.005, cluster extent > 20 voxels) were overlaid on to a 3D inflated surface as in Figure 4-2.

Examination of the letter- and number-preferred activation at the individual subject level confirmed this overall pattern identified in the group-level results. With a relatively strict threshold for multiple comparisons correction (FDR, q < 0.05), fourteen subjects exhibited a significant dissociation between letter and number recognition within the pre-specified anatomical ventral visual mask (either significant letter-preferred activation, significant number-preferred activation, or both). Of the fourteen, seven showed significant activation for letter compared with number recognition, and all seven had more voxels activated in the left hemisphere than in the right hemisphere. Ten of the fourteen subjects showed significant activation for number compared with letter recognition, and nine of the ten had more voxels activated in the right hemisphere. With a more lenient threshold (p < 0.001, uncorrected), all twenty subjects showed a significant dissociation (of any kind) between letter and number recognition within the anatomical mask.

Seventeen subjects exhibited letter-preferred activation, and fourteen of the seventeen had more voxels activated in the left hemisphere than in the right hemisphere. Fifteen subjects exhibited number-preferred activation, and twelve of these subjects showed more voxels activated in the right hemisphere than in the left hemisphere. These results collectively suggest that dissociation is observable on an individual level, and that individuals typically show more activation in the left visual cortex for letters and more activation in the right visual cortex for numbers. More quantitative measures of laterality are reported below in the Laterality Analysis section.

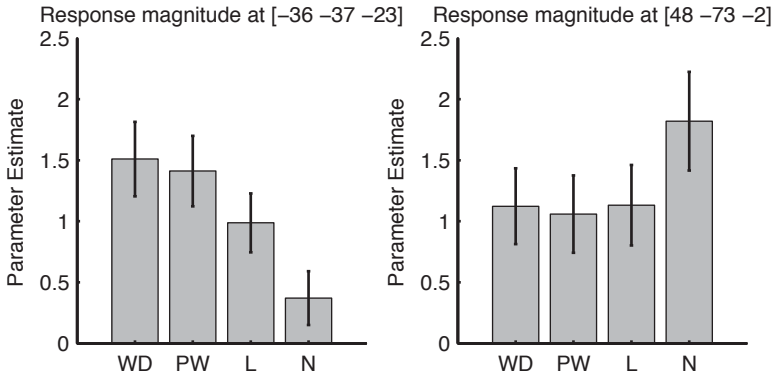

Figure 4-4 Average of the mean beta-values within the 5-mm spherical ROI around the peaks in the visual letter area and the visual number area. The error bar denotes standard error of the mean across 20 subjects (WD: word; PW: pseudoword; L: letter; N: number).

Additionally, we examined the pattern of activation in response to other types of orthographic stimuli (i.e. pseudowords, real words). A 5-mm spherical ROI was constructed around the peak in the visual letter ROI [-36 -37 -23] and the peak in the visual number ROI [48 -73 2] and the average of the mean beta-values across subjects within these spheres was compared across conditions (Figure 4-4). In the

visual letter sphere, there was a linear increase in the beta-values from consonant strings to pseudowords to real words ($F_{1,19}$ = 16.006, p = 0.001, repeated-measures ANOVA with linear contrast). This pattern of activation in the left ventral visual area is consistent with previous findings demonstrating hierarchical organization in the VWFA (Vinckier et al., 2007). In the visual number sphere, no such pattern was observed; this area showed greater BOLD response to numbers than to both pseudowords (t_{19} = 5.858, p < 0.001, paired t-test) and real words (t_{19} = 7.431, p < 0.001, paired t-test). Responses to false fonts in these ROIs were also examined. Like the previous report (Vinckier et al., 2007), false fonts activated more than letters and numbers in both the posterior letter area (t_{19} = 6.558, p < 0.001) and the posterior number area (t_{19} = 6.662, p < 0.001) perhaps they were more demanding and required significantly more time to process.

Laterality Analysis. As can be seen in Figure 4-3, letter-preferred activity was left lateralized while number-preferred activity was right lateralized at the group level. This pattern was quantitatively confirmed at the individual level by the laterality analysis in which letter-preferred activity was left-lateralized across subjects on average (laterality index (LI) = 0.715 ± 0.329, mean and standard deviation) and number-preferred activity was right-lateralized across subjects on average (LI = -0.544 ± 0.305). Positive LI represents left lateralization and negative LI represents right lateralization. However, as indicated by the standard deviations, these laterality indices varied across subjects. The letter-preferred activity LI ranged from 0.451 to 0.987 (excluding one outlier who had a LI = -0.486, see Figure 4-7 subpanel), and the number-preferred activity LI ranged from -0.984 to 0.118.

The letter activity LI and the number activity LI were not correlated (r = -0.124, p = 0.614), suggesting that laterality of letter and number recognition are likely to be independent.

4.2.3 Discussion

In Experiment 1, we confirmed a left-lateralized ventral visual area that responded significantly more to letters than numbers, replicating previous studies (Baker et al., 2007; James et al., 2005; Polk & Farah, 1998; Polk et al., 2002; Reinke, Fernandes, Schwindt, O'Craven, & Grady, 2008). More importantly, we also identified a right-lateralized ventral visual area that responded significantly more to numbers compared to letters. Together, these results constitute a double dissociation between letter and number recognition and provide perhaps the strongest evidence to date that letter and number recognition, at least in part, rely on different neural systems.

While number-preferred activation was strongly right-lateralized in the group analysis, there were substantial individual differences in the laterality of individual participants. What factors might influence the lateralization of number recognition in the brain? One hypothesis is that lateralization depends on patterns of neural connectivity. For example, Cai et al. (2008) found that the laterality of ventral visual activity in response to visual word recognition correlated with the laterality of frontal activity for spoken language (which varied in left- and right-handers). They argued that this finding was due to the important functional connections between written and spoken language.

Following this reasoning, in Experiment 2 we investigated whether a similar mechanism might be at work in the lateralization of number recognition. Specifically, we tested the hypothesis that the lateralization of number recognition might be significantly correlated with the lateralization of higher-order numerical processing (addition, subtraction, counting) which is known to depend on parietal cortex.

4.3 Experiment 2

4.3.1 Methods

Participants. The same 20 healthy young adults (ages 18-29) that participated in Experiment 1 also participated in Experiment 2 within the same fMRI session.

Stimulus Materials and Procedure. There were four types of stimuli used to perform different simple mathematical judgments (examples are shown in Figure 4-5). The number-matching stimuli were comprised of two arrays—one on the left and the other on the right of an equal sign. The items within the two arrays varied in numerosity (from one to four) and shape (triangles, squares or circles). Participants viewed each trial and were asked to make a numerosity judgment, determining whether the number of items in the left array matched the number on the right (regardless of shape). The same stimuli were used for the shape-matching blocks and participants judged whether the left and right arrays contained the same shapes (regardless of numerosity). The only difference between shape and numerosity

stimuli was that an “S” appeared above the equal sign for shape-matching trials and an “N” appeared above the equal sign for number-matching trial.

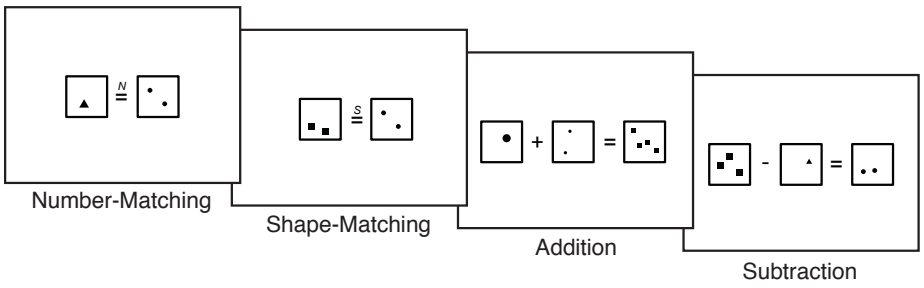

Figure 4-5 Examples of stimuli used in Experiment 2. Participants performed simple numerical tasks on sets of dot arrays differing in numerosity and in shape. They judged whether the numerical operation was correct or not.

Similar stimuli elicited addition and subtraction operations from participants. In addition blocks, participants viewed stimuli consisting of three arrays. On the left were two arrays with a plus sign in the middle, followed by an equal sign and a third array on the right. Participants judged whether the numerosity of stimuli on the right of the equal sign was the same as the sum of the numerosities on the left. The subtraction blocks were similar except that the plus sign was replaced with a minus sign and participants judged whether the numerosity of stimuli on the right was the same as the difference of the numerosities on the left.

This task consisted of five five-minute runs with twenty 16-sec blocks, pseudorandomly ordered (four for each of the four categories in addition to four fixation blocks). Each block was preceded by a 2-sec instruction screen in which the name of the task was displayed on the screen so that the participants could prepare

for the upcoming block. The task was self-paced within each block, and the correct answer was "yes" in half of all the trials.

Data Acquisition. Functional scans were acquired as axial slices, with a faster acquisition (TR = 1.5 s, TE = 25 ms) compared to Experiment 1. This resulted in 246 BOLD repetitions per run with 33 axial slices. Because of the narrowed slice range, cerebellums of some participants were not fully imaged. Other data acquisition parameters were identical to that of Experiment 1.

Activation Analysis. As in Experiment 1, functional images underwent slice-timing correction, realignment, coregistration, segmentation, and normalization as part of preprocessing. The functional images were then modeled using a GLM as in Experiment 1, which included separate regressors for each of the experimental conditions convolved with a canonical hemodynamic response function, as well as six nuisance covariates modeling head translation and rotation. An additional covariate was included to model the 2 sec instructions at the beginning of each experimental block. The contrast maps for numerical processing (addition, subtraction, and number matching vs. shape matching) from each subject were entered into a second-level random effects group analysis in order to estimate neural activity for numerical processing at the group level (see Figure 4-6).

Co-lateralization Analysis. In order to test the hypothesis of co-lateralization of the visual number activity with the parietal activity for numerical processing, we first defined a parietal ROI associated with numerical operations. Similar to the approach used in Experiment 1, we contrasted an aggregate of the three numerical operations conditions (addition, subtraction, and number matching) with the shape

matching condition at the group level ($p < 0.05$, extent > 20 voxels) within a bilateral mask of the superior and inferior parietal cortex. The area isolated from the contrast consisted of 617 voxels in left parietal cortex and 451 voxels in right parietal cortex. The ROI was then defined bilaterally to include the voxels in the opposite hemisphere by flipping the x-coordinates. This bilateral ROI is referred to as the parietal numerical ROI.

In each individual subject, the t-values associated with numerical processing (addition, subtraction, number matching versus the shape-matching condition) in this parietal numerical ROI were used to compute the LI for that subject (see Methods in Experiment 1 for precise methods). The LI for this parietal numerical activity was then correlated with both the LI for the visual letter activity and the visual number activity.

Laterality Analysis in Individualized ROIs. In order to ensure that co-lateralization results are not an artifact of ROIs defined from the group map, co-lateralization analysis was also performed with neural activities within the ROI's defined at the level of individual subjects. In each subject, the visual letter ROI, visual number ROI, and the parietal numerical ROI were defined by each subject's own letter-preferred, number-preferred, and numerical processing activation maps (using a lenient threshold of $p < 0.05$), respectively, within pre-specified anatomical regions (identical to the anatomical masks used in the group-level ROI approach). Then, all the suprathreshold voxels and their opposite hemisphere homologues (flipping x-coordinates) were identified as the individualized ROIs.

4.3.2 Results

Behavioral Results. Accuracy on the numerical tasks was above 90% for all conditions. Reaction times were the fastest for the shape-matching condition followed by the number-matching condition, addition, and subtraction (Table 4-3).

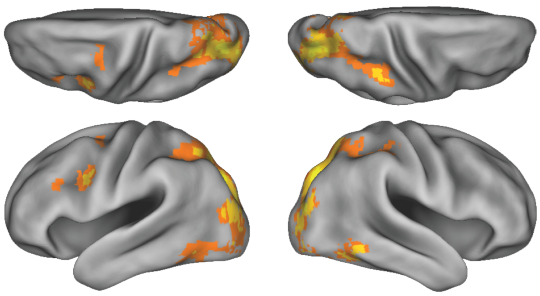

Figure 4-6 Neural activity for numerical processing in the whole brain. Group-level (N=20) activation map of the [addition + subtraction + number matching > shape matching] contrast was displayed on to a 3D inflated surface for visualization as in Figure 2 ($p < 0.001$, cluster extent > 20 voxels).

Table 4-3 Behavioral results of the numerical tasks performed in the scanner (N=20). Mean accuracy and reaction time for the correct trials were measured for each subject, and the average (standard deviations in parentheses) of these scores across subjects are reported.

	Number-matching	Shape-matching	Addition	Subtraction
Accuracy (%)	96.1 (2.94)	95.5 (3.21)	94.8 (3.97)	92.6 (4.99)
Reaction Time (ms)	796.88 (94.87)	684.02 (89.01)	1054.88 (177.36)	1252.62 (210.53)

Co-lateralization Analysis. The primary purpose of Experiment 2 was to test whether lateralization of number recognition in ventral visual cortex is related to lateralization of higher-level numerical processing in parietal cortex. More

specifically, we correlated the visual number LI (as well as the visual letter LI) from Experiment 1 with the parietal numerical LI from Experiment 2. First, we observed individual differences in the lateralization of higher-level numerical processing in parietal cortex. Across subjects, the parietal numerical LI ranged from -0.510 to 0.365 with a median of -0.184. Positive LI represents left lateralization and negative LI represents right lateralization. As hypothesized, the visual number LI, defined from the ROIs constructed at the group level, was significantly correlated with the parietal numerical LI (r = 0.782, p < 0.001; Figure 4-7). That is, subjects who exhibited greater right laterality for visual number processing in the ventral visual cortex exhibited greater right laterality for numerical processing in the parietal area. On the other hand, the visual letter LI showed non-significant correlation with the parietal numerical area LI (r = -0.315, p = 0.189). The results were qualitatively the same when the LIs were computed from the ROIs constructed at the individual level: the parietal numerical LI, ranging from -0.489 to 0.293 with a median of -0.139, was significantly correlated with the visual number LI (r = 0.643, p = 0.002) but not with the visual letter LI (r = -0.041, p = 0.854).

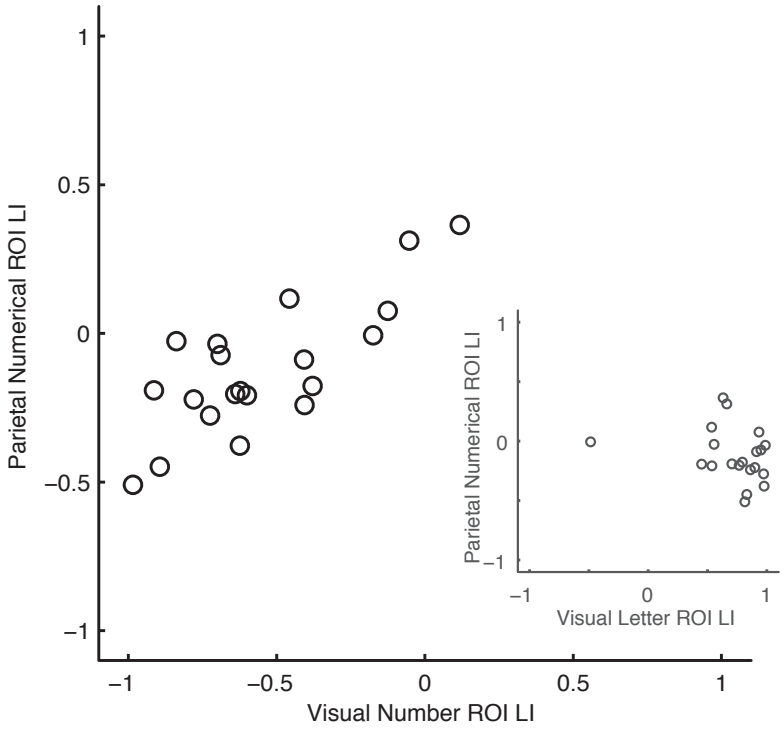

Figure 4-7 Co-lateralization of the visual number area LI and the parietal numerical area LI, in which ROIs were defined from a group-level activation map. The main panel shows the scatter plot between the visual number area LI and the parietal numerical area LI (r = 0.782, p < 0.001). The smaller sub-panel shows how the visual letter area LI is related to the parietal numerical area LI (r = -0.315, p = 0.189). Positive LI represents left lateralization and negative LI represents right lateralization. In the sub-panel, one outlying subject was excluded from the calculation of the correlation coefficients.

One might speculate that visual number activity and parietal numerical activity are primarily right-lateralized in which case variations in the neural activities on the right hemisphere alone could produce such co-lateralization results. However, further analysis showed that there was negligible correlation between the LI measure and the associated Q_R measure in the visual number ROI (r = 0.0512, p = 0.830) and the parietal numerical ROI (r = -0.131, p = 0.580), suggesting that the variance in LI measures cannot be explained solely by the amount of activity in the right hemisphere. Moreover, Q_R in the visual number LI calculation showed no correlation with Q_R in the parietal numerical LI calculation (r = 0.093, p = 0.695),

suggesting that the variability in the right hemisphere activity alone does not explain the present co-lateralization results. Additionally, the visual number LI controlling for the reaction time for number matching and the parietal numerical LI controlling for the reaction time for numerical tasks were correlated with each other ($r = 0.704$, $p = 0.001$), suggesting that the present co-lateralization results still hold even with RT effects excluded.

Note that the parietal activity was first defined by contrasting neural activity for all numerical tasks (addition, subtraction, and number-matching) versus a control task (shape-matching). We tested if the co-lateralization of the visual number activity and the parietal numerical activity would hold true for each of the numerical tasks. That is, within the bilateral ROI (both defined at the group-level and at the individual level) the laterality of each individual's parietal activity was computed from other contrasts, namely, addition versus shape-matching, subtraction versus shape-matching, and number-matching versus shape-matching. The visual number LI showed strong positive correlations with all of the parietal activity LIs defined within the group-based ROI (addition vs. shape-matching LI, $r = 0.680$, $p < 0.001$; subtraction vs. shape-matching LI, $r = 0.712$, $p < 0.001$; number-matching vs. shape-matching LI, $r = 0.420$, $p = 0.065$) and within individual spherical ROIs (addition vs. shape-matching LI, $r = 0.622$, $p < 0.001$; subtraction vs. shape-matching LI, $r = 0.589$, $p = 0.010$; number-matching vs. shape-matching LI, $r = 0.481$, $p = 0.038$).

4.3.3 Discussion

In Experiment 2, we asked whether individual differences in the laterality of visual number activity could be explained by individual differences in the laterality of parietal numerical activity. We found that they could. The co-lateralization analysis showed that subjects with more right-lateralized visual number-preferred activity had more right-lateralized parietal numerical activity. These results cannot be explained by task-independent hemispheric dominance since the visual letter LI was not correlated with the parietal numerical LI (r = -0.315, p = 0.189, ROI defined at the group level; r = -0.041, p = 0.854, ROI defined at the individual level) nor by the variability in right-hemisphere activity alone. Moreover, the co-lateralization results still held when the effects of reaction time were removed. We also verified that the results held true for parietal activity defined from different contrasts (addition, subtraction, or counting), suggesting that the co-lateralization of the visual number activity and the parietal numerical activity generalizes across numerical processes. In addition, there was no significant correlation between the letter activity LI and the number activity LI in the visual cortex suggesting that the development of letter and number recognition may be driven by independent sources.

We found that numerical activity in both parietal and ventral visual cortex was somewhat right-lateralized in most participants, but some previous studies have reported left-lateralized activity for some numerical tasks. One potential explanation for this discrepancy is based on the triple code model of number processing (Dehaene, 1992; Dehaene & Cohen, 1995). According to that model,

numerical tasks that make high demands on verbal processes, such as retrieving memorized multiplication tables, elicit activation primarily in left perisylvian areas (e.g. Chochon et al., 1999; Prado et al., 2011). On the other hand, tasks that put more demands on analog magnitude representations, such as approximate arithmetic, subtraction, number comparison, or even passive adaptation, rely more on bilateral parietal cortex (Chochon et al., 1999; Dehaene et al., 1999; Eger et al., 2009; Piazza et al., 2004; Prado et al., 2011). Our task was designed to make few demands on verbal fact retrieval. Although our task involved addition and subtraction, we reasoned that calculation of non-symbolic numbers in small ranges relies more on analog magnitude representations. These kinds of tasks can be performed by nonhuman primates (Hauser et al., 1996; Rumbaugh et al., 1987), preverbal infants (Wynn, 1992), preschool children (Barth et al., 2005), brain-damaged patients with impaired exact calculation (Lemer et al., 2003), and adults in cultures without large number words (Pica et al., 2004) and therefore presumably do not rely on verbal processes. Therefore, the results of our experiment should be considered in the context of other studies that report more bilateral or even right lateralized (see e.g. Chochon et al., 1999 and Prado et al., 2011) activations for number processing.

An interesting avenue for future research would be to investigate how visual number-preferred activity may be functionally related to different aspects of numerical processing. Since processing of approximate quantity and magnitude serves as a basis of numerical processing (Dehaene et al. 1999), it would be natural to expect a tight functional relationship between approximate numerical processing and number-preferred activity in visual cortex. However, it is also true that humans

typically learn number symbols with extensive schooling on exact number processing and arithmetic. So, one may also hypothesize a close relationship between exact numerical processing and number-preferred activity in visual cortex.

4.4 General Discussion

In this study, we investigated the neural representation underlying the visual recognition of letters and numbers by directly contrasting neural activation patterns elicited by letters and numbers. In Experiment 1, we found letter-preferred activity in left occipitotemporal cortex and number-preferred activity in right occipitotemporal cortex at the group level (Figure 4-3). In Experiment 2, we demonstrated that individual differences in the cerebral lateralization of number-preferred activity in visual cortex could be explained by individual differences in the lateralization of numerical processing in parietal cortex (Figure 4-7).

Left-lateralized letter-preferred activity in ventral visual cortex is consistent with reports showing robust and reproducible neural activation in left occipitotemporal cortex in response to words and letters (Cohen et al., 2000; Petersen, Fox, Snyder, & Raichle, 1990; Polk & Farah, 1998; Polk et al., 2002; Puce et al., 1996). What is more novel in the results from Experiment 1 is the neural dissociation of numbers from letters: the number vs. letter contrast produced significant activation in right lateral occipital cortex at the group level. The identification of this neural double dissociation and the right-lateralized number-preferred activity are important for at least three reasons. First, the double dissociation rules out alternative explanations that assume that the observed letter-

preferred or number-preferred neural activity is an artifact of difficulty or effort. Second, the neural dissociation between letters and numbers is consistent with previously reported behavioral double dissociations (Hamilton et al., 2006; Jonides & Gleitman, 1972), providing further evidence of experience-dependent changes in the neural architecture underlying visual recognition. Third, the fact that number-preferred activity was localized in the right occipitotemporal region is problematic for the "interhemispheric differences hypothesis" which assumes that letter and word recognition are localized in the left hemisphere due to that hemisphere's superiority in processing fine-grained and local visual features (see Robertson & Lamb, 1991 for review). That hypothesis would predict that numbers should also be processed primarily in the left hemisphere given that they also involve processing fine-grained and local visual features.

We also observed individual differences in the lateralization of neural representations for visual and numerical processing, which is a topic that has not yet received much attention. A few studies have reported different patterns of functional cerebral asymmetries between right- and left-handed subjects in the domain of vision. For example, as described in the Introduction, Cai et al. (2008) studied the relationship between cerebral lateralization of VWFA and anterior language processing sites in right- and left-handed subjects. A recent neuroimaging study has also reported that cerebral lateralization for the fusiform face area and the extrastriate body area was coupled with handedness (Willems, Peelen, & Hagoort, 2010). Of course, all of our participants were right-handed, so the

individual differences in lateralization that we observed cannot be attributed to differences in handedness.

The visual processing of numbers has also received relatively little attention in the literature. Besides a previous study by Polk et al. (2002), Arabic digits have typically been used as control stimuli when looking for letter- and word-specific neural activity (Baker et al., 2007; James et al., 2005; Reinke et al., 2008) or have been compared with verbal numerals when looking for notation effects in number processing (Dehaene, 1996; Pinel, Dehaene, Riviere, & LeBihan, 2001; Pinel et al., 1999). Here, we extended the work by Polk et al. (2002) and found significant neural activation in response to numbers compared to letters in right visual cortex.

The observed neural dissociation between letters and numbers is noteworthy given that the distinction between letters and numbers is culturally defined and in some sense arbitrary. How might such a dissociation emerge? Polk & Farah (1995, 1998) proposed a bottom-up model based on a co-occurrence hypothesis. According to this model, letter and number recognition become differentiated because letters tend to co-occur with letters (and number with numbers) in the environment. Correlation-based learning mechanisms in the brain are assumed to pick up on these co-occurrence patterns to lead to neural segregation (Polk & Farah, 1995). While this purely bottom-up hypothesis is plausible for the neural dissociation of letters and numbers, it does not predict why the visual word form area consistently forms in the left hemisphere rather than the right (or why number recognition tends to be right lateralized).

According to the neuronal recycling hypothesis (Dehaene & Cohen, 2007), one of the reasons that VWFA tends to develop in left occipitotemporal cortex is because this area has relatively direct connections to and from anterior language processing sites in the left hemisphere (McCandliss et al., 2003). Consistent with this view, the pattern of activation in VWFA is closely related to components of language-related functions. For instance, it is invariant to letter case (Dehaene et al., 2004; Dehaene et al., 2001; Polk & Farah, 2002) and is greater when the orthographic stimuli are familiar to subjects than when they are unfamiliar (i.e. Hebrew to Hebrew readers versus to non-Hebrew readers) (Baker et al., 2007). Activation in VWFA is hierarchically organized so that the strength of activation increases with orthographic regularities (Vinckier et al., 2007) and bigram frequency (Binder, Medler, Westbury, Liebenthal, & Buchanan, 2006). As noted, it has been shown that VWFA is right lateralized in a subsample of left-handed subjects who showed right-lateralized language sites (Cai, Lavidor, Brysbaert, Paulignan, & Nazir, 2008).

Our findings support another aspect of this hypothesis in the numerical cognition framework. We found that individual differences in the lateralization of numerical processing in the parietal cortex predicted the lateralization of the visual Arabic number form processing in visual cortex. These results are consistent with the hypothesis that top-down influences from the parietal numerical activity play an important role in the neural localization of number recognition in ventral visual cortex. An alternative explanation is that right-lateralized activity in ventral visual cortex influences the laterality of parietal activity for higher-order number

processing (or that a third factor influences the lateralization in both ventral visual and parietal cortex). Given that the processing of numbers may be evolutionarily older than reading (Brannon & Terrace, 1998; Butterworth, Reeve, Reynolds, & Lloyd, 2008; Gallistel & Gelman, 1992; Pica, Lemer, Izard, & Dehaene, 2004) and that numerical competence develops prior to recognizing symbols for numbers (Gebuis, Herfs, Kenemans, de Haan, & van der Smagt, 2009; Wynn, 1992; Xu & Spelke, 2000), we prefer the hypothesis that parietal organization influences ventral visual processes top-down. Our data do not rule out the alternatives however.

To conclude, the current findings demonstrate a neural double dissociation between letter and number recognition and suggest that top-down influences play an important role in experience-dependent neural reorganization.

4.5 References

Allison, T., McCarthy, G., Nobre, A., Puce, A., & Belger, A. (1994). Human extrastriate visual cortex and the perception of faces, words, numbers, and colors. *Cereb Cortex, 4*(5), 544-554.

Anderson, S. W., Damasio, A. R., & Damasio, H. (1990). Troubled letters but not numbers - Domain specific cognitive impairments following focal damage in frontal-cortex. *Brain, 113*, 749-766.

Baker, C. I., Liu, J., Wald, L. L., Kwong, K. K., Benner, T., & Kanwisher, N. (2007). Visual word processing and experiential origins of functional selectivity in human extrastriate cortex. *Proceedings of the National Academy of Sciences of the United States of America, 104*(21), 9087-9092.

Barth, H., La Mont, K., Lipton, J., & Spelke, E. S. (2005). Abstract number and arithmetic in preschool children. *Proceedings of the National Academy of Sciences of the United States of America*, 102(39), 14116-14121.

Binder, J. R., Medler, D. A., Westbury, C. F., Liebenthal, E., & Buchanan, L. (2006). Tuning of the human left fusiform gyrus to sublexical orthographic structure. *Neuroimage, 33*(2), 739-748.

Brannon, E. M., & Terrace, H. S. (1998). Ordering of the numerosities 1 to 9 by monkeys. *Science, 282*(5389), 746-749.

Butterworth, B., Reeve, R., Reynolds, F., & Lloyd, D. (2008). Numerical thought with and without words: Evidence from indigenous Australian children. *Proceedings of the National Academy of Sciences of the United States of America, 105*(35), 13179-13184.

Cai, Q., Lavidor, M., Brysbaert, M., Paulignan, Y., & Nazir, T. A. (2008). Cerebral lateralization of frontal lobe language processes and lateralization of the posterior visual word processing system. *Journal of Cognitive Neuroscience, 20*(4), 672-681.

Cipolotti, L., Warrington, E. K., & Butterworth, B. (1995). Selective impairment in manipulating Arabic numerals. *Cortex, 31*(1), 73-86.

Chochon, F., Cohen, L., van de Moortele, P. F., & Dehaene, S. (1999). Differential contributions of the left and right inferior parietal lobules to number processing. *Journal of Cognitive Neuroscience*, 11(6), 617-630.

Cohen, L., Dehaene, S., Naccache, L., Lehericy, S., Dehaene-Lambertz, G., Henaff, M. A., et al. (2000). The visual word form area - Spatial and temporal characterization of an initial stage of reading in normal subjects and posterior split-brain patients. *Brain, 123*, 291-307.

Cohen, L., Lehericy, S., Chochon, F., Lemer, C., Rivaud, S., & Dehaene, S. (2002). Language-specific tuning of visual cortex functional properties of the Visual Word Form Area. *Brain, 125*, 1054-1069.

Dehaene, S. (1992). Varieties of numerical abilities. *Cognition, 44*(1-2), 1-42.

Dehaene, S. (1996). The organization of brain activations in number comparison: Event-related potentials and the additive-factors method. *Journal of Cognitive Neuroscience, 8*(1), 47-68.

Dehaene, S., & Cohen, L. (1995). Towards an anatomical and functional model of number processing. *Mathematical Cognition, 1*, 83-120.
Dehaene, S., & Cohen, L. (2007). Cultural recycling of cortical maps. *Neuron, 56*(2), 384-398.
Dehaene, S., Jobert, A., Naccache, L., Ciuciu, P., Poline, J. B., Le Bihan, D., et al. (2004). Letter binding and invariant recognition of masked words - Behavioral and neuroimaging evidence. *Psychological Science, 15*(5), 307-313.
Dehaene, S., Naccache, L., Cohen, L., Le Bihan, D., Mangin, J. F., Poline, J. B., et al. (2001). Cerebral mechanisms of word masking and unconscious repetition priming. *Nature Neuroscience, 4*(7), 752-758.
Dehaene, S., Spelke, E., Pinel, P., Stanescu, R., & Tsivkin, S. (1999). Sources of mathematical thinking: Behavioral and brain-imaging evidence. *Science*, 284(5416), 970-974.
Eger, E., Michel, V., Thirion, B., Amadon, A., Dehaene, S., & Kleinschmidt, A. (2009). Deciphering Cortical Number Coding from Human Brain Activity Patterns. *Current Biology*, 19(19), 1608-1615.
Flowers, D. L., Jones, K., Noble, K., VanMeter, J., Zeffiro, T. A., Wood, F. B., et al. (2004). Attention to single letters activates left extrastriate cortex. *Neuroimage, 21*(3), 829-839.
Gallistel, C. R., & Gelman, R. (1992). Preverbal and verbal counting and computation. *Cognition, 44*(1-2), 43-74.
Gebuis, T., Herfs, I. K., Kenemans, J. L., de Haan, E. H. F., & van der Smagt, M. J. (2009). The development of automated access to symbolic and non-symbolic number knowledge in children: an ERP study. *European Journal of Neuroscience, 30*(10), 1999-2008.
Hamilton, J. P., Mirkin, M., & Polk, T. A. (2006). Category-level contributions to the alphanumeric category effect in visual search. *Psychonomic Bulletin & Review, 13*(6), 1074-1077.
Hauser, M. D., MacNeilage, P., & Ware, M. (1996). Numerical representations in primates. *Proceedings of the National Academy of Sciences of the United States of America*, 93(4), 1514-1517.
Ingles, J. L., & Eskes, G. A. (2008). A comparison of letter and digit processing in letter-by-letter reading. *Journal of the International Neuropsychological Society, 14*(1), 164-173.
James, K. H., James, T. W., Jobard, G., Wong, A. C. N., & Gauthier, I. (2005). Letter processing in the visual system: Different activation patterns for single letters and strings. *Cognitive Affective & Behavioral Neuroscience, 5*(4), 452-466.
Jewell, G., & McCourt, M. E. (2000). Pseudoneglect: A review and meta-analysis of performance factors in line bisection tasks. *Neuropsychologia, 38*(1), 93-110.
Jonides, J., & Gleitman, H. (1972). Conceptual category effect in visual search - O as letter or as digit. *Perception & Psychophysics, 12*(6), 457-460.
Joseph, J. E., Cerullo, M. A., Farley, A. B., Steinmetz, N. A., & Mier, C. R. (2006). fMRI correlates of cortical specialization and generalization for letter processing. *Neuroimage, 32*(2), 806-820.

Lemer, C., Dehaene, S., Spelke, E., & Cohen, L. (2003). Approximate quantities and exact number words: dissociable systems. *Neuropsychologia*, 41(14), 1942-1958.

Marangolo, P., Nasti, M., & Zorzi, M. (2004). Selective impairment for reading numbers and number words: a single case study. *Neuropsychologia, 42*(8), 997-1006.

McCandliss, B. D., Cohen, L., & Dehaene, S. (2003). The visual word form area: expertise for reading in the fusiform gyrus. *Trends in Cognitive Sciences, 7*(7), 293-299.

Pernet, C., Celsis, P., & Demonet, J. F. (2005). Selective response to letter categorization within the left fusiform gyrus. *Neuroimage, 28*(3), 738-744.

Petersen, S. E., Fox, P. T., Snyder, A. Z., & Raichle, M. E. (1990). Activation of extrastriate and frontal cortical areas by visual words and word-like stimuli. *Science, 249*(4972), 1041-1044.

Piazza, M., Izard, V., Pinel, P., Le Bihan, D., & Dehaene, S. (2004). Tuning curves for approximate numerosity in the human intraparietal sulcus. *Neuron*, 44(3), 547-555.

Pica, P., Lemer, C., Izard, W., & Dehaene, S. (2004). Exact and approximate arithmetic in an Amazonian indigene group. *Science, 306*(5695), 499-503.

Pinel, P., Dehaene, S., Riviere, D., & LeBihan, D. (2001). Modulation of parietal activation by semantic distance in a number comparison task. *Neuroimage, 14*(5), 1013-1026.

Pinel, P., Le Clec'H, G., van de Moortele, P. F., Naccache, L., Le Bihan, D., & Dehaene, S. (1999). Event-related fMRI analysis of the cerebral circuit for number comparison. *Neuroreport, 10*(7), 1473-1479.

Polk, T. A., & Farah, M. J. (1995). Brain localization for arbitrary stimulus categories: A simple account based on Hebbian learning. *Proceedings of the National Academy of Sciences of the United States of America, 92*(26), 12370-12373.

Polk, T. A., & Farah, M. J. (1998). The neural development and organization of letter recognition: Evidence from functional neuroimaging, computational modeling, and behavioral studies. *Proceedings of the National Academy of Sciences of the United States of America, 95*(3), 847-852.

Polk, T. A., & Farah, M. L. (2002). Functional MRI evidence for an abstract, not perceptual, word-form area. *Journal of Experimental Psychology-General, 131*(1), 65-72.

Polk, T. A., Stallcup, M., Aguirre, G. K., Alsop, D. C., D'Esposito, M., Detre, J. A., et al. (2002). Neural specialization for letter recognition. *Journal of Cognitive Neuroscience, 14*(2), 145-159.

Prado, J., Mutreja, R., Zhang, H., Mehta, R., Desroches, A. S., Minas, J. E., et al. (2011). Distinct representations of subtraction and multiplication in the neural systems for numerosity and language. *Human Brain Mapping*, n/a-n/a.

Puce, A., Allison, T., Asgari, M., Gore, J. C., & McCarthy, G. (1996). Differential sensitivity of human visual cortex to faces, letterstrings, and textures: A functional magnetic resonance imaging study. *Journal of Neuroscience, 16*(16), 5205-5215.

Rumbaugh, D. M., Savagerumbaugh, S., & Hegel, M. T. (1987). Summation in the chimpanzee (Pan Troglodytes). *Journal of Experimental Psychology-Animal Behavior Processes*, 13(2), 107-115.

Reinke, K., Fernandes, M., Schwindt, G., O'Craven, K., & Grady, C. L. (2008). Functional specificity of the visual word form area: General activation for words and symbols but specific network activation for words. *Brain and Language, 104*(2), 180-189.

Robertson, L. C., & Lamb, M. R. (1991). Neuropsychological contributions to theories of part whole organization. *Cognitive Psychology, 23*(2), 299-330.

Roux, F. E., Lubrano, V., Lauwers-Cances, V., Giussani, C., & Demonet, J. F. (2008). Cortical areas involved in Arabic number reading. *Neurology, 70*(3), 210-217.

Shallice, T. (1988). From Neuropsychology to mental structure. *Shallice, T. From Neuropsychology to Mental Structure. Xv+462p. Cambridge University Press: Cambridge, England, Uk; New York, New York, USA. Illus*, XV+462P.

Starrfelt, R. (2007). Selective alexia and agraphia sparing numbers-a case study. *Brain Lang, 102*(1), 52-63.

Suarez, R. O., Whalen, S., Nelson, A. P., Tie, Y., Meadows, M. E., Radmanesh, A., et al. (2009). Threshold-independent functional MRI determination of language dominance: A validation study against clinical gold standards. *Epilepsy & Behavior, 16*(2), 288-297.

Vinckier, F., Dehaene, S., Jobert, A., Dubus, J. P., Sigman, M., & Cohen, L. (2007). Hierarchical coding of letter strings in the ventral stream: Dissecting the inner organization of the visual word-form system. *Neuron, 55*(1), 143-156.

Vogel, J. J., Bowers, C. A., & Vogel, D. S. (2003). Cerebral lateralization of spatial abilities: A meta-analysis. *Brain and Cognition, 52*(2), 197-204.

Willems, R. M., Peelen, M. V., & Hagoort, P. (2010). Cerebral lateralization of face-selective and body-selective visual areas depends on handedness. *Cereb Cortex, 20*(7), 1719-1725.

Wong, A. C., Gauthier, I., Woroch, B., DeBuse, C., & Curran, T. (2005). An early electrophysiological response associated with expertise in letter perception. *Cogn Affect Behav Neurosci, 5*(3), 306-318.

Wynn, K. (1992). Addition and subtraction by human infants. *Nature, 358*(6389), 749-750.

Xu, F., & Spelke, E. S. (2000). Large number discrimination in 6-month-old infants. *Cognition, 74*(1), B1-B11.

Chapter 5

Conclusion

This dissertation investigates experiential effects on the neural basis of visual word and number processing. Visual representations of words and numbers are cultural inventions that appeared only very recently on an evolutionary time scale. Furthermore, other species do not read words and numbers. So, while generic visual mechanisms might be hardwired to some extent, our unique ability to process words and numbers is likely to be a result of extensive experience during development. Therefore, investigating the neural basis of the visual processing of words and numbers provides a window into answering an interesting question about experience-dependent properties in the functional organization of the human brain. In this last Chapter, I present a summary of the dissertation and provide future directions to investigate this matter further.

5.1 Summary

In this dissertation, answers to a series of scientific questions are reported in one methodological study (Chapter 2) and two empirical studies (Chapters 3 and 4). First, in Chapter 2, I developed a novel statistical method that can estimate intraclass correlation and heritability measures in each point in spatial data. Both a

simulation study and a real data study suggest that the proposed spatial decomposition method provides a better estimate of correlation and heritability in a spatial dataset than conventional methods such as a voxelwise method or a mean-ROI (region of interest) method. The motivation for this novel statistical method is to allow a trade-off between bias and variance. By introducing a somewhat restricted set of basis volumes, the method is able to effectively estimate the correlation and heritability captured by these basis volumes. As a result, the estimation typically has lower variance at a cost of a slight increase in conservative bias compared to the voxelwise method. By having better control of variance, the proposed method was able to detect significantly heritable regions even with a modest sample size in the real data study in Chapter 2. One limitation of the spatial decomposition method compared to the voxelwise method is that the scope of investigation, in terms of spatial dependencies, is limited to a region of interest. Therefore, the selection of the region of interest that adequately captures the cognitive process of interest would be an important issue to consider.

Compared to the mean-ROI approach, this novel technique allows us to capture correlated/heritable subregions within the region of interest. This is an important advance because the assumption of spatial homogeneity within an ROI (which the mean-ROI method assumes) is often violated in fMRI studies.

In Chapter 3, I used this method to investigate how the environment we experience influences the visual word form area (VWFA). While previous studies have shown inconsistent results as to whether VWFA activation is greater for familiar words or unfamiliar words, a monozygotic (MZ) twin study in this Chapter

provided a clearer way of quantifying the environmental effects. The results showed greater unique environmental effects for neural activity associated with familiar word recognition than neural activity associated with unfamiliar word recognition. In addition, the unique environmental contribution was the greatest in the word recognition condition, where orthography, phonology, and semantics are fully embedded. The pseudoword condition, which does not involve semantic processing, showed exhibited a slightly smaller unique environmental contribution compared to the word condition. The consonant strings condition, which further removes the need for phonological processing, showed a much smaller unique environmental contribution. This pattern suggests that experience-based phonological processing may make the largest contribution in shaping VWFA.

Unique environmental effects are broadly defined in this study, including any prenatal experiences or epigenetic changes. In short, this effect is what makes monozygotic twins different from one another. Thus, the present findings support the idea that the VWFA is shaped by how each of us uniquely encounters orthographic stimuli in the environment over the course of development. The present findings incorporating a twin study provide direct evidence for environmental contributions to the neural representations of written words, suggest the relative importance of phonological processing in shaping VWFA, and overcome the limitations of previous studies based exclusively on the mean response magnitude.

In Chapter 4, I asked whether the neural representation of letters and numbers is doubly dissociated and what might be the underlying reasons for such a

dissociation. I report that letter recognition uniquely activates the left occipitotemporal region while number recognition uniquely activates the right lateral occipital region, thus establishing a double dissociation. Considering the fact that letters and numbers are physically arbitrary and culturally defined, these results suggest that early schooling experiences can lead to qualitative changes in neurocognitive architecture. In the second part of Chapter 4, I tested whether the number-preferred activation in right lateral occipital cortex can be explained by the localization of higher-order numerical processes. I found that individual differences in the laterality of visual number activation could be explained by individual differences in the laterality of numerical processing in parietal cortex. These results suggest that the emergence of neural segregation between letter and number recognition may be due to top-down influences from higher-level cognitive functions.

5.2 Future Directions

While the findings in this dissertation provide a better understanding of experiential effects on the neural substrates of visual word and number recognition, many related interesting questions immediately follow. In Chapter 4, I investigated the functional relationship between number processing in ventral visual cortex and parietal cortex by correlating a measure of cerebral laterality. While this approach provides indirect evidence for functional connections between the two sites, a stronger form of functional connectivity can be measured from a within subject functional connectivity analysis such as time-series correlation analysis,

psychophysiological interactions, or dynamic causal modeling (Biswal, Yetkin, Haughton, & Hyde, 1995; Friston, et al., 1997; Friston, Harrison, & Penny, 2003). Unfortunately, these types of analyses were not directly applicable to the current data due to the nature of the experimental design. An experimental modulation (e.g. less attentional state versus more attentional state) is typically necessary to run these models. In addition, by identifying individual's prefrontal and superior temporal language processing sites in addition to the parietal numerical processing sites, one should be able to test whether functional connections involved in word and number recognition show double dissociation.

There is some evidence that two types of higher-order numerical processing exist—an approximate numerosity system and an exact calculation system (Dehaene, Spelke, Pinel, Stanescu, & Tsivkin, 1999). The numerical processing task used in Chapter 4 did not make a strong distinction between the two systems. Therefore, it is unknown whether the emergence of number-preferred neural activation in the right lateral occipital area is related to a more fundamental approximate numerosity processing system or is related to learning of exact calculation during development.

Investigating the developmental trajectory of the neural systems involved in word and number processing is another important topic for future study. When during development do the neural representations for letters and numbers doubly dissociate in the visual cortex? Does this neural trajectory lead or follow the behavioral double dissociation between letters and numbers (i.e. the categorical effect between letters and numbers shown by Jonides & Gleitman, 1972)? Can the

location of the neural site for letter and number recognition in the visual cortex be predicted based on top-down connections from prefrontal language and parietal numerical processing sites, perhaps even before children learn to read?

There are also many ways to further explore the potential of the novel statistical method introduced in Chapter 2. One way is to investigate ways to better construct the basis volumes. In a practical setting when the basis volumes are limited in number, the extent of the spatial variation that can be captured well is certainly limited. Therefore, finding ways to capture spatial dependencies more efficiently would be an important improvement. Also, intraclass correlation is a useful measure to assess the reliability of a measure. Thus, applying this novel statistical method to the context of neuroimaging reliability (e.g., Specht, Willmes, Shah, & Jancke, 2003) would be an important contribution to the field.

While Chapter 3 explored the amount of unique environmental effects in VWFA in response to familiar words and unfamiliar words, the absence of dizygotic twins and a relatively small sample size prevented me from assessing the genetic influence. With both monozygotic and dizygotic twins reared together, it is possible to decompose the phenotypic variance into the additive genetic effects, common environmental effects and the unique environmental effects. Being able to estimate the heritability of VWFA activity in response to various visual stimuli would shed light on the role of genetics in shaping the VWFA. At the same time, by comparing genetic and environmental effects in VWFA activation in different age groups, one would be able to answer questions about the role of genetics and environment across the developmental trajectory (e.g., Byrne, et al., 2005). For example, based on

my results showing strong experiential role on VWFA activity, I predict that children who have not yet learned to read should exhibit more genetic effects in VWFA activity than children or adults who have gained knowledge about words.

5.3 References

Biswal, B., Yetkin, F. Z., Haughton, V. M., & Hyde, J. S. (1995). Functional connectivity in the motor cortex of resting human brain using echo-planar MRI. *Magnetic Resonance in Medicine, 34*(4), 537-541.

Byrne, B., Wadsworth, S., Corley, R., Samuelsson, S., Quain, P., DeFries, J. C., et al. (2005). Longitudinal twin study of early literacy development: Preschool and kindergarten phases. *Scientific Studies of Reading, 9*(3), 219-235.

Dehaene, S., Spelke, E., Pinel, P., Stanescu, R., & Tsivkin, S. (1999). Sources of mathematical thinking: Behavioral and brain-imaging evidence. *Science, 284*(5416), 970-974.

Friston, K. J., Buechel, C., Fink, G. R., Morris, J., Rolls, E., & Dolan, R. J. (1997). Psychophysiological and modulatory interactions in neuroimaging. *Neuroimage, 6*(3), 218-229.

Friston, K. J., Harrison, L., & Penny, W. (2003). Dynamic causal modelling. *Neuroimage, 19*(4), 1273-1302.

Jonides, J., & Gleitman, H. (1972). Conceptual category effect in visual search - O as letter or as digit. *Perception & Psychophysics, 12*(6), 457-460.

Specht, K., Willmes, K., Shah, N. J., & Jancke, L. (2003). Assessment of reliability in functional imaging studies. *Journal of Magnetic Resonance Imaging, 17*(4), 463-471.